THE HONG KONG
POLYTECHNIC UNIVERSITY
香港理工大學
Pao Yue-kong Library
包玉剛圖書館

Copyright Undertaking

This thesis is protected by copyright, with all rights reserved.

By reading and using the thesis, the reader understands and agrees to the following terms:

1. The reader will abide by the rules and legal ordinances governing copyright regarding the use of the thesis.
2. The reader will use the thesis for the purpose of research or private study only and not for distribution or further reproduction or any other purpose.
3. The reader agrees to indemnify and hold the University harmless from and against any loss, damage, cost, liability or expenses arising from copyright infringement or unauthorized usage.

IMPORTANT

If you have reasons to believe that any materials in this thesis are deemed not suitable to be distributed in this form, or a copyright owner having difficulty with the material being included in our database, please contact lbsys@polyu.edu.hk providing details. The Library will look into your claim and consider taking remedial action upon receipt of the written requests.

Pao Yue-kong Library, The Hong Kong Polytechnic University, Hung Hom, Kowloon, Hong Kong

http://www.lib.polyu.edu.hk

LATTICE BOLTZMANN SIMULATION OF HEAT AND MASS TRANSFER PROCESS IN FALLING FILM BASED LIQUID DESICCANT AIR CONDITIONING

LU TAO

PhD

The Hong Kong Polytechnic University

2020

The Hong Kong Polytechnic University

Department of Building Services Engineering

LATTICE BOLTZMANN SIMULATION OF HEAT AND MASS TRANSFER PROCESS IN FALLING FILM BASED LIQUID DESICCANT AIR CONDITIONING

LU TAO

A thesis submitted in partial fulfillment of the requirements for the

Degree of Doctor of Philosophy

February 2020

Certificate of Originality

I hereby declare that this thesis is my own work and that, to the best of my knowledge and belief, it reproduces no material previously published or written, nor material that has been accepted for the award of any other degree or diploma, except where due acknowledgement has been made in the text.

__ _ (Signed)

_LU TAO____(Name of student)

Abstract

Indoor thermal environment is quite important for both indoor occupants and indoor building materials, especially in hot and humid regions. Temperature and humidity control of indoor air is the core part of indoor thermal environment. In the conventional HVAC system that removes moisture by condensation, air is cooled and dehumidified simultaneously. However, the overcooling and reheating process is energy-intensive, which leads to low evaporating temperature, a poor COP value for the chiller and higher energy consumption of the system. In the conventional HVAC system, energy consumption on treating fresh air is extensive. About 20-40% of the overall energy consumption of air conditioning system is consumed in fresh air handling process. Moreover, the ratio of sensible load to latent load varies largely due to the changes of outdoor climate, number of indoor occupants, indoor equipment utilization situation and so on. Therefore, the indoor temperature and humidity can hardly be satisfied with condensation by the cooling coil only.

Falling film is widely used in heat engineering fields, such as falling film heat exchangers, evaporators and cooling towers, for its simple structure, low temperature difference and considerable heat and mass transfer efficiency. Falling film liquid desiccant air dehumidification is a promising alternative to traditional vapor compression air-conditioning system due to its lower energy consumption and less

pollution. It is reported that the liquid desiccant air conditioning system based on this kind of dehumidifier can save about 10-30% of energy compared with the low temperature dehumidification using conventional gas compression system. Many researchers have studied the effect of various design operating parameters and conditions on the performance of the falling film. The factors are evaluated specifically, including the desiccant fluid properties (like density, viscosity, and specific heat capacity and so on), the flow configuration, the desiccant distribution, the inlet flow rate and condition of the desiccant solution, moist air and cooling media, energy store capacity and so on. However, further studies are also needed on some aspects. Firstly, most researches focus on the macroscopic parameter change rather than the microscopic heat and mass transfer process in falling film. Secondly, many researches take the falling film as a single phase problem, which means the surface tension and phase change are neglected. Thirdly, in conventional numerical models, the turbulence flow is usually simulated with semi-experimental turbulence models, which may not have solid physical backgrounds.

The lattice Boltzmann method (LBM), which is a numerical method rooted in kinetic theory, is becoming popular in the fields of computational fluid dynamics in last decades. Due to the particle-based mesoscopic nature which connects the micro and macro worlds, the LBM has an advantage in simulation fidelity and computational efficiency especially for multiphase flows. Generally, there are four popular LBM models

so far to solve the multiphase flow problems, including the color-gradient model, the free energy model, the Shan-Chen model and the phase-field model. The phase-field model is more appropriate to solve the falling film problems due to its advantage in handing high density ratio problem. To solve the heat and mass transfer problem in falling film process, thermal phase-field LB models are proposed by many researches. However, in these previous models, there are still some fundamental problems that have not been solved. First, most of the existing works are focused on the lattice Boltzmann (LB) models for Cahn-Hilliard (C-H) equation, but these models suffer from the poor stability, difficulty in simulating the large density ratio problems, and the mass non-conservation. Second, most of the existing LB models are only suitable for steady state flow instead of dynamic problems. Thirdly, most existing LB models still have problems in dealing with the phase change problem. For above problems, we have carried out the following works:

(1) A mass conservative lattice Boltzmann model (LBM) is proposed to simulate the two-phase flows with moving contact lines at high density ratio. The proposed model consists of a phase field lattice Boltzmann equation (LBE) for solving the conservative Allen-Cahn (A-C) equation, and a pressure evolution LBE for solving the incompressible Navier-Stokes equations. In addition, a modified wall boundary treatment scheme is developed to ensure the mass conservation. The wetting dynamics are treated by incorporating the cubic wall energy in the expression of the total free

energy. The current model is characterized by mass conservation, proper treatment of wetting boundary and high density ratio. We applied the model on a series of numerical tests including equilibrium droplets on wetting surface, co-current flow and a droplet moving by gravity along inclined wetting surfaces. Theoretical analysis and experiments are conducted for model validation. The numerical results show good performances on mass conservation even with a density contrast up to 1000. Furthermore, the results show that the moving contact line can be successfully recovered, which proves that this model is applicable on the study of moving contact line issue and further related applications.

(3) Based on the above thermal LB model, we simulated the complete development processes of the falling film from beginning to steady state at different Reynolds numbers. The results are compared with the experiments of previous researches.

In conclusion, a thermal multi-phase lattice Boltzmann model is established for simulating the heat and mass transfer process in falling film based liquid desiccant air conditioning. The model can well predict the temperature and concentration distribution of the falling film process and has a better computational efficiency than traditional simulation methods. The model has made contributions in the aspects of two-phase flow interaction, high density ratio flow and phase-change problems. The model can provide suggestions in the future design and optimization of the falling film

based liquid desiccant air conditioning.

Publications during PhD study

Journal papers

[1] **Tao, Lu**, and Fu Xiao. "Lattice Boltzmann Simulation of Falling Film Flow under Low Reynolds Number." Heat Transfer Engineering 39.17-18 (2018): 1528-1539.

[2] **Tao Lu**, Xuguang Yang, Fu Xiao and Tao Wen. "A Mass Conservative Lattice Boltzmann Model for Two-Phase Flows with Moving Contact Lines at High Density Ratio." Communications in Computational Physics 26 (2019): 1098-1117.

[3] **Tao Lu**, Xuguang Yang and Fu Xiao. "Lattice Boltzmann simulation of heat and mass transfer in falling film dehumidifier", International Journal of heat and mass transfer (under review).

[4] 王凌士, 肖赋*, **陆韬**. (2019). 3 种填料型溶液除湿器性能对比分析. *暖通空调*. 49 (7): 130-134.

[5] 王凌士, 肖赋*, **陆韬**. (2017). 高效填料型除湿器新传质关联式实验研究.*制冷学报*, 2017, 38(6): 1-6. **（2017 年度《制冷学报》优秀论文奖）**

Conference papers

[1] **Tao Lu** and Fu Xiao, Lattice Boltzmann Simulation of Falling Film Flow under Low Reynolds Number, the 5th International Symposium on Heat Transfer and Energy Conservation (ISHTEC2016), November 11-14, 2016, Guangzhou, China

[2] **Tao Lu**, Fu Xiao, A Mass Conservative Lattice Boltzmann Model for the Wavy Falling Film Flow with High Density Ratio, the International Conference on cryogenics Refrigeration (ICCR 2018), April 12-14, 2018, Shanghai, China

[3] **Tao Lu**, Xuguang Yang and Fu Xiao, Simulation of Two-phase Flows on Wetting Surface with High Density Ratio by A Mass Conservative Lattice Boltzmann Model, 31st International Conference on Efficiency, Cost, Optimization, Simulation and Environmental Impact of Energy Systems (ECOS 2018), June 17-21, 2018, Guimarães, Portugal

[4] Lingshi Wang, Fu Xiao*, **Tao Lu**. (2017). Performance analysis of the packed-type liquid desiccant dehumidifier using different packing materials. 16th International Conference on Sustainable Energy Technologies, July 17-20, 2017, Bologna, Italy.

[5] 王凌士, 肖赋*, **陆韬**. (2017). 填料材料对填料型除湿器的性能影响分析.

2017 年全国空调学术年会, 2017 年 11 月 1-3 日，浙江杭州. **（2017 年全国空调学术年会优秀论文）**

[6] 王凌士, 肖赋*, **陆韬**. (2016). 高效填料型除湿器新传质关联式实验研究. *2016 年第九届全国制冷空调新技术研讨会*, 2016 年 8 月 3-6 日, 河南洛阳.

Acknowledgements

First and foremost, I would like to express my deepest appreciation and gratitude to my chief supervisor, Prof. Xiao Fu. During my pursuing of the doctoral degree, she always gave me valuable advices, continuous encouragement, patient guidance and generous support. Without her, it is impossible for me to complete the thesis on time. What's more, her optimism and friendly personality also set an example for my life-long learning.

My special appreciation is also devoted to Prof. Wang Shengwei, for his insightful view and valuable suggestions on my research work.

I also wish to express sincerest gratitude to Prof. Cheng Ping from Shanghai Jiao Tong University, for his valuable suggestions and providing me the opportunity to study in his research group.

Furthermore, I would like to express my thanks to all the members in the Intelligence Building Group for their help and company during the PhD study. I'm deeply indebted to Dr. Wang Lingshi, who is already a research staff of Oak Ridge National Laboratory in USA, for his kind guidance, especially at the beginning of my PhD study.

My special thanks go to the Research Grant Council (RGC) of Hong Kong and the

Hong Kong Polytechnic University for financially supporting this research work.

My heartfelt appreciation goes to my beloved parents, for their love and sacrifice without expecting any return.

Table of Contents

List of Figures

Chapter 5

Nomenclature

A	Area	m^2
c_p	Specific heat capacity	kJ/(kg·℃)
d	Width of the air channel	m
D	Width of the rim part	m
D_a	Diffusion coefficient	m^2/s
f	Friction factor	
F	Wetting factor	
G, m	Mass flow rate	kg/s
h	enthalpy	kJ/kg
h_c	Heat transfer coefficient between air and desiccant	$W/(m^2 \cdot K)$
h_d	Mass transfer coefficient	$kg/(m^2 \cdot s)$
h_f	Heat transfer coefficient between cooling water and desiccant	$W/(m^2 \cdot K)$
H	Height	m
J	Colburn J factor	
K	Thermal conductivity	$W/(m \cdot K)$
Le	Lewis number	
NTU	Number of transfer unit	

n	Element number	
Nu	Nusselt number	
P	Pressure	Pa
Pr	Prandtl number	
Q	Heat	W
Re	Reynolds number	
Sc	Schmidt number	
SC	Sensitivity coefficient	
Sh	Sherwood number	
T	Temperature	℃
V	Velocity	m/s
U	Uncertainty	
W	Width or air humidity	m or g/kg
Δx	Shrinkage distance	m
X	Concentration	%

Greek letters

α	Contact angle	°
β	Shrinkage angle	°
γ	Latent heat	kJ/kg
ω	Humidity ratio	g/kg

$\Delta\omega$	Moisture removal rate	g/kg
σ	Surface tension	N/m
ε	Deformation factor	
ρ	Density	kg/m^3
δ	Film thickness	mm
μ	Dynamic viscosity	$Pa \cdot s$

Subscripts

a	Air
ave	Average
cen	Central part
eff	effective
equ	equilibrium
f	Cooling water
g,G	air
in	Inlet
L	Liquid
m	Maximum
Out	Outlet
s	Desiccant solution
S	Solid

v	vapor
x	x coordinate
y	y coordinate
z	z coordinate

CHAPTER 1

INTRODUCTION

1.1 Background of building energy consumption

Energy is playing key role in modern society, in which the building energy is closely related to daily life. A great amount of energy is consumed by buildings to create a comfortable indoor environment. During the past decades, the energy consumed by building has increased rapidly with the development of society [P. Tuominen et al., 2014]. In developed countries, 20% and 40% of the total energy are consumed by buildings, including both residential and commercial, which exceeds the industry and transportation sectors [L. Perez-Lombard et al., 2011]. In China, the building energy consumption accounts for about 33% of total energy (China Energy Statistical Yearbook 2014). In Hong Kong, buildings contribute up to 90% of total electricity consumption (http://www.beeo.emsd.gov.hk/en.mibec_beeo.html) and 64% of total energy consumption (Fig 1.1, Hong Kong Energy End-use Data 2018).

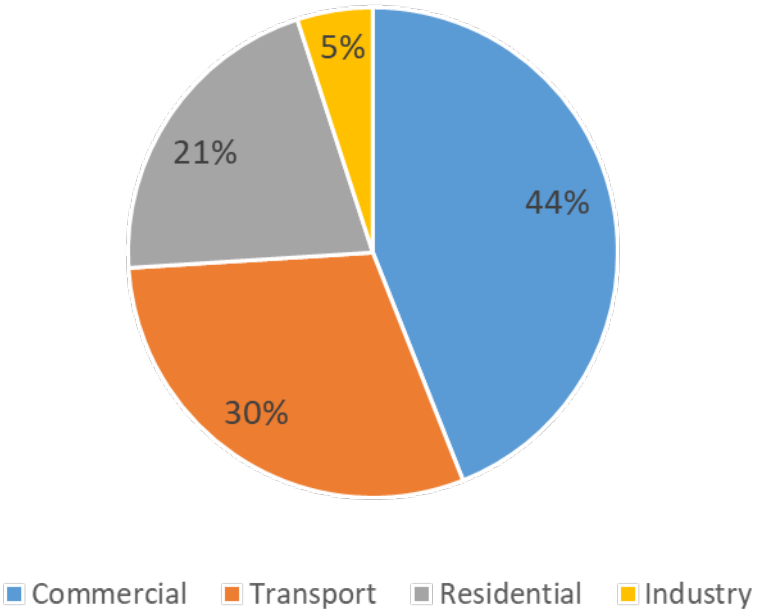

Fig 1.1 Breakdown of total energy consumption in Hong Kong in 2018

Air conditioning systems are the most energy consuming devices among all the building service equipment. According to the Hong Kong Energy End-use Data 2018, the electricity energy usage of air conditioning accounts for 55% (commercial building) and 25% (residential building) of the total electricity energy consumption as shown in Fig 1.2. In addition, considering the global warming and increasing living standard, it is expected that more energy will be consumed by air conditioning system to create a comfortable indoor environment. Therefore, energy saving in air conditioning system is of great importance, especially in Hong Kong.

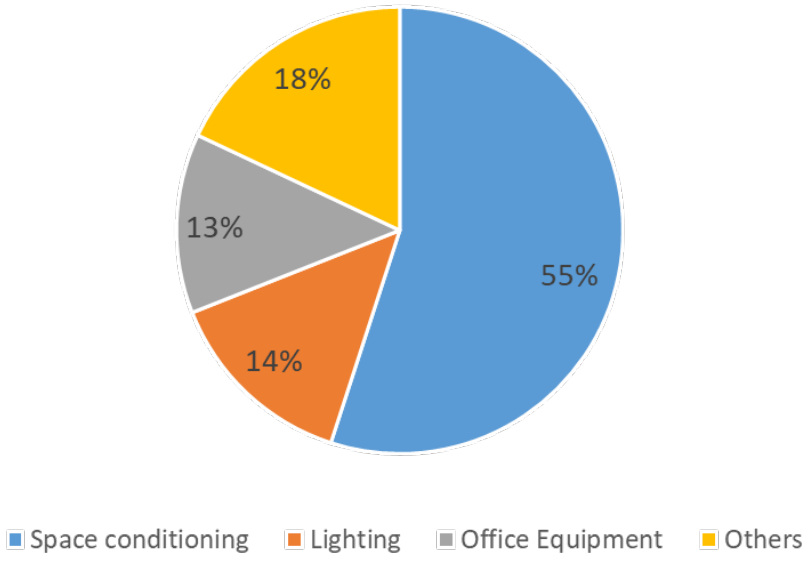

(a) Breakdown of electric energy usage in commercial buildings in Hong Kong

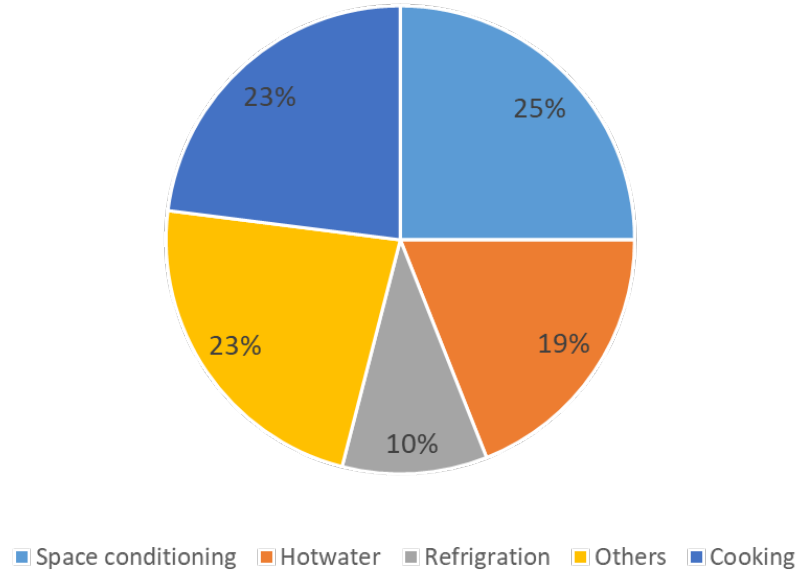

(b) Breakdown of electric energy usage in residential buildings in Hong Kong

Fig 1.2 Hong Kong Energy End-use Data 2018

1.2 Introduction of falling film based liquid desiccant dehumidification

Air conditioning system is to create a comfortable indoor thermal environment, which includes two key parameters: temperature and humidity of indoor air. Fig 1.3 shows the traditional dehumidification process. In the conventional HVAC system that removes moisture by condensation, air is cooled and dehumidified simultaneously. However, as the required cooling source temperature of dehumidification is much lower than that of cooling, the chilled water temperature has to be reduced to meet the demand for condensation dehumidification. The cooled air often needs to be reheated. The overcooling and reheating process is energy-intensive, which leads to low evaporating temperature, a poor COP value for the chiller and higher energy consumption of the system.

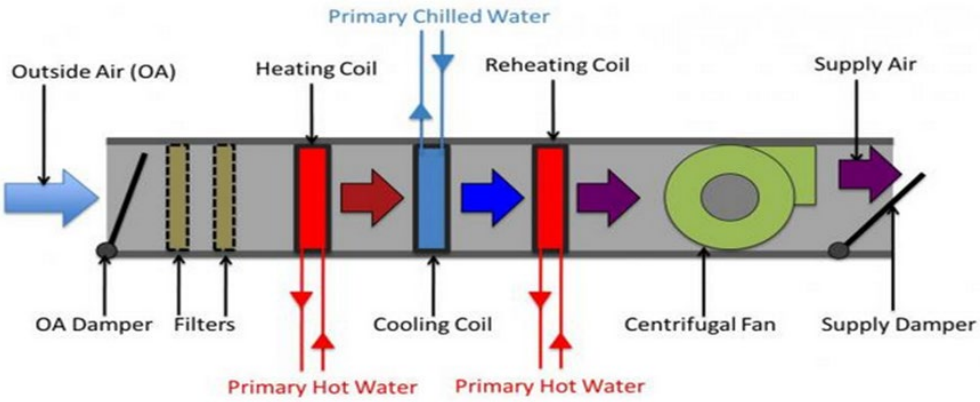

Fig 1.3 Schematic of traditional dehumidification process

In the conventional HVAC system, energy consumption on treating fresh air is extensive. About 20-40% of the overall energy consumption of air conditioning system is consumed in fresh air handling process. The ratio can be even higher in hot and humid regions where latent load from fresh air is as heavy as 50% of the cooling load [Zhang and Xiao, 2008].

Moreover, the ratio of sensible load to latent load varies largely due to the changes of outdoor climate, number of indoor occupants, indoor equipment utilization situation and so on. Therefore, the indoor temperature and humidity can hardly be satisfied with condensation by the cooling coil only [Zhao et al., 2011].

In order to improve system energy performance and solve the above-mentioned problems, more effective humidity control method should be developed.

Basically, there are two methods for air humidity control: mechanical dehumidification method and chemical dehumidification method.

The mechanical dehumidification method is the air cooling below dew point which was mentioned above. The chemical dehumidification method is to reduce the water vapor content of moist air by solid or liquid desiccants. Solid desiccants widely used in air conditioning systems include silica gel and molecular sieves, while liquid

desiccants include lithium chloride (LiCl), lithium bromide(LiBr), calcium chloride (CaCl2), and triethylene glycol. Liquid desiccants have many advantages over solid desiccants, including a lower pressure drop in air-flow across the desiccant material, energy storage capacity, and the capability to remove pollutants. Moreover, a liquid desiccant system can be driven by low-grade heat sources such as solar energy or waste heat [Factor et al., 1980]. Analyses of air conditioning and industrial drying processes showed the potential application of liquid desiccant dehumidification [Lazzarin et al., 1999]. Liquid desiccant dehumidification is a promising dehumidification method, which has prominent superiority in humidity control [Ma et al., 2006], energy saving [Niu et al., 2012], indoor air quality improvement [Mei and Dai, 2008] over conventional dehumidification by mechanical cooling.

Fig 1.4 presents a schematic of a liquid desiccant dehumidification system. The liquid desiccant air conditioning system removes latent load (and, possibly, sensible heat) from process air via a liquid desiccant material, such as lithium chloride(LiCl), lithium bromide (LiBr). It consists of two primary units, a dehumidifier where concentrated liquid desiccant solution absorbs moisture from the process air, and a regenerator where the moisture taken on by the liquid desiccant in the absorber is removed from the liquid desiccant, thus regenerating the liquid desiccant to the higher concentration air.

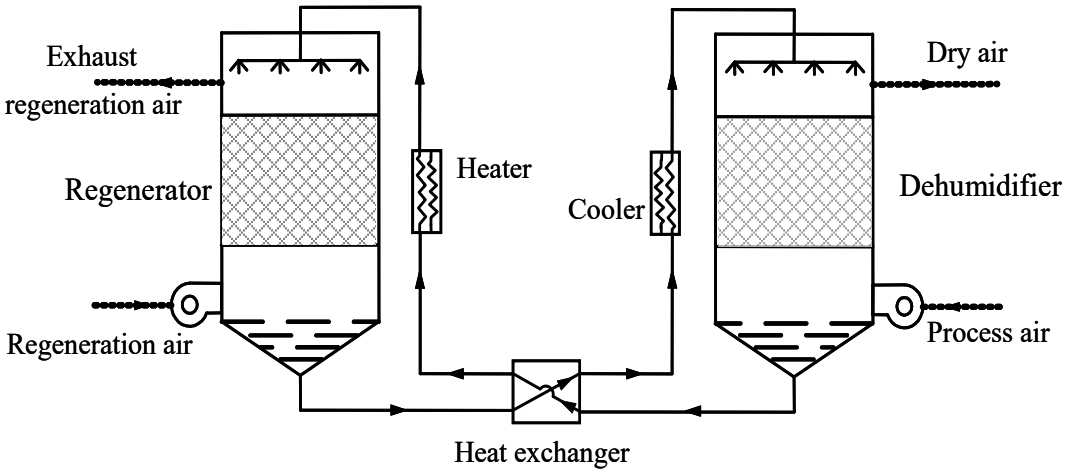

Figure 1.4 Schematic of a liquid desiccant dehumidification system

Falling film flow is a special type of multi-phase flow, characterized by a thin liquid layer at a wall and some gas in the remainder of domain (for a graphical representation see Fig. 1.5). The layer thickness is typically below a few millimeters. Contrary to pure-gas flows, liquid film flows provide superior heat and mass transfer conditions due to the thin liquid layer, which improves the performance even better when being wavy or turbulent and phase–change takes place. Falling film is widely used in industries like thermal engineering, energy engineering [Roques and Thome 2007] and air conditioning engineering, especially the liquid desiccant air conditioning [Ahn et al. 2016] due to its simple structure, low temperature difference and considerable heat and mass transfer efficiency. Fig. 1.6 is the two-dimensional schematic side view of the falling film. Complicated heat and mass transfer process including phase change can occur between the liquid layer and the gas, which makes falling film appropriate

for heat and mass exchange. When the desiccant solution (such as the $LiCl_2$ solution) is chosen as the working liquid and the moist air takes the role of gas, the falling desiccant solution film becomes a dehumidifier [Lowenstein 2008]. It is reported that the liquid desiccant air conditioning system based on this kind of dehumidifier can save about 10-30% of energy compared with the low temperature dehumidification using conventional gas compression system [Yin et al. 2014]. Thus, it is important and valuable to better understand the characteristics of falling film flow to enhance the mass/moisture transfer, so as to improve the performance of the falling film based liquid desiccant technology.

Figure 1.5 Typical falling film

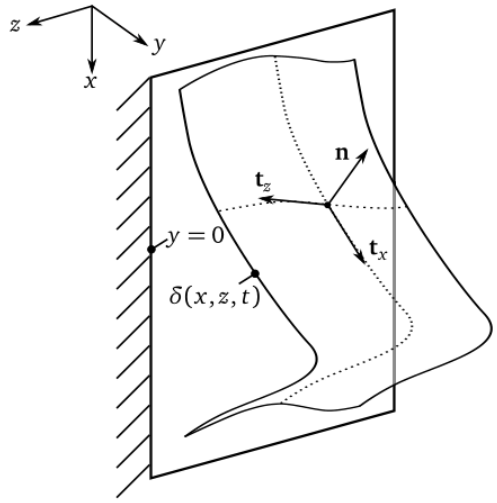

Figure 1.6 Three-dimensional sketch of a wavy liquid film flowing down a vertical wall with the film thickness δ, and the interfacial unit normal n and unit tangents tx and tz

1.3 Introduction of lattice Boltzmann method (LBM)

The previous researches on falling film are reviewed in Chapter 2. Generally, there are some improvement can be made in some aspects:

Many researchers take the falling film as a single-phase problem, which means the surface tension and phase change are neglected.

The numerical researches on falling film are most based the traditional CFD tools, which rely on the continuity hypothesis. However, considering the thin liquid layer (less than 1 micrometer in our experiment) and cutoff phenomenon, the traditional

numerical methods may have great difficulties in falling film research.

Lattice Boltzmann method (LBM) is a promising solution to the falling film problem. Over the past few decades, tremendous progress has been made in the development of particle-based discrete simulation methods versus the conventional continuum-based methods. In particular, the lattice Boltzmann (LB) method has evolved from a theoretical novelty to a ubiquitous, versatile and powerful computational methodology for both fundamental research and engineering applications. It is a kinetic-based mesoscopic approach that bridges the microscales and macroscales, which offers distinctive advantages n simulation fidelity and computational efficiency. Applications of the LB method are now found in a wide range of disciplines including physics, chemistry, materials, biomedicine and various branches of engineering. Chapter 2 provides a comprehensive review of the LB method for thermo-fluids and energy applications, focusing on multiphase flows, thermal flows and thermal multiphase flows with phase change.

1.4 Research objectives of the thesis

The falling film liquid desiccant dehumidifier is a promising alternative to traditional air dehumidification technologies for lower energy consumption, environment-friendly and more flexible humidity control. Besides, the liquid desiccant dehumidifier

possesses some other advantages, such as lower possibility of droplet carryover and lower pressure drop. The study on the falling film phenomenon can be traced back to early last century. Since then many theoretical models have been proposed to study the effect of various design operating parameters and conditions on the performance of the falling film. With the development of computational fluid dynamics (CFD), numerical methods become popular in falling film research in recent decades. However, traditional methods are mostly based on the continuity hypothesis, which may not be appropriate in some falling film cases. In addition, most traditional methods including the theoretical and numerical models study the performance of the stable falling film flow, while the dynamic characters are less focused. Furthermore, the high computational cost of traditional CFD tools in handling falling film cases is a challenge in real applications.

Over the past few decades, the lattice Boltzmann method (LBM) is becoming popular in the fields of computational fluid dynamics. It is a kinetic-based mesoscopic approach that bridges the microscales and macroscales, which offers distinctive advantages on simulation fidelity and computational efficiency especially for multiphase flows. Compared with traditional CFD tools, the LB model on falling film has a solid physical background (continuity hypothesis not needed) and shows better computational efficiency. To solve the heat and mass transfer problem in falling film

process, thermal LB models are proposed by many researches. However, in these previous models, there are still some fundamental problems that have not been solved. First, most of the existing works are focused on the (LB) models for Cahn-Hilliard equation, but these models suffer from the poor stability, difficulty in simulating the large density ratio problems, and the mass non-conservation. Second, most of the existing LB models are only suitable for steady state flow instead of dynamic problems. Thirdly, most existing LB models still have problems in dealing with the phase change problem.

This thesis aims to propose a lattice Boltzmann model to study the falling film based liquid desiccant dehumidifier. The main objectives of the project are summarized as follows:

(1) To develop a lattice Boltzmann model to trace the density distribution of two-phase flow with high density ratio. In falling film the density ratio of liquid/gas can be up to 1000. The developed model is the basic of falling film simulation.

(2) To propose a wetting boundary scheme which can handle the three-phase contact problem. Wetting boundary is the typical characteristic in falling film. In present work the contact angle is taken to feature the wetting ability.

(3) To develop a mass conservative lattice Boltzmann model (LBM) to simulate the two-phase flows with moving contact lines at high density ratio. The developed model is characterized by mass conservation, proper treatment of wetting boundary and high density ratio, which are the typical characteristics in falling film simulation. Based on this model the isothermal falling film can be complete simulated.

(4) To develop a thermal lattice Boltzmann model for simulating the heat and mass transfer process in falling film dehumidifier. The model is based on the model in previous step. Instead of the traditional continuity hypothesis based numerical methods, the proposed model treats the heat and mass transfer in multi-phase flow from the point of kinetic theory, which has a solid physical background. .

(4) To find the parameters which influence the performance of falling film, and give suggestions on the improvement of falling film based liquid desiccant air conditioning.

1.5 Organization of the thesis

The overall structure of this thesis takes the form of seven chapters. Chapter 1 gives a brief introduction of consumption of building energy, falling film based liquid desiccant air-conditioning system and lattice Boltzmann method. As a possible alternative of the traditional vapor compression air conditioner, the advantages of the liquid desiccant air conditioning system are summarized. The falling film liquid

desiccant air dehumidification technology, handling the latent and sensible load separately, is a promising alternative to traditional air dehumidification technologies. Meanwhile, lattice Boltzmann method is a promising method to numerically study the falling film problem, especially the heat and mass process inside. Falling film dehumidifier is the research focus of the thesis, and lattice Boltzmann methods is the research method. The general objective is to develop a lattice Boltzmann model to simulate the complete falling film process, especially the heat and mass transfer process. The research objectives of this project are also summarized in Chapter 1.

Chapter 2 provides a comprehensive literature review of falling film and lattice Boltzmann method. Firstly, the researches on laminar flow and wavy film flow are discussed respectively, and the relationship between film Reynolds number and flow type is summarized. Then, the researches on heat and mass transfer process in falling film are detailed reviewed. The theoretical, numerical and experimental model are introduced respectively. Thirdly, the limitations of the previous researches on falling film are summarized, and the reason of taking lattice Boltzmann method as the research methodology is explained. Fourthly, the development of the lattice Boltzmann method is reviewed and the characteristics are highlighted. The basic ideas and equations of lattice Boltzmann method are introduced. Finally, the limitations of previous lattice Boltzmann models on multi-phase flows are summarized.

Chapter 3 developed a new two-dimensional LBM simulation model to capture the density distribution of two phase flows with high density ratio. In this chapter the interaction force scheme was first discussed in this chapter. Two kinds of difference formats, the isotropic difference format and mixed difference format, were introduced and adopted in the developed model. The developed model has taken the problems such as the high density ratio, surface tension, gravity, inlet and outlet open boundary conditions into consideration. Three test cases were studied to validate the two-phase model. The first case was to simulate the droplets on flat plates with different contact angles to test the approach to handling the liquid-solid interface. The second case was to simulate the typical two phase co-current flow in a channel, which has been analytically solved [Huang et al. 2013]. This case is to examine the external forces (such as gravity) added in the model. The third case aimed to test the performance of the fully developed outlet boundary by simulating a droplet flowing in an infinitely long channel. The numerical results show that the developed model can trace the density distribution properly even at the density ratio 1000. And the developed model in this chapter lays the foundation for the study of falling film based liquid desiccant dehumidifier.

Chapter 4 proposed the wetting boundary treatment method. In falling film research, the wetting area of liquid desiccant is an important parameter in the dehumidifier. In

early stage of the simulation model for liquid desiccant dehumidifier, the working plate was usually assumed to be fully wetted by liquid desiccant, which did not comply with the experimental observation. In actual situations, the working surfaces were usually observed to be incompletely wetted by the liquid desiccant. Therefore, it is very important to properly simulate the wetting boundary in falling film. In this chapter, the cubic form of surface free energy density is taken. The proposed wetting boundary treatment method is used in the lattice Boltzmann model developed in Chapter 3, and numerical test is performed by this model. The result shows that the proposed wetting boundary treatment method can properly handles the contact angle issue.

Chapter 5 proposed a mass conservative lattice Boltzmann model (LBM) to simulate the two-phase flows with moving contact lines at high density ratio. The proposed model consists of a phase field lattice Boltzmann equation (LBE) for solving the conservative Allen-Cahn (A-C) equation, and a pressure evolution LBE for solving the incompressible Navier-Stokes equations. In addition, a modified wall boundary treatment scheme is developed to ensure the mass conservation. The wetting dynamics are treated by incorporating the cubic wall energy in the expression of the total free energy. The current model is characterized by mass conservation, proper treatment of wetting boundary and high density ratio. We applied the model on a series of numerical tests including equilibrium droplets on wetting surfaces, co-current flow and a droplet

moving by gravity along inclined wetting surfaces. Theoretical analysis and experiments were conducted for model validation. The numerical results show good performances on mass conservation even with a density contrast up to 1000. Furthermore, the results show that the moving contact line can be successfully recovered, which proves that this model is applicable on the study of moving contact line issue and further related applications.

Chapter 6 proposed a thermal lattice Boltzmann model based on the model developed in chapter 5. This thermal lattice Boltzmann model is proposed to simulate the heat and mass transfer process in fall film. Instead of the traditional continuity hypothesis based numerical methods, the proposed model treats the heat and mass transfer in multi-phase flow from the point of kinetic theory, which has a solid physical background. The proposed model consists of a phase-field lattice Boltzmann equation (LBE) for solving the conservative Allen-Cahn (A-C) equation, a pressure evolution LBE for solving the incompressible Navier-Stokes equations, a temperature evolution LBE for solving the internal energy equation and a concentration evolution LBE for solving the mass diffusivity equation. The proposed model was adopted to simulate the heat and mass transfer process in the falling LiCl solution film at different Reynolds number and the results were compared with the numerical and experimental tests. The comparison results show that the proposed can well predict the temperature

and concentration distribution of the falling film absorption process and has a better computational efficiency than traditional simulation methods.

Chapter 7 summarizes the contributions of this work and concludes the thesis.

CHAPTER 2

LITERATURE REVIEW AND METHODOLOGY

2.1 Introduction

Complicated heat and mass transfer occur in a falling film dehumidifier. The process can be described in detail: water vapor spreads from the air to the air side surface of the gas-liquid two phase interface, then water vapor condensates on the interface and enters into the liquid phase, and finally the condensed water diffuses from the liquid side of the interface to the desiccant solution. The driving force for heat transfer is the temperature difference between the air and desiccant solution, and for mass transfer is the water vapor pressure difference between the air and the surface of the desiccant solution.

In this chapter, the origins and research methods of this thesis are presented in detail. Section 2.2 reviews the researches on laminar flow and wavy film flow respectively, and the relationship between film Reynolds number and flow type is summarized. Also the researches on heat and mass transfer process in falling film are detailed reviewed. The theoretical, numerical and experimental model are introduced respectively. Section 2.3 summarizes the limitations of the previous researches on falling film, and explains the reason of taking lattice Boltzmann method as the research methodology.

the development of the lattice Boltzmann method is reviewed and the characteristics are highlighted in Section 2.4. Through literature review it can be concluded that the lattice Boltzmann method is appropriate for falling film simulation.

2.2 Literature review of falling film technology

As a special type of multi-phase flow, falling film is widely used in industries like thermal engineering, energy engineering and air conditioning engineering, especially the liquid desiccant air conditioning due to its simple structure, low temperature difference and considerable heat and mass transfer efficiency. Fig. 2.1 is the two-dimensional schematic side view of the falling film. The falling film is usually characterized by a thin liquid layer on an inclined or vertical plate and some gas in the remaining space. Complicated heat and mass transfer process including phase change can occur between the liquid layer and the gas, which makes falling film appropriate for heat and mass exchange. When the desiccant solution (such as the $LiCl_2$ solution) is chosen as the working liquid and the moist air takes the role of gas, the falling desiccant solution film becomes a dehumidifier. It is reported that the liquid desiccant air conditioning system based on this kind of dehumidifier can save about 10-30% of energy compared with the low temperature dehumidification using conventional gas compression system [Yin et al. 2014].

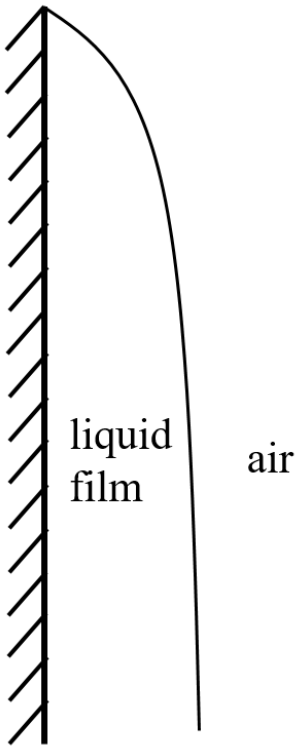

Figure 2.1 Schematic of the two-dimensional falling film

Given the advantages, liquid film flows are widely in use in energy and process engineering. One can find them in the condenser of power stations, in chemical industries for rectification and distillation, in food industries for densification of milk and juice, in cooling devices utilizing heat pipes (also known as thermo-siphons), and geothermal heat exchangers based on phase–change processes. The typical geometry of heat exchanger utilization liquid film flow is a tube, a flat-plate, or a packed bed.

2.2.1 Laminar film slow assumptions

The study on falling film can date back to early 1900s. Nusselt (Nusselt 1916) theoretically studied the falling film phenomenon, he assumed that the film is smooth laminar and gave an analytical solution of film thickness

$$Re_{L=}4\frac{\rho.u_{av}.\delta}{\mu}=4\frac{\Gamma}{\mu} \qquad (1.)$$

Where ρ is liquid density, u_{av} is the average film velocity, δ is the mean film thickness, μ is liquid viscosity and is mass flow rate per unit flow width.

Kholpanov et al. [Kholpanov et al. 1982] present an analysis similar to that developed by Nakoryakov and Grigor' equations but allow for the effect of tangential shear stress or a surface tension gradient at the solution-vapor interface. The solution is only valid for regions near the beginning of the absorption process where the thermal and concentration boundary layers developing from the interface do not reach the wall since the transfer of heat and mass from the interface into the film is assumed to be confined to a thin boundary layer. They also assume that the velocity profile within this thin boundary is uniform, even in the presence of shear and surface tension gradients. The authors develop expressions for concentration and temperature within the film that they state reduce to the inlet region approximations developed by Nakoryakov and Grigor' equations for the case of no interface shear or surface tension gradients. Additionally, local and mean heat and mass fluxes are also developed from

these expressions.

Le Goff et al. [Le Goff et al. 1986] give a brief summary of several methods for modeling absorption heat and mass transfer. In other works not translated into English they developed analytical, numerical, and approximate models of laminar falling film absorption over an adiabatic wall, however these are not reviewed here. Le Goff et al. discuss some of the features, limitations, and usefulness of the different solution methods including analytical and approximate methods, numerical methods with Laplace transforms and finite difference approximations. They also briefly discuss methods for wavy and turbulent films. The authors also refer to other publications (in French) in which they have utilized each of the solution methods, compared them with each other and with experimental data. One interesting concept presented by the authors is the idea of "tie lines" and "trajectories". A "trajectory" is a line on a temperature-concentration plot representing the progression of temperature and concentration of a particular location within the film, such as the interface, bulk or wall, as the film proceeds along the wall. "Tie lines" connect the trajectories at any given cross-section of the film. This is a unique plotting method not found elsewhere in the literature.

Conlisk [Conlisk, 1992, Conlisk 1995] presents the development of a solution to the

vertical，laminar film absorption problem employing the Laplace transform technique. His assumptions are essentially the same as Grossman except that the film thickness is not required to be constant， the transverse velocity component，v，is not neglected in the species conservation equation although it is neglected in the energy equation， the wall temperature can either be constant or an empirically derived function of downstream position， and infinite dilution of water in the film is not assumed. It is assumed that mass transfer is confined to a boundary layer (i.e. doesn't reach the wall) but this assumption is justified for moderate lengths; for a typical operating condition， Conlisk suggests that this length is about 3m， increasing or decreasing with Reynolds number. Conlisk notes that the use of the Laplace transform eliminates the difficulty often encountered in finding solutions at the inlet discontinuity. Considering an expansion series formulation for the film thickness along the absorber， he mathematically demonstrates that "to a leading order"，the film thickness is constant because the mass transfer rate is limited by the physical parameters of the problem. However， his solution for the concentration profile depends on the leading order term for variation in film thickness (absorption rate) which is determined approximately from the inlet and equilibrium conditions for the isothermal case. For the non-isothermal case， a more complex relationship is needed for determining this leading order term of the film thickness variation. Determining the temperature profile requires numerically evaluating a Laplace inversion integral. Conlisk shows that in the

region near the inlet where heat transfer is confined to a boundary layer near the interface, a solution for the concentration distribution can be determined which does not require numerical evaluation.

Conlisk presents the results of the model in several ways. For both an isothermal and non-isothermal wall, plots of temperature profiles are given at various downstream locations for two solution flow rates. Also the leading order term for absorption rate (film thickness variation) is plotted for the case of constant and variable wall temperature and curve fits are given which can be used to simplify subsequent analyses. Comparisons with experimental data are also presented for two operating conditions. The total absorption rate predicted is within 20% of the experimental values, overpredicting the experimental data in both cases. The author concludes that the potential of waves to affect the results is small.

Noting that the temperature profiles predicted by the above model become substantially conduction dominated at a small downstream length, Conlisk presents fully analytical solutions for the problem by assuming that the temperature profile within the film must be linear. The total absorption rate at the two operating conditions used for comparison with experimental data in Conlisk is within 1% of the original model. It is shown that at positions very near the film inlet, the prediction of local

absorption rate differs greatly between the two models. But because this region is small compared to the length of the tube (1.5 m in this case) the effect on overall model performance is small. Based on the analytical expressions developed, Conlisk shows that as the initial thickness of the film is reduced, the heat transfer coefficient increases but the mass transfer coefficient decreases, although no further physical interpretation of why this happens is given. Also, Conlisk notes that the total absorbed mass flux is almost completely independent of the difference between the film inlet and wall temperatures. Presumably this is because the sensible heat load associated with inlet temperature differences is small compared to the heat load of absorption for long absorbers. This conclusion is in sharp contrast to the findings of Andberg and Vliet for the horizontal tube case where the film flow length is small.

Condisk extends his earlier model to include heat transfer to the coolant by assuming specific heat mass flow rate and average heat transfer coefficient of the coolant, as well as wall thickness and conductivity. Obtaining the solution requires numerical evaluation of two integrals, and two methods for predicting absorbed mass are given. It is demonstrated that the model results are not overly sensitive to the choice of correlation for heat transfer coefficient. Additionally, comparison with four sets of experimental data reveals that total mass absorption rate is generally predicted within 10%. Conlisk also notes that only a 10% increase in absorbed mass is achieved from

a four-fold increase in coolant flow rate, and suggests that "attempting to increase the mass absorbed by modifying the coolant-side flow has limited return." This is presumably due to the relatively significant thermal resistance of the falling film, compared to the coolant-side resistance.

2.2.2 Wavy film flow

As was stated earlier， it is well known that falling films are inherently unstable， even at low Reynolds numbers. This instability leads to the growth of waves visible on the film surface even in the absence of any disturbances due to the motion of the vapor. A recent review of the literature on the hydrodynamics of wavy falling films is presented by Miller. Commenting on several key investigations， Miller states "their results imply that all vertical falling films are naturally wavy".

The waves that may develop on a falling film are not all alike. Many investigators have suggested categorization methods based on the non-dimensional Reynolds and Kapitza numbers. A simple classification is proposed by Brauner who suggests the existence of two primary types of waves:

(1) capillary waves which are characterized by their low amplitude，sinusoidal shape， regular frequency， and tendency of the wave-front to be aligned perpendicular to the

flow direction

(2) Inertial wave, often called roll waves, which can obtain high amplitudes (several times the underlying film thickness) have a steep wave-front and long wave- back，may travel as solitary waves with long spans of smooth film in between successive waves, or may interact with each other to form complex threedimensional wave patterns with wave-fronts that are not necessarily aligned across the flow direction.

Inertial waves may also contain regions of recirculation that play a role in the transport processes between the film interface and bulk. It is also important to note that wave shape generally travels several times faster than the fluid in the film (this speed ratio is called wave celerity) and consequently wavy films have a higher mass flow rate than a smooth film with an equivalent mean film thickness. The majority of the mass flow may be carried within the wave shape itself leaving only a fraction of the flow in the thin film substrate between and underneath the waves.

To model the absorption process in the presence of wavy falling films, investigators must make assumptions regarding the film hydrodynamics which involve a number of simplifications. In each case presented in this section, the hydrodynamics are assumed a priori, neglecting the potential influences of the heat and mass transfer processes on the hydrodynamics. However, several investigators, for example Cosenza and Vliet

[Cosenza & Vliet 1991] and Miller and Keyhani [Miller and Keyhani 1999], have noted significant differences in the observed hydrodynamics and surface wetting when absorption is occurring; this is generally attributed to surface tension gradients resulting from uneven absorption over the film surface. It is also typical to neglect the actual development of the waves from an initially smooth film in favor of using an asymptotic steady-state solution. Also, often only a small number of wavelengths are modeled representing a short length of the absorber. Models have been developed for absorption in the presence of both capillary and inertial wavy-laminar films, but in either case most investigators assume that the waves are periodic. Experimental investigations of wavy films reveal that the waves themselves, especially at Reynolds numbers greater than 100, are unstable and often develop into seemingly chaotic three-dimensional patterns perhaps requiring a statistical description. The general conclusion of all of these investigations is that the presence of waves significantly enhances the transport processes compared with a laminar film. The exact mechanism attributed to the enhancement and its quantitative value depend on the investigator.

One of the simplest methods for modeling the effect of waves is to assume that a passing wave completely mixes the film, resulting in uniform concentration and temperature profiles at regular intervals corresponding to the characteristic wavelength. This assumption allows results such as those of Nakoryakov and Grigor'

equations for the absorption near the inlet region of a fall-ing film absorber to be applied to the regions in between each wave. This technique is used in Burdukov et al. and Nakoryakov et al.

Burdukov et al. [Bergero & Chiari 2010] and Nakoryakov et al. [Nakoryakov et al. 1982] presented the data from experimental measurements of absorption rate on a vertical tube absorber. It is noted that beyond a position of 350 millimeters down the tube, the absorption rate and film temperature become nearly constant. This does not agree with the theoretical solutions of Nakoryakov and Grigor' eqution for laminar films which predict that the transfer rates should vary as the inverse of the square root of the downstream position. The authors also note the presence of "irregular three-dimensional waves" in this region beyond 350 millimeters. To account for the waves, the authors adopt the postulate of Kholpanov et al. [Kholpanov et al. 1982] that the effect of the waves is to completely mix the film. They use photography to determine the characteristic wavelength and then assume that the laminar theory for the inlet region holds within each wavelength. Comparison with experimental data shows that this wavy model at least qualitatively predicts the trends in the data.

Nakoryakov et al. [Nakoryakov et al. 1982] presented a new set of experimental results for vertical falling film absorption and a slightly modified model to account for film

waviness. The difference from the previous model is that instead of using photography to characterize the average wavelength, the authors use existing experimental correlations for wave velocity and for wave frequency to calculate the wavelength. This wavy film model predicts the observed trends in the experimental data better than a laminar film model, but as in the previous models, quantitative agreement is only fair.

Kholpanov [Kholpanov et al. 1982] first presented the results of solving a simplified version of the Navier-Stokes equations for the wave motion. The predicted wave amplitude is shown to agree reasonably well with some experimental data from the literature. A plot of non-dimensional flow rate against wave number shows local minima and maxima, the maxima corresponding to the "optimal" regime which will be established. By assuming a parabolic stream-wise velocity profile throughout the film, the author develops a boundary layer solution for mass transfer only, and another solution for combined heat and mass transfer. Neither the temperature boundary layer nor the concentration boundary layer developing from the interface is allowed to reach the wall; thus the solution is insensitive to wall conditions. For the pure mass transfer problem, the model results are compared with data from "long pipes" and show good agreement. No validation or discussion of limitations is given for the combined heat and mass transfer problem. However, since the transport processes are even more rapid

due to presence of waves, the entry region where absorption is insensitive to wall conditions will presumably be shorter than for the smooth film case. Kholpanov also considers wavy flow over a rough surface with gas shear using a linear stream-wise velocity profile and flow along the inside of a rotating cylinder. A very similar problem is also considered by Tsvelodub. He assumes a constant stream-wise velocity within the boundary layers and develops analytical relationships for heat and mass transfer coefficients in terms of non-dimensional parameters.

Kholpanov [Kholpanov 1985] analytically developed expressions for coupled heat and mass transfer coefficients for absorption on a wavy film with a purely sinusoidal surface. A constant stream-wise velocity is assumed within the film, and wall conditions are not specified. Wavy film transfer coefficients are expressed as a correction to the laminar film transfer coefficients. The expressions for these corrections are functions of wave amplitude and frequency (or phase velocity), which the author suggests may be determined from experimental data or from approximate expressions presented.

Uddholm and Setterwall [Uddholm and Setterwall 1988] modelled the absorption process on a vertical isothermal wall where the film exhibits inertial wavy-laminar flow (roll waves). Their assumption for the hydrodynamics within the wave is based

on early work by Brauner et al. who divide a typical roll wave into four sections: wave front, wave back, wave trail, and substrate. They use a finite difference scheme to solve the problem. Other assumptions include constant thermophysical properties, infinite dilution of water within the film, and no heat transfer to the vapor. The front of the wave is apparently modeled assuming a parabolic velocity profile although within the wave back, the laminar substrate is assumed to be developing; a solution for boundary layer thickness and velocity profile for a wall suddenly set in motion is used for the wave back. The wave trail is assumed to have a velocity profile derived from a fifth-order polynomial for the stream function proposed by Brauner et al. [Brauner et al. 1989]. Finally, in the substrate region between waves, a parabolic velocity profile is assumed.

Results of photography of falling films allowed Uddholm and Setterwall to develop a correlation for wave frequency based on downstream position [[Uddholm and Setterwall 1988]]. Their experimental results show that near the inlet, the wave frequency may be 20 Hz, but it reduces to about 10 Hz further along the tube as the roll waves develop. The authors consider four different models for the wave frequency: constant 20 Hz waves, constant 9 Hz waves, linearly varying 20-9 Hz waves, and no waves. The predictions of average overall heat transfer coefficients are compared with experimental data from a water lithium bromide heat transformer. When assuming

only low frequency (9 Hz) roll waves, the model over-predicts the experimental data. The other three assumptions under-predict the data by varying degrees. The predicted heat transfer coefficient is between 35 and 120% greater with waves than with a laminar film model.

Morioka and Kiyota [Morioka & Kiyota 1993] modelled the absorption in the presence of capillary waves. The key assumptions of Morioka and Kiyota are that the film surface is sinusoidal, the stream-wise velocity profile is parabolic, the wave speed and length are determined from a linear stability analysis by Pierson and Whitaker, but the wave amplitude is arbitrarily assumed to be 30% of the average film thickness to ensure what the authors felt are reasonable velocity profiles within the film. Other assumptions include constant thermophysical properties, isothermal wall linear interface equilibrium model and no heat transfer to the vapor phase. The authors note that for a concentration range of 54-60%, the error from the linear equilibrium assumption is +_0.12C.

A numerical solution is generated using a grid structure fit to the shape of the wavy film over three wave lengths and governing equations transformed in such a way as to eliminate cross-derivatives. Local absorption rates for film Reynolds numbers of 20, 50 and 100 are presented along with the predictions from a smooth film model.

Temperature and concentration profiles shown at the wave crests and troughs for a Reynolds number of 20 and 50 demonstrate the development of a “depression” in the concentration profile due to the motion of the waves and the enhanced absorption rates. The authors point out “the absorption mass flux shows a maximum at the troughs of the wave where the film thickness is minimum. At these points the mass flux is approximately 3 times larger than the smooth flow case.” The authors propose that the enhanced absorption rates are due to both the increase in the transverse velocity and the action of the waves effectively exposing and covering sections of an underlying film. They note that their predicted absorption rate is nearly independent of Reynolds number for the range considered. On average they report that the absorption rate in wavy films is 70 to 140% higher than for the smooth laminar film case. In a later experimental study which includes photographs of wavy falling films on vertical tubes. Morioka et al. measure absorption rates that are generally higher than their predicted values and sensitive to Reynolds number.

Yang and Jou [Yang & Jou 1998] also considered the problem of absorption on a film with capillary waves. The hydrodynamic solution is presented in an earlier work but is based on the following assumptions: the stream-wise velocity profile is parabolic, the wave velocity and wave number correspond to the “most unstable wave” determined by the linear stability analysis of Pierson and Whitaker, and the solution is

the asymptotic periodic steady-state wave pattern. The profile of the film interface is described by a Fourier expansion series，the coefficients of which are determined numerically. The resulting profiles vary with Reynolds number (up to 500), and it is noted that the solution for the wave profile always corresponds to the maximum wave amplitude and minimum average film thickness at any given flow rate. The resulting profiles are not purely sinusoidal as in Morioka and Kiyota but exhibit shortened wave fronts and elongated wave backs suggesting characteristics of roll waves; however, the amplitude is much lower than what is normally labeled a roll wave perhaps due to the linear model used in the stability analysis. A comparison of predicted wave lengths and amplitudes with several sets of experimental measurements from the literature shows fair agreement. The authors develop a numerical solution for absorption using several other assumptions including: constant thermophysical properties no heat transfer to the vapor infinite dilution in Fick's law and an isothermal wall. To speed up the calculation procedure the results of a smooth film model are used as initial conditions for the wavy film model. For a baseline operating condition bulk concentration plotted against time at three downstream positions shows that the solution becomes periodic after about the second wave period. Total absorption rate plotted against downstream position reveals that the absorption rates predicted with the wavy model are about double the results with a smooth film. It is also shown that absorption rate increases with Reynolds number the effect diminishing somewhat for

higher Reynolds numbers. This trend does not agree with the conclusions of Morioka and Kiyota; the discrepancy may be due to the fact that the hydrodynamic solution of Yang and Wood varies with Reynolds number and is not purely sinusoidal.

Jernqvist and Kockum [Jernqvist & Kockum 1996] suggested that their model for smooth laminar film absorption may be extended to wavy (or turbulent) flow regimes by assuming complete mixing within the film at regular intervals (similar to Burdukov et al. and Nakoryakov et al. They introduce a mixing density parameter and suggest that it could be related to Reynolds number to account for changing film hydrodynamics although no quantitative relationships are presented. As was mentioned before the laminar film predictions of absorption rate decrease with increasing film flow rate under-predicting the experimental data which show the opposite trend. The authors show that by increasing the mixing density parameter at higher Reynolds numbers the model can be made to predict absorption rates closer to the experimental results. Interestingly though the error in heat transfer rate at the wall which is over-predicted for even the purely laminar case is increased when the mixing density is increased. The fact that wall heat transfer rates are overpredicted even when absorption rates are underpredicted may suggest that the assumption of no heat transfer to the vapor is leading to appreciable errors.

With the development of CFD technology, numerical method is becoming popular in the falling film research, especially the wavy film.

Sabir et al. [Sabir et al. 1999] generated numerical solutions for the problem of absorption on films with capillary waves. They assume the hydrodynamics proposed by Penev et al. [Penev et al. 1972] including a streamwise velocity profile which the authors point out does not allow for any circulation of liquid within a wave (described as surface renewal). This profile is based on a parabolic function with coefficients that are calculated from a truncated expansion series of sinusoidal functions. The film thickness profile is a similar truncated expansion series of sinusoidal functions. Other assumptions used include: constant thermophysical properties isothermal wall at solution inlet temperature linearized interface equilibrium model and no heat transfer to the vapor. Plots of bulk concentration and temperature against downstream position reveal that initially the wavy film shows great enhancement over the smooth film assumption. However further downstream the results of the two models converge as the limit of absorption is approached. The authors also note that the enhancement of mass transfer appears to be greater than that of heat transfer. They attribute this to the fact that the mass transfer is governed by conditions at the interface where wave effects are strongest while heat transfer occurs across the entire film and the enhancement near the wall due to the waves is less. The authors conclude that the enhancement

effect is due to the additional transverse velocity components occurring in the wavy flow not mixing within the waves although they eliminate the latter possibility purely by assumption.

Kapitz et al [Kapitz, 1964] found that the assumption by Nusselt is not appropriate. They found the interfacial waves and solitary wave (Fig 2.2) by experiments for the first time.

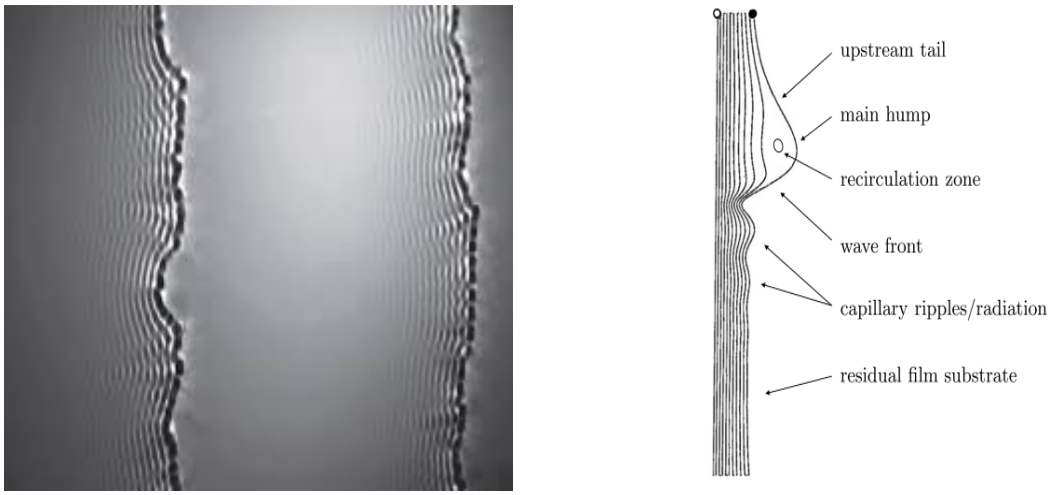

Figure 2.2 Solitary wave found by Kapitz et al [Kapitz, 1964]

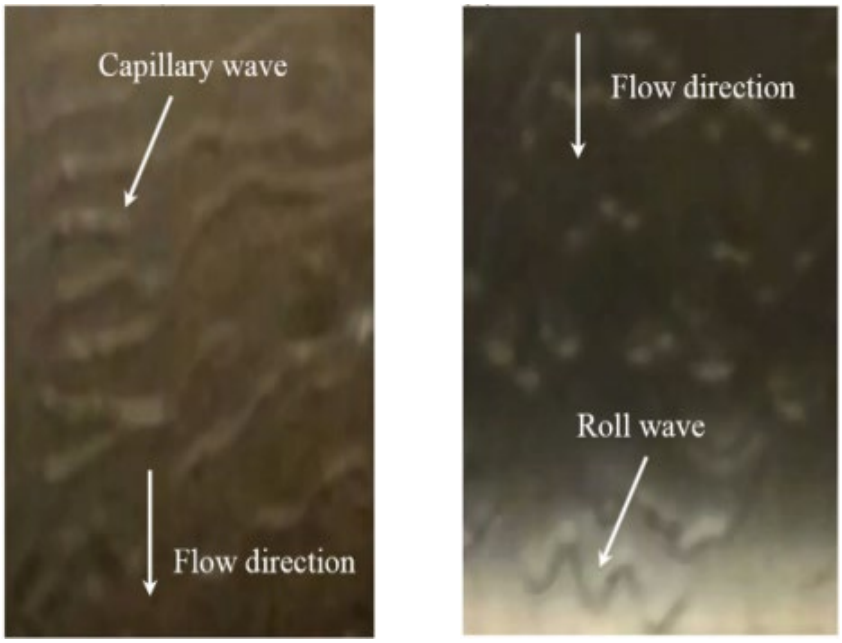

Figure 2.3 Capillary wave and roll wave found by Brauner and Maron [Brauner & Maron 1983]

Brauner and Maron [Brauner & Maron 1983] built a physical model for the hydrodynamic mechanisms of thin liquid film and compared it with experimental results. They pointed out that the well-develop smooth film and wavy flow can be regarded as two equilibrium states and the interfacial waves can be classified as capillary wave and roll wave (Fig 2.3).

After a period of experiments, Killion JD and Garimella [Killion JD & Garimella 2001] found that the falling film flow pattern is highly associated with Reynolds number of solution Re_L.

For Re_L < 20, the falling film flow is laminar and the interface is smooth;

For 20 < Re_L < 4000, the flow become partially turbulent and the interfacial waves appear;

For Re_L > 4000, the film flow is fully turbulent and the interface returns to smooth;

Thus, the falling film flow becomes partially turbulent and unsteady even when the solution Reynolds number Re_L > 20.

Miyara [Miyara 2000] numerically simulated the wavy liquid film with the finite difference method and compared the results with experimental observations (Fig 2.4 Nosoko et al. [Nosoko et al. 1996]). Film thickness can be simulated well by the numerical method and the formation of solitary wave was discussed.

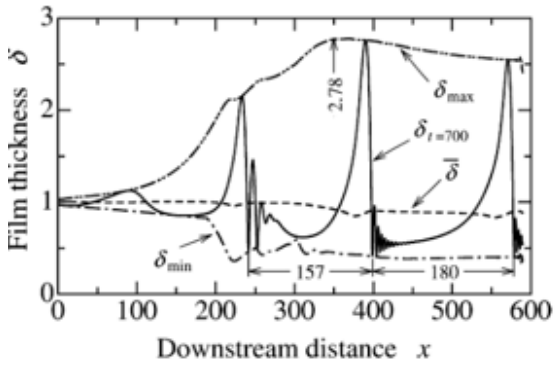

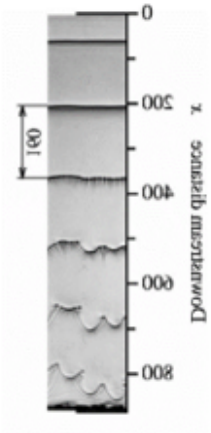

Figure 2.4 Instantaneous and time averaged film thickness behavior by simulation and experiments

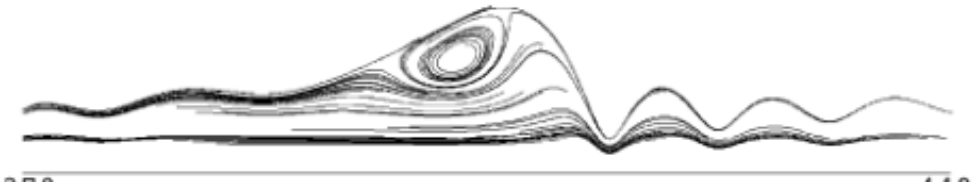

Figure 2.5 The simulated solitary wave

Lu H and Lu L (2016) numerically simulated the formation of falling film flow. The studied the dynamic characteristics of unsteady interface and with the CFD models and compared with the experimental results (Fig 2.6).

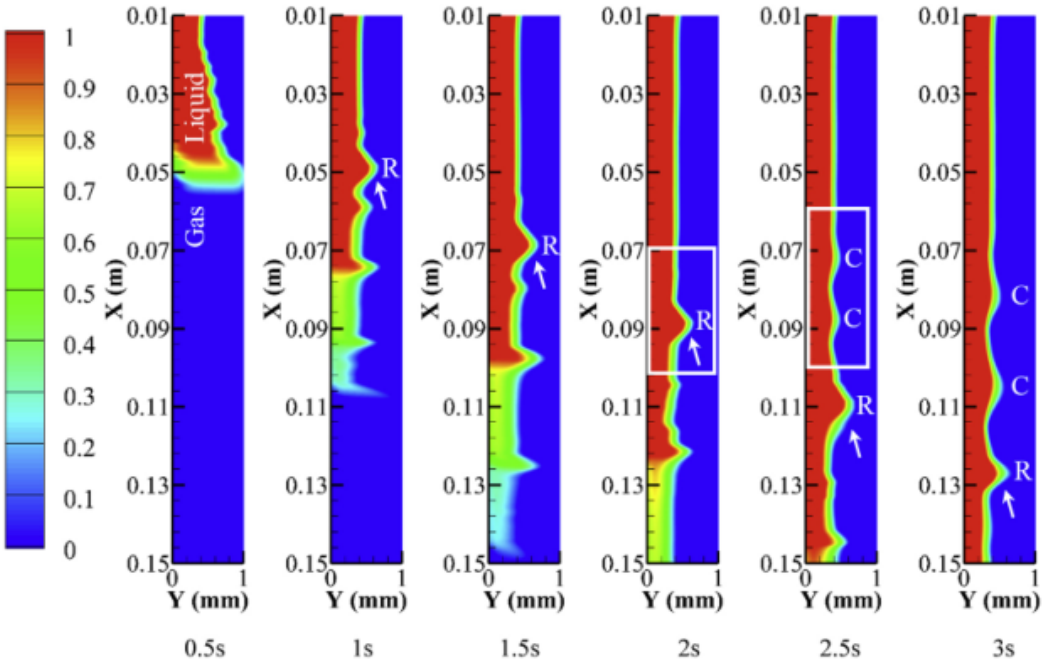

Figure 2.6 Falling film formation process

2.2.3 Heat and mass transfer in falling film

The system heat transfer coefficient is mainly decided by the heat conduction through the wall and heat convection.

Brauner et al. [Brauner et al 1989] present solutions valid near the inlet region using the similarity technique as in Nakor- yakov and Grigor' equations. The key difference is that the application of Fick's law of diffusion at the interface is formulated without assuming infinite dilution in the liquid film. Regarding the term which was neglected in Fick's law, Brauner et al. state, "the convective term …can be omitted for either $XA^{\wedge 0}$ or NAy = —NBy, neither of which holds for the case of hygroscopic condensation. For instance, the minimum molar fraction of water which corresponds to a saturated salt solution of $MgCl_2$, $CaCl_2$, LiBr, NaOH, is about XA = 0.8." All other assumptions are identical to Nakoryakov and Grigor' equations.

The solutions presented are valid near the inlet of the film; the effect of heat transfer to the wall is not included and the velocity in the boundary layers developing from the liquid-vapor interface is assumed to be uniform. For determining the range of validity of the solution, Brau- ner et al. suggest that the uniform velocity assumption deviates only 10% from a parabolic profile for the third of the film closest to the interface. Thus, to quantify the length over which their assumptions hold, they present a relationship

for calculating the distance along the film at which the developing concentration boundary layer reaches any arbitrary penetration depth. However, the development of the thermal boundary layer, which is much faster in water-lithium bromide films, is not discussed.

The equations presented for the temperature and concentrations within the film require an iterative solution. Once the solutions are obtained, relationships are presented for calculating heat and mass transfer coefficients. A comparison with the expressions developed by Nakoryakov and Grigor' equations shows significant deviations in temperature and concentration when the finite concentration of the film is considered. Brauner et al. show that including this effect leads to predictions of enhanced transfer rates and penetration depth of the concentration boundary layer. An expression for the enhancement factor is also presented.

Brauner develops new solutions to the vertical laminar film absorption problem for any downstream location for both adiabatic and isothermal wall cases. Her assumptions are the same as those of Grossman [Grossman, 1988] with two significant extensions. First, as in her previous work, the application of Fick's law of diffusion at the interface is formulated without assuming infinite dilution of the water in the film. Second, the film thickness is allowed to vary with absorbed mass; the resulting

transverse velocity component, v is not neglected. This leads to the following forms of the governing equations:

$$u\frac{\partial T}{\partial x} + v\frac{\partial T}{\partial y} = a\frac{\partial^2 T}{\partial y^2} \qquad (2.)$$

$$u\frac{\partial C_A}{\partial x} + v\frac{\partial C_A}{\partial y} = D_{AB}\frac{\partial^2 C_A}{\partial y^2} \qquad (3.)$$

She divides the solution domain into three regions: (a is thermal diffusivity)

(1) the region where both thermal and concentration boundary layers are developing from the liquid-vapor interface,

(2) the region where the thermal boundary layer has reached the wall but the concentration profile is still developing, and

(3) the region where both boundary layers are fully developed.

Within each region, she assumes parabolic profiles of temperature and concentration which satisfy the required boundary conditions. The temperature profile may reduce to a linear profile in the isothermal wall case. These assumed profile shapes are then substituted into the contimuity, energy, and species conservation equations. The equations are translated into integral form and require numerical integration. By

varying the parameter corresponding to solution concentration, she demonstrates that the solutions for the film temperature, concentration, heat and mass fluxes all change significantly when the concentration of the film is taken into account. Additionally by examining the non-dimensional coefficients of heat and mass transfer, she shows that the heat transfer coefficient is unaffected by the solution concentration and that the modification to the predicted heat transfer is due to the coupling of the heat and mass transfer problems.

Jayaniti and Hewitt [Jayaniti & Hewitt 1997] experimentally studied the sine wave (a special capillary wave) and solitary wave, they proposed that the heat transfer is mainly decided by the heat conduction through the wall even with the existence of waves. The reason why waves can strengthen the heat transfer is that the film thickness is reduced when there are waves.

When there is air flow, shear force on the film will make some changes.

Guo et al [Guo et al. 2009] analytically solve the energy equation of the laminar falling film with co-current/counter air flow. They found that the co-current air can strengthen the heat transfer and the Nusselt number increases with the air velocity, since the concurrent shear force can reduce the film thickness, while the counter air is exactly opposite.

The Marangoni effect is the appearance of flow or the modification of an existing flow due to surface tension nonuniformity caused by temperature or pressure gradients.

Zhang et al (2006) studied the Marangoni effect and found the formula of temperature distribution, film thickness and other factors. They concluded the ways Marangoni effect strengthen the heat and mass transfer:

(1) Heat capillary effect drives the centric liquid to the sides so the film thickness is reduced

(2) The effect causes the deformation of the film surface and reduces the average film thickness

(3) The convection caused by the effect increases the heat and mass transfer

Luo and Yang (2014) built a numerical model for simultaneous heat and mass transfer with the volume of fluid(VOF) method. In their model, the penetration mass transfer theory has been employed to make it possible to observe the dynamic heat and mass transfer process of falling film (Fig 2.7 and 2.8).

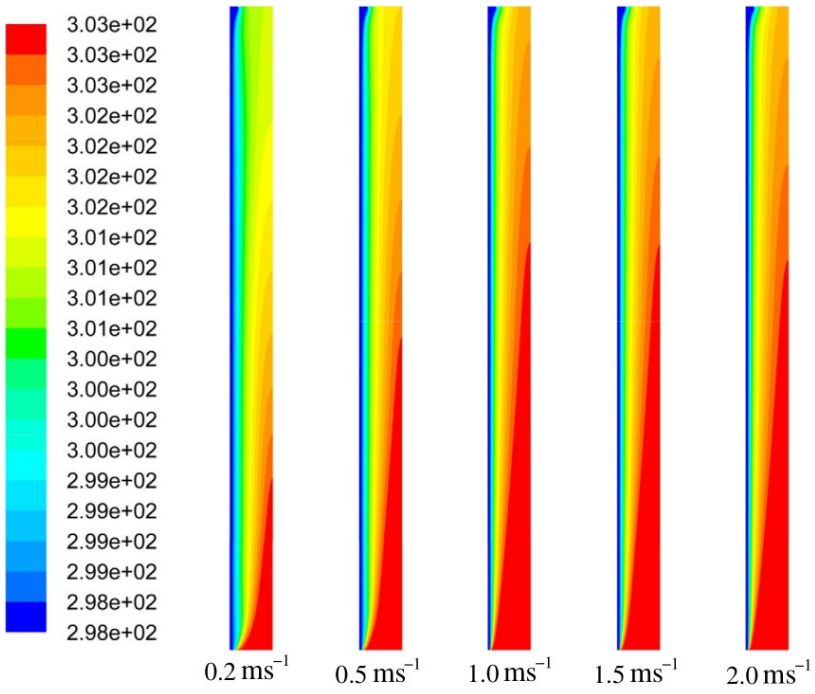

Figure 2.7 Temperature distribution under different inlet air velocities

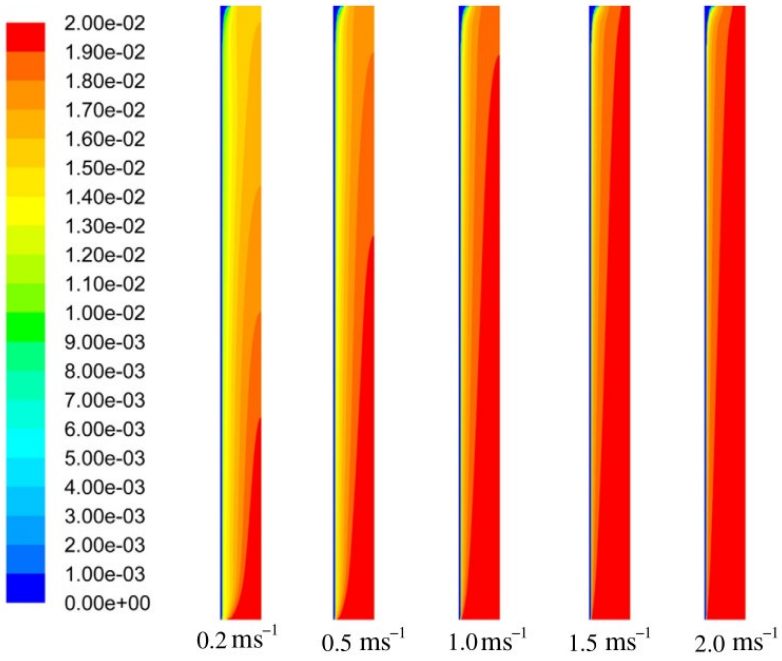

Figure 2.8 Mass fraction of water vapor under different inlet air velocities

2.3 Research methodology: lattice Boltzmann method

Over the past few decades, tremendous progress has been made in the development of particle-based discrete simulation methods versus the conventional continuum-based methods. In particular, the lattice Boltzmann (LB) method has evolved from a theoretical novelty to a ubiquitous, versatile and powerful computational methodology for both fundamental research and engineering applications. It is a kinetic-based mesoscopic approach that bridges the microscales and macroscales, which offers distinctive advantages n simulation fidelity and computational efficiency. Applications of the LB method are now found in a wide range of disciplines including physics, chemistry, materials, biomedicine and various branches of engineering. The present work provides a comprehensive review of the LB method for thermofluids and energy applications, focusing on multiphase flows, thermal flows and thermal multiphase flows with phase change.

2.3.1 Numerical methods for fluid flows

Energy and combustion systems typically involve fluid dynamics, chemical reactions, heat transfer, multiphase flows and phase change that occur over scales ranging from macroscale via mesoscale to microscale. Extensive examples are found in batteries, fuel cells, gas turbines, fluidized beds, coal-fired power plants, solar thermal power plants and nuclear power plants. The performance, reliability and safety of these

technologies depend crucially on how to organize the fundamental thermal-fluids processes, which in turn requires accurate and reliable predictive and diagnostic methods. Since the 1970s, general-purpose computational fluid dynamics (CFD) based on solving the Reynolds-averaged Navier–Stokes (RANS) equations, pioneered by D. B. Spalding and others, has been developed to compute fluid flow, heat transfer and combustion with considerable success. With the emergence of supercomputers in the 1990s, more accurate but computationally demanding methods such as large eddy simulation (LES) and direct numerical simulation (DNS) have been in increasing use. These macroscopic methods, however, are all based on the assumption of continuum, which makes it difficult or even impossible to treat certain physical phenomena, especially at micro- and meso-scales.

More fundamental approaches are particle-based (i.e. molecu- larcluster-based) discrete methods, such as molecular dynamics(MD), direct simulation Monte Carlo (DSMC), and dissipative particle dy- namics(DPD). These methods are capable of simulating phenomena where the continuum assumption breaks down. On the other hand, the high computational cost renders these methods impractical for the majority of problems of practical concern in energy and combustion. The lattice Boltzmann (LB) method, sitting in the middle of the hierarchy of modeling and simulation methods (see Fig 2.9), is a mesoscopic approach based on the kinetic theory expressed

by the original Boltzmann equation. The LB equation can be either viewed as a special discrete solver for the Boltzmann equation or a minimal form of the Boltzmann equation in which the microscopic kinetic principles are preserved to recover the hydrodynamic behavior at the macroscopic scale. Therefore, the LB method is based on a particle picture, but principally aims to predict macroscopic properties. This scale-bridging nature of the LB method is a fundamental advantage, which allows it to incorporate the essential microscopic or mesoscopic physics while recovering the macroscopic laws and properties at affordable computational cost.

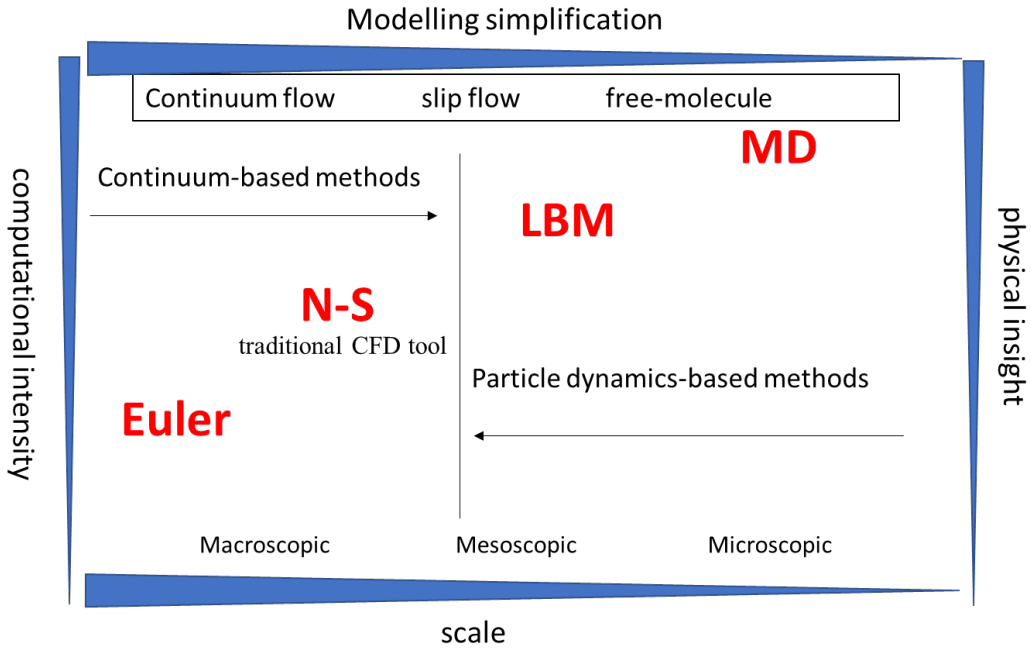

Figure 2.9 A hierarchy of modelling and simulation approaches

2.3.2 Development of lattice Boltzmann method

In the last 25 years, the LB method has been developed into an efficient and powerful simulation method for a wide range of phenomena and processes, such as single-phase flows, multiphase flows, turbulence, heat transfer, and phase change, as well as a numerical tool for nonlinear partial differential equations. It exhibits many distinctive advantages over conventional numerical methods. First, in the LB equation the convective operator (the streaming process) is completely linear, whereas the convective terms of the Navier-–Stokes equations are nonlinear. Second, in conventional numerical methods it is usually necessary and costly to solve a Poisson equation for the pressure field of incompressible flows, while in the LB method the fluid pressure can be simply calculated with an equation of state (such an advantage can also be found in the artificial compressibility method, but only for steady-state flows). Third, complex boundary conditions in the LB method can be formulated with elementary mechanical rules such as bounce-back and reflection according to the interactions of the LB “molecules” with solid walls. Moreover, the LB method is ideal for parallel computing because of its explicit scheme, local interactions, and consequently very low communication/computation ratio. It is ideally situated to exploit the massively parallel super computers based on either CPUs or GPUs or heterogeneous architectures. Meanwhile, it should be noted that, as a natural born dynamic scheme, the LB method is not a method of choice for steady-state

computations. In addition, the standard LB method is not well suited to body-fitted coordinates and adaptive time stepping.

2.3.3 Multiphase lattice Boltzmann models

Since the emergence of the LB method, its application in multiphase flows has always been a very important theme of the method. With the development in the past two decades, many multiphase LB models have been proposed. These models mostly fall into one of the following categories: the color-gradient LB method [Gunstensen et al. 1991], the pseudopotential LB method [Shan & Chen 1993], the free-energy LB method [Swift et al. 1995], and the phase-field LB method [He et al. 1999]. The comparison of these four models is summarized in Table 1. In addition, several multiphase LB models were recently developed based on the entropic LB method and the discrete Boltzmann equation. The color-gradient LB method was introduced by Gunstensen et al., who employed red and blue particle distribution functions to represent two different fluids. Besides the standard collision operator, an additional collision operator was also utilized in this method, which can be regarded as a source term for generating the surface tension. Furthermore, to separate different phases and maintain interfaces, a recoloring process is required in the color gradient LB models.

The free-energy LB method was proposed by Swift et al. based on thermodynamics

considerations. The second-order moment of the equilibrium density distribution function was modified to include a non-ideal thermodynamic pressure tensor. The phase separation was therefore described by a non-ideal equation of state in the thermodynamic theory such as the van der Waals equation of state. However, the original free-energy LB model suffered from the lack of Galilean invariance owing to some non-Navier–Stokes terms, which resulted from the incorporation of pressure tensor using the equilibrium distribution function. To restore the Galilean invariance, some correction terms should be added to the equilibrium distribution function. A similar problem also exists in the color-gradient LB method, in which the pressure is changed by modifying the equilibrium distribution function. Therefore, the color-gradient multiphase LB models also need some correction terms to eliminate the non-Navier–Stokes terms in the recovered macroscopic equations.

The pseudopotential LB method, which is the simplest multiphase LB method, was devised by Shan and Chen. In this method, the fluid interactions are mimicked by an interparticle potential, through which the separation of fluid phases or components can be achieved automatically, without resorting to any techniques to track or capture interfaces. In fact, the interparticle potential will lead to a non-ideal pressure tensor, although it is different from that in the free-energy LB method. The pseudopotential LB method has become very popular in the multiphase LB community due to its

conceptual simplicity and computational efficiency and has been applied with great success to many problems.

The fourth category, the phase-field LB method, represents the multiphase LB models that are based on the phase-field theory, in which the interface dynamics is described by an order parameter that obeys the Cahn–Hilliard equation or a Cahn–Hilliard-like equation. In 1999, an incompressible multiphase LB model was proposed by He et al. In this model, the liquid-gas interface was captured with the evolution of an index function (order parameter). Meanwhile, the recovered interface-capturing equation was found to be a Cahn–Hilliard-like equation. In this regard, He et al.'s model is a phase-field LB model, even though the model was not directly built on the phase-field theory. Similarly, the multiphase LB model devised by Lee and Lin also belongs to this category.

Table 2.1 Comparison of lattice Boltzmann multiphase models

Model	**Maximum density ratio**	**Efficiency**	**Accuracy**	**Pros and cons**
Color-	$O(10)$	Less efficient	Accurate	Only useful for

gradient				density-matched cases
Shan-Chen	$O(10^2)$	Very efficient	Less accurate	Easy to implement
Free energy	$O(10)$	Less efficient	Accurate	Not convenient to specify wetting condition
Phase-field	$O(10^3)$	Efficient	Accurate	Not convenient to specify wetting condition

Much progress has been made in the above four categories of multiphase LB methods since the aforementioned early studies. However, these multiphase LB methods exhibit different performances in simulating dynamic multiphase flows at large liquid-gas density ratios in real world, which may be related to the following issues. First, it can be found that in these multiphase LB methods, the physical quantities that need to be evaluated across the liquid-gas interface are different. For instance, in the free

energy and the pseudopotential LB methods, the density and the pseudopotential are used, respectively. Second, as just mentioned, the free-energy and the color-gradient LB methods need some correction terms to remove the non-Navier-Stokes terms in the macroscopic equations. These correction terms will introduce additional sources of numerical instability as they involve many density-gradient terms such as $v\nabla\rho$ and $v\cdot\nabla\rho$, where v is the velocity. This is one of the reasons why the free energy and the color-gradient multiphase LB methods usually suffer from severe numerical instability in simulating dynamic multiphase flows at large density ratios and high Reynolds numbers, although they are successful in static or quasi-static cases with large density ratios.

In comparison with the free-energy and the color-gradient LB methods, the pseudopotential LB method and the phase-field LB method have been successfully applied to dynamic multiphase flows at large density ratios and relatively high Reynolds numbers (e.g., droplet splashing and droplet collision). Moreover, the pseudopotential and the phase field multiphase LB methods have been widely employed to simulate multiphase flows in fuel cells (water-gas two-phase transport) and batteries (the electrolyte transport dynamics) as well as phase-change heat transfer (boiling, evaporation, etc.). It is noticed that these two multiphase LB methods play an increasingly important role in modeling multiphase flow and phase change heat

transfer that are involved in energy science and technologies from the viewpoint of a mesoscopic numerical approach.

With the increase of practical applications of the LB method, it is very necessary to review the related theories and clarify some theoretical issues that are crucial to applications. The purpose of this article is therefore to present a comprehensive review of the advances in the pseudopotential and the phase-field multiphase LB methods. Various theoretical aspects will be addressed, such as the fundamental theory and basic models, the elimination of thermodynamic/hydrodynamic inconsistency, the surface tension treatment, the adjustment of interface thickness, and the implementation of contact angles. Meanwhile, the thermal LB models based on these two multiphase LB methods for simulating liquid vapor phase change will also be critically reviewed. Furthermore, we will summarize several forcing schemes that are widely used in the LB method, which also play a crucial role in the multiphase LB methods. In addition, the thermal LB approaches on standard lattices, which are extensively involved in the LB simulations of phase change heat transfer, will be discussed in detail.

2.3.4 The basic lattice Boltzmann formulations

Historically, the LB method originated from the lattice gas automata method, which can be considered as a simplified fictitious molecular dynamics model in which the space, time, and particle velocities are all discrete. Later it was demonstrated that the

LB equation can be rigorously derived from the Boltzmann equation in the kinetic theory, which not only establishes a direct connection between the LB method and the kinetic theory but also greatly solidifies the physics base of the LB method. Nevertheless, it should be noted that the LB method is not limited to dilute gases (a limitation of the Boltzmann equation) because it can be extended to incorporate non-ideal interactions through the effective interactions in the spirit of density functional theory. In this paper we start with the Boltzmann equation, which can be written as (without external forces)

$$\frac{\partial f}{\partial t} + \boldsymbol{\xi} \cdot \boldsymbol{\nabla} f = \boldsymbol{\Omega_f} \tag{4.}$$

where $f = f(\boldsymbol{r}, \boldsymbol{\xi}, t)$ is the single particle distribution function, $\boldsymbol{\xi}$ is the microscopic velocity, and $\boldsymbol{\Omega_f}$ is the collision term. Using the Bhatnagar–Gross–Krook (BGK) collision operator, the collision term is given by

$$\boldsymbol{\Omega_f} = -\frac{[f(\boldsymbol{r}, \boldsymbol{\xi}, t) - f^{eq}(\boldsymbol{r}, \boldsymbol{\xi}, t)]}{\tau_f} \tag{5.}$$

in which τ_f is the relaxation time and f^{eq} is the continuous Maxwell–Boltzmann distribution function

$$f^{eq} = \frac{\rho}{(2\pi RT)^{\frac{D}{2}}} \exp\left[-\frac{(\boldsymbol{\xi} - \boldsymbol{v})^2}{2RT}\right] \tag{6.}$$

where R is the gas constant, D is the spatial dimension, ρ is the density, T is the temperature, and $\boldsymbol{v}$ is the macroscopic velocity. By discretizing the velocity $\boldsymbol{\xi}$ into a set of lattice velocities:

$$\boldsymbol{\xi} - -\{\boldsymbol{e_0}, \boldsymbol{e_1} \dots, \boldsymbol{e_N}\} \tag{7.}$$

the following discrete Boltzmann–BGK equation can be obtained

$$f_\alpha(\boldsymbol{r} + \boldsymbol{e}_\alpha \delta_t, t + \delta_t) - f_\alpha(\boldsymbol{r}, t) = -\frac{1}{\tau}[f_\alpha(\boldsymbol{r}, t) - f_\alpha{}^{eq}(\boldsymbol{r}, t)] \tag{8.}$$

where f_α is the discrete density distribution function and f^{eq} is its equilibrium distribution.

The space $\boldsymbol{x}$ is usually discretized in such a way that $\boldsymbol{e}_\alpha \delta_t$ is the distance between two neighboring grid points. Then after one time step δ_t, $f_\alpha(\boldsymbol{r}, t)$ will arrive at its neighboring grid site along the lattice velocity direction e α . Hence the LB equation can be split into two processes:

the “collision” process

$$f_\alpha(\boldsymbol{r}, t + \delta_t) - f_\alpha(\boldsymbol{r}, t) = -\frac{1}{\tau}[f_\alpha(\boldsymbol{r}, t) - f_\alpha{}^{eq}(\boldsymbol{r}, t)] \tag{9.}$$

and the “streaming” process

$$f_\alpha(\boldsymbol{r} + \boldsymbol{e}_\alpha \delta_t, t + \delta_t) = f_\alpha(\boldsymbol{r}, t + \delta_t) \tag{10.}$$

From above equations we can see that the collision process is completely local and the streaming process is completely linear. Actually, many advantages of the LB method arise from such a feature. For instance, it can be seen that most of the computations take place locally at the collision process, which makes the LB method highly amenable to parallel computing.

2.4 Limitations in previous researches

2.4.1 Limitations in previous researches on falling film

In summary, the effect of various design operating parameters and conditions on the performance of the falling film has been theoretically analyzed, numerically simulated and experimentally studied in previous studies. The factors are evaluated specifically, including the desiccant fluid properties (like density, viscosity, and specific heat capacity and so on), the flow configuration, the desiccant distribution, the inlet flow rate and condition of the desiccant solution, moist air and cooling media, energy store capacity and so on. However, through the literature review there are also several limitations to be listed out. Generally, there are some improvement can be made in some aspects:

(1) Many researchers take the falling film as a single-phase problem, which means the surface tension and phase change are neglected, while the falling film is a typical two-

phase flow. This kind of simplification may cause unexpected errors in falling film research.

(2) The numerical researches on falling film are mostly based the traditional CFD tools, which rely on the continuity hypothesis. However, considering the thin liquid layer (less than 1 micrometer in our experiment) and cutoff phenomenon, the continuity hypothesis may be not appropriate in falling film research.

(3) In conventional numerical models, the turbulence flow is usually simulated with semi-experimental turbulence models, which may not have solid physical backgrounds.

(4) In conventional numerical models, the computational cost is too high. It is reported that even one week is required to calculate a typical two-dimensional case of a computation area size of 150mm×100mm [Luo et al. 2014].

Considering the limitations listed above, the lattice Boltzmann method, which is reported to have advantage over the aspects such as multi-phase flows, non-continuity hypothesis and computational efficiency, was chosen as the method to simulate the falling film in this work.

2.4.2 Limitations in previous researches on lattice Boltzmann method

The lattice Boltzmann method (LBM), which is a numerical method rooted in kinetic theory, is becoming popular in the fields of computational fluid dynamics in last decades. Due to the particle-based mesoscopic nature which connects the micro and macro worlds, the LBM has an advantage in simulation fidelity and computational efficiency especially for multiphase flows. Many lattice Boltzmann models were proposed for multiphase flows which are similar to falling film. Through the literature review, however, there are also several limitations to be listed out. Generally, there are some improvement can be made in some aspects:

(1) Although great progress has been made on using LBM to simulate multiphase flow, it is still great challenge to simulate high density ratio, especially up to 1000.

(2) The boundary treatment, especially the wetting boundary problem, which is of great importance in falling film, has not been focused in previous researches.

(3) Most lattice Boltzmann models are proposed for the equilibrium problems, whether the method can be applied on the dynamic problem is rarely mentioned.

2.5 Summary

This chapters provides a comprehensive literature review of falling film and lattice

Boltzmann method. Firstly, the researches on laminar flow and wavy film flow are discussed respectively, and the relationship between film Reynolds number and flow type is summarized. Then, the researches on heat and mass transfer process in falling film are detailed reviewed. The theoretical, numerical and experimental model are introduced respectively. Thirdly, the limitations of the previous researches on falling film are summarized, and the reason of taking lattice Boltzmann method as the research methodology is explained. Fourthly, the development of the lattice Boltzmann method is reviewed and the characteristics are highlighted. The basic ideas and equations of lattice Boltzmann method are introduced. Finally, the limitations of previous lattice Boltzmann models on multi-phase flows are summarized. Through literature review it can be concluded that the lattice Boltzmann method is appropriate for falling film simulation.

CHAPTER 3

DEVELOPMENT OF A LATTICE BOLTZMANN MODEL CAPTURING DENSITY DISTRIBUTION OF TWO PHASE FLOWS WITH HIGH DENSITY RATIO

3.1 Introduction

The dynamic characteristics of the lattice Boltzmann equation make it possible to directly handle the interaction between molecules, and the macroscopic interface dynamic behavior is obtained, which gives the lattice Boltzmann equation great advantage on the two phase flow problem. However, the lattice Boltzmann method also has some limitations when dealing with two-phase flow, for example, in many cases the density distribution obtained by the lattice Boltzmann model deviates from the theoretical solution [Cristea & Sofonea 2003, Shan 2006]. And, as the density ratio increases, The deviation between the simulation and the theoretical solution also becomes worse.

Many scholars have noticed this limitation of the lattice Boltzmann method. For example, through theoretical analysis Shan and Chen [Shan & Chen 1994] pointed out that their model is inconsistent with thermodynamic equilibrium. Yuan [Yuan & Schaefer 2006] pointed out that in Shan and Chen's model, whether the density of the

equilibrium state obtained by the simulation matches the theoretical solution depends on the state formula adopted. On the other hand, Cristea and Sofonea [Cristea & Sofonea 2003] also observed the density errors when studied the spurious velocity using finite difference lattice Boltzmann model.

A model that cannot capture the density distribution correctly may cause some non-physical phenomena when studying some complex flows and complex geometry. For example, when study the contact line problem, if the numerical density distribution is inconsistent with the theory, it will lead that the original hydrophobic structure in the numerical model becomes hydrophilic, which is a total mistake. However, the lattice Boltzmann model has been widely used to study complex flow dynamics and flow in complex geometric structures, such as the critical point phenomenon [Gross & Varnik 2012], flows in complex porous media [Wiklund et al. 2011], and the breakup and merging of droplets [Xing et al. 2007], and for the above problems, the small density errors may cause the calculation results to deviate seriously from actual physical phenomena. Also, the high density ratio in two phase flows makes it harder to capture the density properly. Thus, it is necessary to propose a two-phase flow model which can properly capture the density distribution in two phase flow.

3.2 The interaction force scheme in lattice Boltzmann model for two phase flows

As mentioned in the Chapter 2, the complex interface dynamics of multiphase flow involves large time and space scales, and the traditional numerical method of fluid mechanics faces great difficulties in studying two-phase flow, especially at high density ratio. Due to the micro-nature and mesoscopic characteristics, lattice Boltzmann method can describe the interaction between different phases by adding the interaction force of the ideal gas. As long as these interaction forces are described accurately, complex interface dynamics will occur naturally. Therefore, in the lattice Boltzmann method, the interaction force handling is particularly important.

The force terms of different forms are mathematically consistent, and different discrete gradient operators can converge to the same gradient operator under continuous conditions. However, when it comes to the non-continuous situation, previous researchers pointed out that different force schemes have a great influence on the interface dynamics [Sbragaglia et al. 2007, Seta & Okui 2007, Pooley & Furtadov 2008]. Thus, it is necessary to study the influence of different force schemes in lattice Boltzmann method on the interface dynamics.

Generally, all the lattice Boltzmann models consist of a standard evolution equation

and a force term [He et al. 1998]

$$f_a(\boldsymbol{e}_\alpha + \delta_t, t + \delta_t) - f_a(\boldsymbol{r}, t) = -\frac{1}{\tau}[f_a(\boldsymbol{x}, t) - f_a{}^{eq}(\boldsymbol{x}, t)] + \delta_t F_a \qquad (11.)$$

where f_α represents the particle distribution function, $\boldsymbol{e}_\alpha$ is the velocity of particle in direction α, $\boldsymbol{u}$ is the macro velocity, c_s is the lattice sound speed and λ is the relaxation time, $\Gamma_a = \Gamma_a(\boldsymbol{u}) = f_\alpha^{eq}/\rho$, and f_α^{eq} is the equilibrium distribution function which is defined as:

$$f_\alpha^{eq} = \omega_\alpha \rho \left[1 + \frac{\boldsymbol{e}_\alpha \cdot \boldsymbol{u}}{c_s^2} + \frac{(\boldsymbol{e}_\alpha \cdot \boldsymbol{u})^2}{2c_s^4} - \frac{(\boldsymbol{u} \cdot \boldsymbol{u})}{2c_s^2}\right] \qquad (12.)$$

where ω_α donating the weight factor [He et al. 1998].

F_a in Eq. 11 is the force term, which means the influence of the interaction force $\boldsymbol{F}$ on distribution function. There are different schemes of F_a in previous researches. Here we take the scheme proposed by He et al [He et al. 1999]

$$F_a = \left(1 - \frac{1}{2\tau}\right)\frac{(\boldsymbol{e}_\alpha - \boldsymbol{u}) \cdot \boldsymbol{F}}{\rho c_s^2} f_\alpha^{eq} \qquad (13.)$$

For an isothermal system, the density and velocity of the fluid are define as

$$\rho = \sum_\alpha f_a \qquad (14.)$$

$$\rho \boldsymbol{u} = \frac{1}{c_s^2} \sum_{\alpha} \boldsymbol{e}_{\alpha} f_a - \frac{\delta t}{2} \boldsymbol{F} \tag{15.}$$

For Van der Waals fluids, the interaction force can be written as follows

$$\boldsymbol{F} = \nabla \rho c_s^2 - \rho \nabla \mu = \nabla (\rho c_s^2 - p_0) + \rho \kappa \nabla \nabla^2 \rho \tag{16.}$$

where μ is the chemical potential is defined as $\mu = \mu_0 - \kappa \nabla^2 \phi$, μ_0 is the bulk chemical potential, κ is a constant related to the surface energy. By the Chapman-Enskog expansion, the model can be recovered to Navier – Stokes equation,

$$\frac{\partial \rho}{\partial t} + \nabla \cdot (\rho \boldsymbol{u}) = 0 \tag{17.}$$

$$\frac{\partial (\rho \boldsymbol{u})}{\partial t} + \nabla \cdot (\rho \boldsymbol{u} \boldsymbol{u}) = -\nabla p_0 + \nabla (\rho v S) + \rho \kappa \nabla \nabla^2 \rho \tag{18.}$$

Where $v = c_s^2 (\tau - 0.5) \partial t$ is the kinematic viscosity.

He et al. [He et al. 1999] proposed the potential form (Eq. 19) and pressure form (Eq. 20), these two expressions are mathematically equal. However, the results they obtained are not consistent due to numerical errors on discrete degree.

$$\boldsymbol{F} = \nabla\rho c_s^2 - \rho\nabla(\mu_0 - \kappa\nabla^2\phi v) \tag{19.}$$

$$\boldsymbol{F} = \nabla(\rho c_s^2 - p_0) + \rho\kappa\nabla\nabla^2\rho \tag{20.}$$

In this chapter, we consider two different finite difference schemes for the gradient operator in Equation *F*. The first format is the isotropic difference format (CD),

$$\nabla\phi = \sum_{\alpha} \frac{w_i \boldsymbol{e}_\alpha \phi(\boldsymbol{x} + \boldsymbol{e}_\alpha \delta t)}{c_s^2 \delta t} \tag{21.}$$

The second scheme for the gradient operator is the mix difference format (MD) proposed by Lee & Fisher [Lee & Fisher 2006]. In the scheme, the force term consists of two parts,

$$F_a{}^{MD} = \frac{1}{2}[\left(1 - \frac{1}{\tau}\right) F_a{}^{c} + F_a{}^{b}]$$

The superscript “c” and “b” means the central difference and biased difference.

In this work these two difference formats are both adopted to guarantee the stability and accuracy on the lattice Boltzmann model.

3.3 Lattice Boltzmann model for capturing density distribution of two phase flows with high density ratio

The model developed in this paper is based on the multi-phase lattice Boltzmann model proposed by Lee and Liu [Lee & Liu 2010], and the gravity and open boundary conditions are proposed and incorporated in the original model. In this model, $\widetilde{\rho_m}$ and $\boldsymbol{u_m}$, which donate the local density and velocity of the two kinds of fluids respectively, satisfy the continuity equation

$$\frac{\partial \widetilde{\rho_m}}{\partial t} + \nabla \cdot \widetilde{\rho_m} \boldsymbol{u_m} = 0, \;\; m = 1,2 \qquad (22.)$$

The heavier fluid is referred as Fluid 1 ($m = 1$) and the other as Fluid 2 ($m = 2$). The mixture density, $\rho = \sum_{m=1}^{2} \widetilde{\rho_m}$, should also be conserved. The composition function$C$, which is defined as $C = \widetilde{\rho_1}/\rho_1$, is then taken to describe the binary fluid, and the density can be expressed as a linear function of C

$$\rho = C\rho_1 + (1 - C)\rho_2 \qquad (23.)$$

According to the phase-field theory, the fluid system can be represented by a continuous variable which is known as the order parameter. In this study, the composition function C plays the role of the order parameter, and the free energy of the whole fluid system can be expressed as follows:

$$\Phi_b + \Phi_s = \int_V \left(E_0(C) + \frac{\kappa}{2}|\nabla C|^2\right) dV$$
$$+ \int_S \left(\varphi_0 - \varphi_1 C_s + \varphi_2 {C_s}^2 - \varphi_3 {C_s}^3 + \cdots\right) dS \qquad (24.)$$

where E_0 is the bulk energy density and usually it takes the form as $E_0 = \beta C^2(C-1)^2$, κ is a constant related with surface energy, β is a constant related with bulk energy, C_s is the composition at the solid surface. The chemical potential is defined as $\mu = \frac{\partial E_0}{\partial C} - \kappa\nabla^2 C$. The free energy is minimized when the system reaches an equilibrium state, with the result that the equilibrium interfacial profile is

$$C(z) = 0.5 + 0.5 tanh\left(\frac{2z}{\xi}\right) \qquad (25.)$$

where ξ is the thickness of the interface and z is the coordinate normal to the interface. With Eq. 25, the density distribution around two phase interface is shown in Fig 3.1.

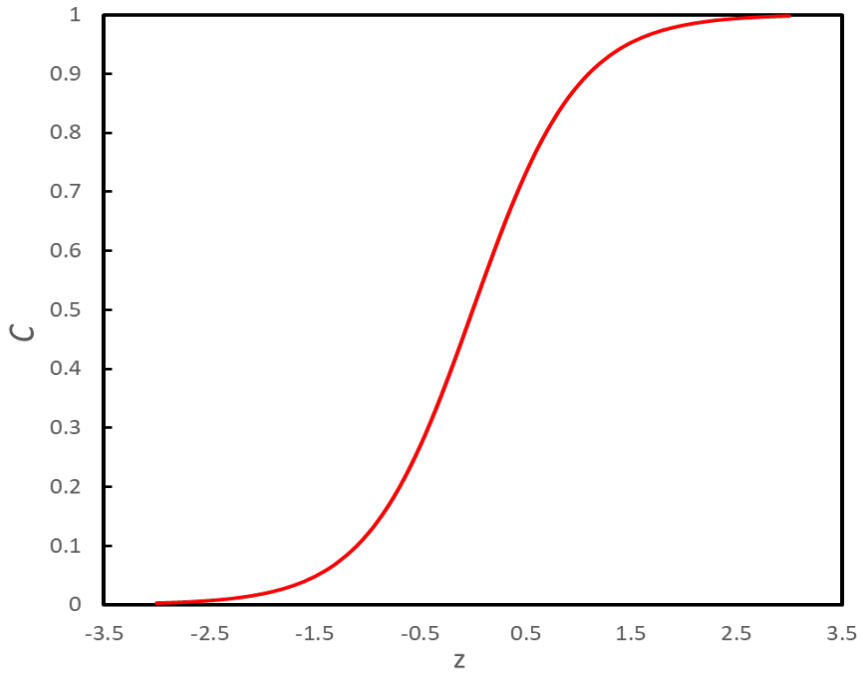

Fig 3.1 Interface density profile

3.3.1 Discrete Boltzmann equations

The discrete Boltzmann equation (DBE) for the transportation of density and momentum of the mixed fluid [He et al. 1999] is :

$$\frac{Df_\alpha}{\partial t} = (\frac{\partial}{\partial t} + \boldsymbol{e}_\alpha \cdot \nabla) f_\alpha = -\frac{1}{\lambda}\left(f_\alpha - f_\alpha^{eq}\right) + \frac{1}{{c_s}^2}(\boldsymbol{e}_\alpha - \boldsymbol{u}) \cdot \boldsymbol{F}\Gamma_a \qquad (26.)$$

where f_α represents the particle distribution function, $\boldsymbol{e}_\alpha$ is the velocity of particle in direction α, $\boldsymbol{u}$ is the macro velocity, c_s is the lattice sound speed and λ is the relaxation time, $\Gamma_a = \Gamma_a(\boldsymbol{u}) = f_\alpha^{eq}/\rho$, and f_α^{eq} is the equilibrium distribution function

which is defined as:

$$f_\alpha^{eq} = \omega_\alpha \rho \left[1 + \frac{\boldsymbol{e}_\alpha \cdot \boldsymbol{u}}{c_s^2} + \frac{(\boldsymbol{e}_\alpha \cdot \boldsymbol{u})^2}{2c_s^4} - \frac{(\boldsymbol{u} \cdot \boldsymbol{u})}{2c_s^2}\right] \quad (27.)$$

where ω_α donating the weight factor [He et al. 1998].

The $\boldsymbol{F}$ in DBE is the intermolecular force and it comprises:

$$\boldsymbol{F} = \nabla \rho c_s^2 - (\nabla p - C\nabla\mu) + \rho \boldsymbol{g} \quad (28.)$$

where p is the dynamic pressure which ensures the incompressibility, and $\rho \boldsymbol{g}$ is the gravity.

Two new particle distributions are defined to describe the evolution of pressure p and composition C. For pressure p we define

$$g_\alpha = f_\alpha c_s^2 + (p - \rho c_s^2)\Gamma_a(0) \quad (29.)$$

and the corresponding equilibrium distribution function

$$g_\alpha^{eq} = f_\alpha^{eq} c_s^2 + (p - \rho c_s^2)\Gamma_a(0) = \omega_\alpha \left[p + \rho c_s^2 \left(\frac{\boldsymbol{e}_\alpha \cdot \boldsymbol{u}}{c_s^2} + \frac{(\boldsymbol{e}_\alpha \cdot \boldsymbol{u})^2}{2c_s^4} - \frac{(\boldsymbol{u} \cdot \boldsymbol{u})}{2c_s^2}\right)\right] (30.)$$

The DBE for the new variable g_α is taken as

$$\frac{Dg_\alpha}{Dt} = \left(\frac{\partial}{\partial \boldsymbol{t}} + \boldsymbol{e}_\alpha \cdot \nabla\right) g_\alpha =$$

$$-\frac{1}{\lambda}\left(g_\alpha - g_\alpha^{eq}\right) + (\boldsymbol{e}_\alpha - \boldsymbol{u}) \cdot \left[\nabla \rho c_s^2 \left(\Gamma_a - \Gamma_a(0)\right) - C\nabla\mu\Gamma_a\right] \qquad (31.)$$

For composition C we define

$$h_\alpha = \frac{C}{\rho} f_\alpha \qquad (32.)$$

and the corresponding equilibrium distribution function

$$h_\alpha^{eq} = \frac{C}{\rho} f_\alpha^{eq} \qquad (33.)$$

The DBE for the new variable h_α is taken as

$$\frac{Dh_\alpha}{Dt} = -\frac{1}{\lambda}\left(h_\alpha - h_\alpha^{eq}\right) + M\nabla^2\mu\Gamma_a + (\boldsymbol{e}_\alpha - \boldsymbol{u}) \cdot \left[\nabla C - \frac{C}{\rho c_s^2}(\nabla p - C\nabla\mu)\right]\Gamma_a \quad (34.)$$

3.3.2 Lattice Boltzmann equations

In this study, we choose the D2Q9 scheme so the weight factor ω_α is taken as

$$\omega_\alpha = \begin{cases} \frac{4}{9} & \alpha = 0 \\ \frac{1}{9} & \alpha = 1\sim4 \\ \frac{1}{36} & \alpha = 5\sim8 \end{cases} \qquad (35.)$$

and the discrete velocity $\boldsymbol{e}_\alpha$ is

$$\boldsymbol{e}_\alpha = \begin{cases} (0,0)c & \alpha = 0 \\ (\pm 1,0)c, (0,\pm 1)c & \alpha = 1\sim 4 \\ (\pm 1,\pm 1)c & \alpha = 5\sim 8 \end{cases} \quad (36.)$$

in which $c = \delta_x/\delta_t$ is the lattice speed, with δ_x and δ_t representing the lattice spacing and time spacing, respectively.

The discrete Boltzmann equations (20) and (23) for g_α and h_α can be integrated over time step δ_t under the D2Q9 scheme and then the lattice Boltzmann equations (LBEs) for these two distribution functions are obtained. To simplify the calculation, two modified distribution functions $\bar{g}_\alpha, \bar{h}_\alpha$ as well as their equilibrium functions $\bar{g}_\alpha^{eq}$, $\bar{h}_\alpha^{eq}$ are introduced as follows:

$$\bar{g}_\alpha = g_\alpha + \frac{1}{2\tau}\left(g_\alpha - g_\alpha^{eq}\right) - \frac{\delta_t}{2}(\boldsymbol{e}_\alpha - \boldsymbol{u}) \cdot \left[\nabla^{CD}\rho c_s^2\left(\Gamma_a - \Gamma_a(0)\right) - C\nabla^{CD}\mu\Gamma_a\right] \quad (37.)$$

$$\begin{aligned} \bar{g}_\alpha^{eq} &= g_\alpha^{eq} - \frac{\delta_t}{2}(\boldsymbol{e}_\alpha - \boldsymbol{u}) \cdot [\nabla^{CD}\rho c_s^2\left(\Gamma_a - \Gamma_a(0)\right) - C\nabla^{CD}\mu\Gamma_a \bar{g}_\alpha^{eq} \\ &= g_\alpha^{eq} - \frac{\delta_t}{2}(\boldsymbol{e}_\alpha - \boldsymbol{u}) \cdot [\nabla^{CD}\rho c_s^2\left(\Gamma_a - \Gamma_a(0)\right) - C\nabla^{CD}\mu\Gamma_a \#(38.) \end{aligned}$$

$$\bar{h}_\alpha = g_\alpha + \frac{1}{2\tau}\left(h_\alpha - h_\alpha^{eq}\right) - \frac{\delta_t}{2}(\boldsymbol{e}_\alpha - \boldsymbol{u}) \cdot \left[\nabla^{CD}C - \frac{C}{\rho c_s^2}(\nabla^{CD}p + C\nabla^{CD}\mu)\right]\Gamma_a \quad (39.)$$

$$\bar{h}_\alpha^{eq} = h_\alpha^{eq} - \frac{\delta_t}{2}(\boldsymbol{e}_\alpha - \boldsymbol{u}) \cdot \left[\nabla^{CD} C - \frac{C}{\rho c_s^2}(\nabla^{CD} p + C\nabla^{CD}\mu)\right] \Gamma_a \qquad (40.)$$

and the LBEs for functions $\bar{g}_\alpha, \bar{h}_\alpha$ are as followed.

$$\bar{g}_\alpha(\boldsymbol{x} + \boldsymbol{e}_\alpha \delta_t, t + \delta_t) = \bar{g}_\alpha(\boldsymbol{x}, t) - \frac{1}{\tau + 0.5}\left(\bar{g}_\alpha - \bar{g}_\alpha^{eq}\right)|_{(\boldsymbol{x},t)}$$

$$+\delta_t(\boldsymbol{e}_\alpha - \boldsymbol{u}) \cdot \left[\nabla^{MD}\rho c_s^2\left(\Gamma_a - \Gamma_a(0)\right) - C\nabla^{MD}\mu\Gamma_a\right]_{(\boldsymbol{x},t)} \qquad (41.)$$

$$\bar{h}_\alpha(\boldsymbol{x} + \boldsymbol{e}_\alpha \delta_t, t + \delta_t) = \bar{h}_\alpha(\boldsymbol{x}, t) - \frac{1}{\tau + 0.5}\left(\bar{g}_\alpha - \bar{g}_\alpha^{eq}\right)|_{(\boldsymbol{x},t)} + \frac{\delta_t}{2} M\nabla^2\mu\Gamma_a|_{(\boldsymbol{x},t)}$$

$$+\frac{\delta_t}{2} M\nabla^2\mu\Gamma_a|_{(\boldsymbol{x}+\boldsymbol{e}_\alpha\delta_t,t)} + \frac{\delta_t}{2}(\boldsymbol{e}_\alpha - \boldsymbol{u}) \cdot [\nabla^{MD} C - \frac{C}{\rho c_s^2}(\nabla^{MD} p + C\nabla^{MD}\mu)]\Gamma_a|_{(\boldsymbol{x},t)} (42.)$$

The superscript “CD” and “MD” mean the central difference and the mixed difference approximation of the derivative, respectively.

After the collision process, the hydrodynamic parameters such as the composition, average velocity and dynamic pressure can be calculated by taking the zeroth and first moments of the particle distribution

$$C = \sum_\alpha \bar{h}_\alpha \qquad (43.)$$

$$\rho\boldsymbol{u} = \frac{1}{c_s^2}\sum_\alpha \boldsymbol{e}_\alpha \bar{g}_\alpha - \frac{\delta t}{2} C\nabla^{CD}\mu \qquad (44.)$$

$$p = \sum_{\alpha} \bar{g}_{\alpha} + \frac{\delta t}{2} \boldsymbol{u} \cdot \nabla^{CD} \rho c_s^2 \qquad (45.)$$

3.3.3 Boundary conditions

In this falling film case, the computational domain is shown in Fig. 3. Both the solid-liquid and the liquid-gas boundaries are considered as no-slip walls, which was realized by the bounce-back scheme at the boundary nodes ($\boldsymbol{x}_s$), $f_{\bar{\alpha}}(\boldsymbol{x}_s) = f_{\alpha}(\boldsymbol{x}_s)$ ($\bar{\alpha}$ is the opposite direction of α). With this scheme the unknown variable outside the wall boundary can be approximated by

In this falling film case, the computational domain is shown in Fig. 3. Both the solid-liquid and the liquid-gas boundaries are considered as no-slip walls, which was realized by the bounce-back scheme at the boundary nodes ($\boldsymbol{x}_s$), $f_{\bar{\alpha}}(\boldsymbol{x}_s) = f_{\alpha}(\boldsymbol{x}_s)$ ($\bar{\alpha}$ is the opposite direction of α). With this scheme the unknown variable outside the wall boundary can be calculated by

$$\phi(\boldsymbol{x}_s + \boldsymbol{e}_{\alpha}\delta t) = \phi(\boldsymbol{x}_s - \boldsymbol{e}_{\alpha}\delta t) \qquad (46.)$$

$$\phi(\boldsymbol{x}_s + 2\boldsymbol{e}_{\alpha}\delta t) = \phi(\boldsymbol{x}_s - 2\boldsymbol{e}_{\alpha}\delta t) \qquad (47.)$$

The upper (inlet) and lower (outlet) boundaries are considered as open boundaries.

Velocity inlet boundary and fully developed outlet boundary were developed in this study. The validation tests were conducted to ensure the boundary conditions are appropriate. The boundary conditions are different from those adopted in Lee and Liu's [Lee & Liu 2010] original work in which periodic boundary conditions were taken. Open boundary is more appropriate for the falling film simulation and so it is adopted in this work.

3.4 Benchmark cases

First of all, three test cases were studied to validate the two-phase model. The first case was to simulate the droplets on flat plates with different contact angles to test the approach to handling the liquid-solid interface. The second case was to simulate the typical two phase co-current flow in a channel, which has been analytically solved [Huang et al. 2013]. This case is to examine the external forces (such as gravity) added in the model. The third case aimed to test the performance of the fully developed outlet boundary by simulating a droplet flowing in an infinitely long channel.

3.4.1 Equilibrium droplet on flat plate

In this case, a rectangle computational domain with a grid size of 160×60 ($NX \times NY$) was chosen. A two-dimensional liquid droplet with a radius of 25 was initially generated at the center of a plate. The periodic boundaries were implemented at the

left and right sides and bounce back scheme was taken for the upper and lower boundary. In this case, the density ratio (the heavier over the lighter fluid, ρ^*) is taken as 100. The different contact angles $\theta^{eq} = 30°, 60°, 90°, 120° \, and \, 150°$ were simulated by choosing different wetting potential ω. The equilibrium contact angles were measured by the geometric formula of droplet height and the length of contact line. Fig 3.2 shows the comparison between the measured contact angles and analytical ones. It can be observed that the angles obtained by the model agree well with the analytical ones. Furthermore, the droplet recovering process on the plate with contact angle $\theta^{eq} = 30°$ is shown in Fig. 3.3, in which the color represents the density while the red part and blue part are corresponding to the liquid droplet and the gas, respectively. The droplet automatically achieved equilibrium state from initial state after a short period, which indicates that the proposed model is appropriate to treat the contact angle issue.

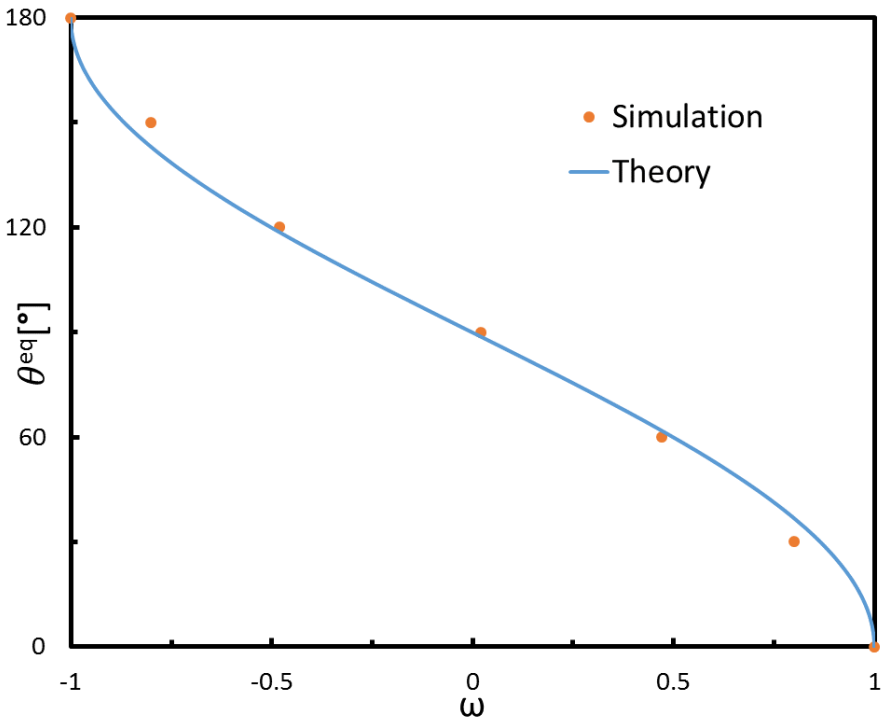

Figure 3.2 The comparison between the equilibrium contact angles between simulation results and analytical data

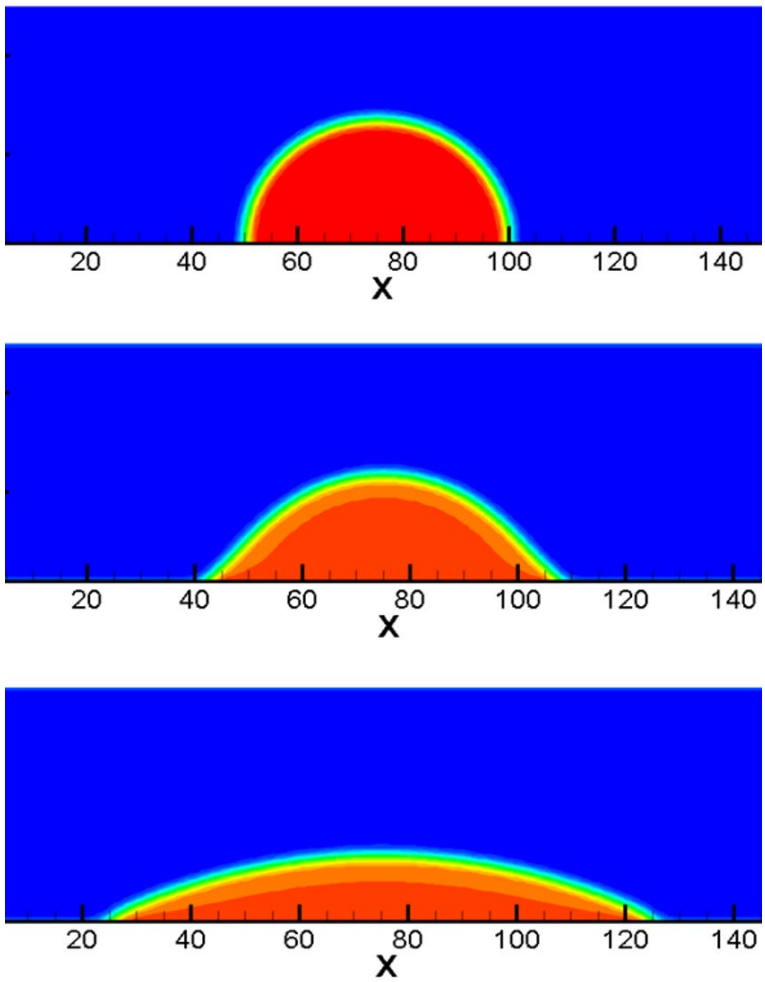

Figure 3.3 Droplet recovering process on the plate with contact angle 30°

3.4.2 Two-phase co-current flow in a channel

In this case, the two-phase co-current flow driven by external forces in a channel was simulated. The computational domain consisted of a 200×100 ($NX \times NY$) rectangle girds system, while the liquid phase occupied the areas in which $NY = 0{\sim}25$ and $NY = 75{\sim}100$, and the remaining area was occupied by the gas phase. In this case, the density ratio is taken as 100, i.e. $\rho^* = 100$ The periodic boundaries were

implemented at the left and right sides and no-slip walls were applied for the top and bottom boundaries, where the θ^{eq} for these two boundaries were both set as $90°$. An external force F_x was applied on the gas phase to simulate the gravity. The analytical solution for this case can be found in Huang *et al.* [Huang et al. 2013]. The velocity profiles of u_x in the channel flow obtained from the model developed in this study and the analytical solution are compared in Fig 3.4. It can be observed that the velocity profiles agree well, which means the incorporation of the gravity in the proposed model is appropriate.

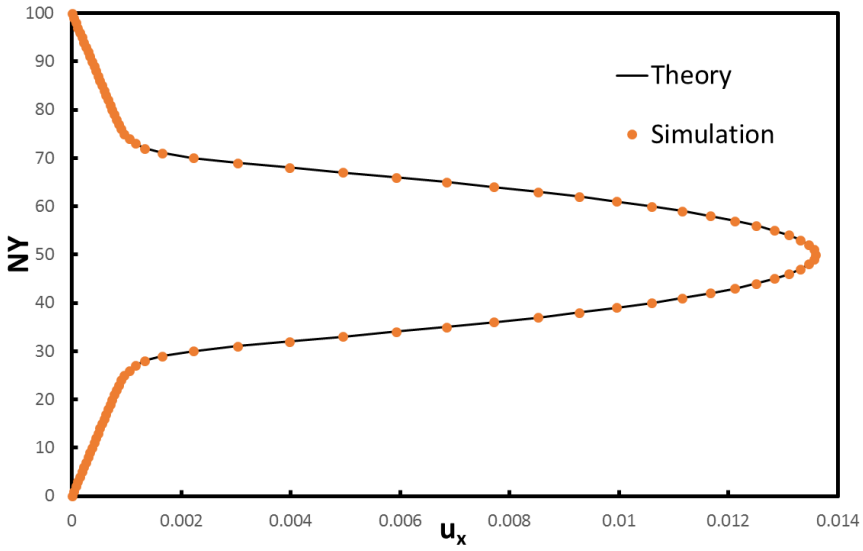

Figure 3.4 The comparison between the velocity profiles of $\boldsymbol{u_x}$ of co-current flow between simulation results and analytical data

3.4.3 Droplet flowing in infinite long channel

This case aimed to test the fully developed outlet boundary condition of the proposed model. Similar to the two-phase co-current flow in a channel, a rectangle computational domain with a grid size of 200×100 $(NX \times NY)$ was chosen. A two-dimensional liquid droplet with a radius of 25 was initially generated at the left side of the domain, with an initial velocity

$$u_{x,droplet} = U, u_{y,droplet} = 0$$

$$u_{x,gas} = u_{y,gas} = 0$$

The channel was assumed to be infinitely long so deformation should not take place when the droplet flowed across the right boundary if the boundary was appropriate chosen. The no-slip wall boundary conditions were applied on the upper and lower sides, and the velocity boundary was implemented on the left side. The outlet boundary, which referred the right side of the simulation domain, was set as fully developed outlet boundary. In this case, $\rho^* = 100, \mathrm{Re} = \frac{2UR}{v}$. Snapshots of the droplet at different times are shown in Fig. 3.5. Slight deformation can be observed at the outlet while the droplet keeps the shape in the main process. Considering that falling film interface is much smoother than the droplet surface under low Reynolds number, this fully developed outlet boundary is acceptable.

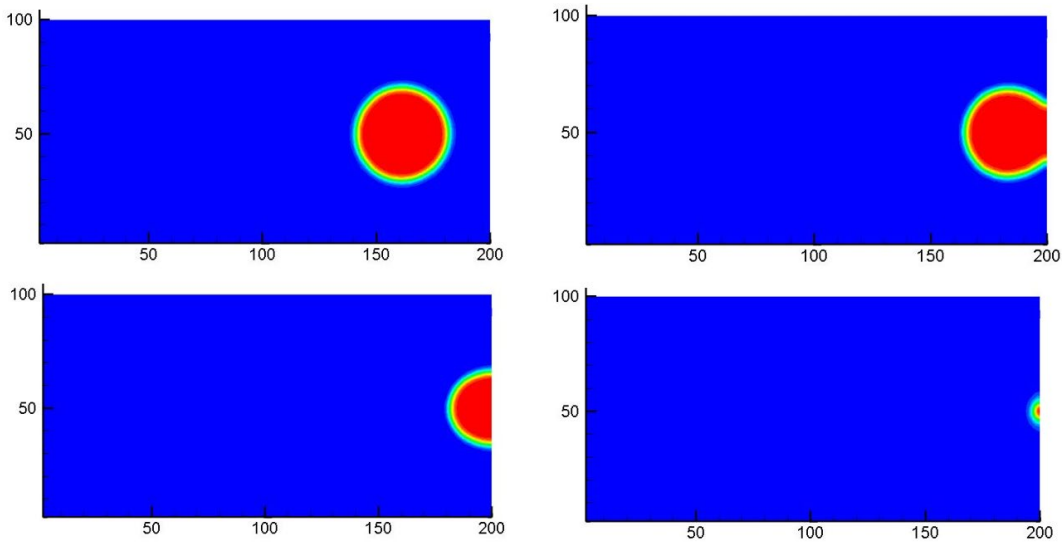

Figure 3.5 Snapshots of the droplet at different times

3.5 Summary

In this chapter, a new two-dimensional LBM simulation model was developed to capture the density distribution of two phase flows with high density ratio. The dynamic characteristics of the lattice Boltzmann equation make it possible to directly handle the interaction between molecules, and the macroscopic interface dynamic behavior is obtained, which gives the lattice Boltzmann equation great advantage on the two phase flow problem. However, the lattice Boltzmann method also has some limitations when dealing with two-phase flow, for example, in many cases the density distribution obtained by the lattice Boltzmann model deviates from the theoretical solution. And, as the density ratio increases, The deviation between the simulation and the theoretical solution also becomes worse. Thus, it is necessary to propose a two-

phase flow model which can properly capture the density distribution in two phase flow.

The interaction force scheme was first discussed in this chapter. Two kinds of difference formats, the isotropic difference format and mixed difference format, were introduced and adopted in the developed model. The developed model has taken the problems such as the high density ratio, surface tension, gravity, inlet and outlet open boundary conditions into consideration. Three test cases were studied to validate the two-phase model. The first case was to simulate the droplets on flat plates with different contact angles to test the approach to handling the liquid-solid interface. The second case was to simulate the typical two phase co-current flow in a channel, which has been analytically solved [Huang et al. 2013]. This case is to examine the external forces (such as gravity) added in the model. The third case aimed to test the performance of the fully developed outlet boundary by simulating a droplet flowing in an infinitely long channel. The numerical results show that the developed model can trace the density distribution properly even at the density ratio 1000. And the developed model in this chapter lays the foundation for the study of falling film based liquid desiccant dehumidifier.

CHAPTER 4

WETTING BOUNDARY TREATMENT

4.1 Introduction

In falling film research, the wetting area of liquid desiccant is an important parameter in the dehumidifier. In early stage of the simulation model for liquid desiccant dehumidifier, the working plate was usually assumed to be fully wetted by liquid desiccant, which did not comply with the experimental observation. In actual situations, the working surfaces were usually observed to be incompletely wetted by the liquid desiccant, as shown in Fig. 4.1. Therefore, it is very important to properly simulate the wetting boundary in falling film.

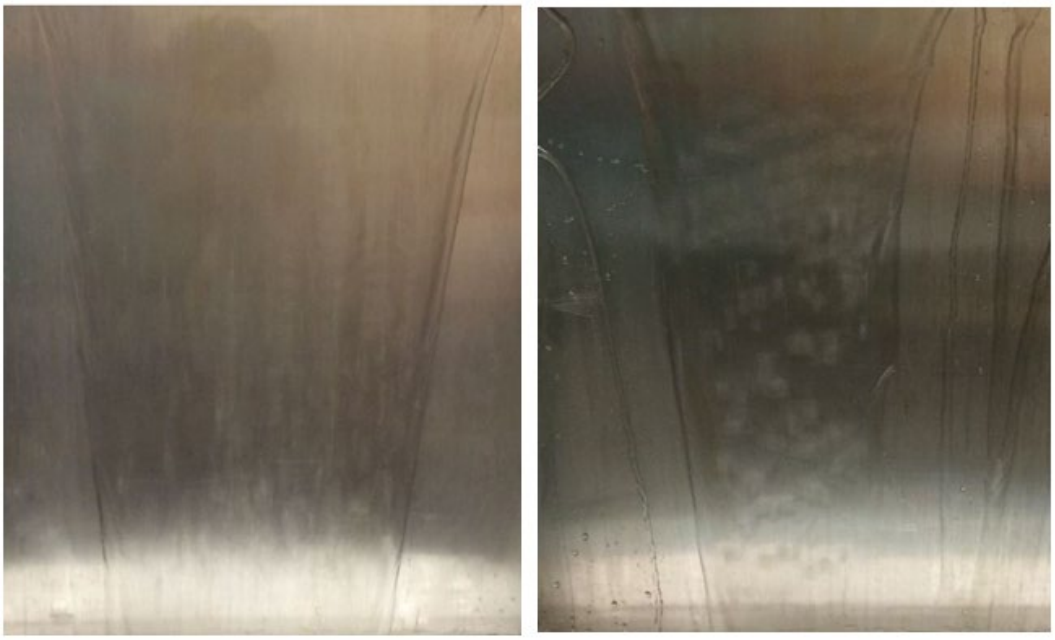

Fig 4.1 Pictures of working surfaces incompletely wetted by the liquid desiccant

4.1.1 Surface wettability

Surface wettability represents the ability of the liquid wetting on the solid surface. The wettability of the solid surface is mainly determined by surface forces, including the adhesive and cohesive forces. The adhesive forces between the solid force and liquid cause the liquid to spread over the solid surface, while the cohesive forces within the liquid droplet cause the liquid to avoid contact with the solid surface.

The wettability can be categorized according to the contact angles of the liquid droplets on the surface. The contact angle is the angle at which the liquid-vapor interface meets the solid-liquid interface. Fig 4.2 shows the water droplets on different wetting surfaces. Surface A is hydrophobic surface and Surface B is hydrophilic surface. Surface A has a large contact angle, and the surface B has a small contact angle. The contact angle is determined by the resultant between adhesive and cohesive forces. As the tendency of a drop to spread out over a flat, solid surface increases, the contact angle decreases. As shown in Table 4.1, the wettability can be dived into four stages, i.e., super-hydrophilic, hydrophilic, hydrophobic and super-hydrophobic, according to the contact angles.

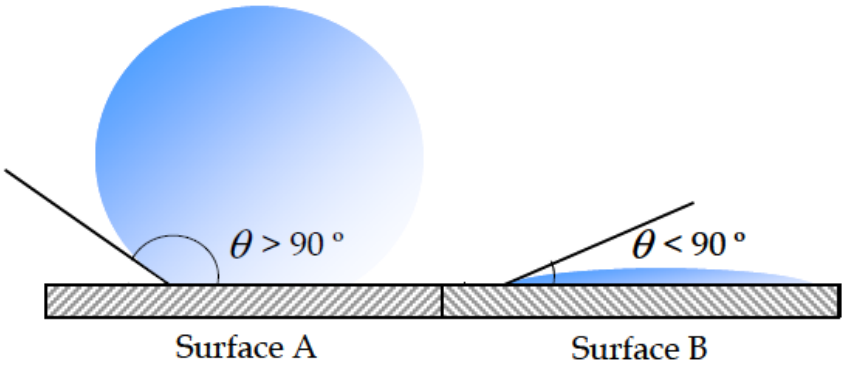

Fig 4.2 Water droplets on different wetting surfaces

Table 4.1 Wettability and contact angels

Surface types	Contact angles (°)
Super-hydrophilic surface	θ<10°
Hydrophilic surface	10°< θ <1°
Hydrophobic surface	90°< θ <150°
Super-hydrophobic surface	150°< θ <180°

4.1.2 Wetting models

There are several models for interface force equilibrium. Young [Young 1805] developed a simple equation to describe the relationship between the interface force among the three phases, as shown in Fig 4.3.

$$\gamma_{SG} = \gamma_{SL} + \gamma_{LG} \cos\theta^{eq} \quad (48.)$$

where γ_{SG}, γ_{SL}, γ_{LG} represent solid-gas surface tension, solid-liquid surface tension and liquid-gas surface tension, respectively. Subsequently, this predicts the contact angle of a liquid droplet on a solid surface from knowledge of the three surface energies involved.

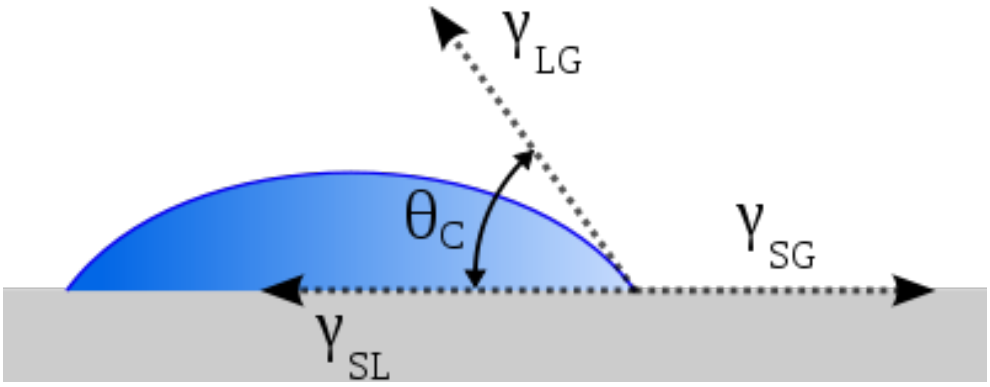

Fig 4.3 Contact angle of the liquid droplet on the solid surface

As Young Equation can only be applied in ideal smooth solid surface, many investigators developed improved models based on Young Equation to describe the force equilibrium on rough solid surface. Amongst the existing models, Wenzel model [Wenzel 1936] and Cassie-Baxter model [Cassie-Baxter 1944] are the two main models that attempt to describe the wettability on rough solid surface.

Wenzel [Wenzel 1936] developed an equation to describe the relationship between the apparent contact angle on rough solid surface and the ideal contact angel on smooth surface calculated by Young Equation. Fig. 4.4(a) shows the schematic of Wenzel model.

$$cos\theta_r = rcos\theta \qquad (49.)$$

where θ_r is the apparent contact angle on rough solid surface and θ is the ideal contact angle on ideal smooth solid surface. *r* is the roughness ratio, which is defined as the ratio of the actual area of the solid surface to the apparent area. In Wenzel's model, the roughness grooves of the solid surface was assumed to be fully filled with liquid, as shown in Fig. 4.4 (a), therefore, the roughness ratio *r* was usually bigger than one.

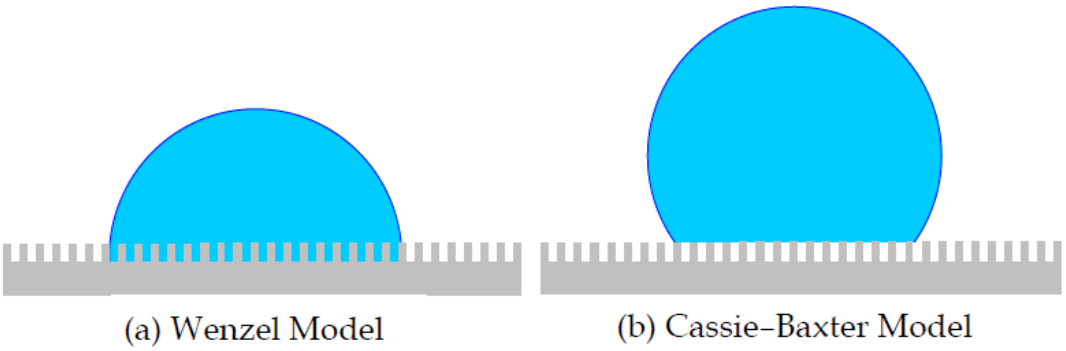

Fig 4.4 Models for rough surface

As the small grooves of the solid surface cannot be filled by the liquid due to the surface tension effect in some cases, Cassie and Baxter [Cassie & Baxter 1944] developed a compound model based on Wenzel model. In Cassie-Baxter model, the roughness grooves was filled by gas instead of liquid, as shown in Fig 4.4(b). Two wetting area factors, f_1 and f_2, were introduced in the model. f_1 represents the ratio of the contact area between the liquid and the solid surface to the total area, while f_2 represents the ratio of the contact area between the liquid and gas in the roughness grooves to the total area.

$$cos\theta_c = f_1 cos\theta + f_2 cos\theta_g \qquad (50.)$$

where θ_g is the contact angle of the liquid in the air, which is usually assumed to be 180°. Therefore, Eq. 50 can be simplified as follows:

$$cos\theta_c = f_1(cos\theta + 1) - 1 \qquad (51.)$$

4.2 Lattice Boltzmann models on wetting boundary

The wetting boundary treatment is a big challenge in lattice Boltzmann simulation. Yan and Zu [Yan & Zu 2007] developed a LB model for simulate the liquid droplet behavior on partial wetting surfaces with density ratio with a simple bounce back boundary scheme applied. While the results of their simulations agreed well with the theoretical prediction in equilibrium situations, the comparison of transient profiles

between simulation and theory or experiments was not reported. Mazloomi et al [Mazloomi et al. 2015] applied the entropic lattice Boltzmann stabilization mechanism to control the dynamics at the liquid-vapor interface and developed a novel entropic lattice Boltzmann model (ELBM) for multiphase flows. The model is used to investigate the dynamics of the contact line in a wide range of applications, from capillary filling to liquid drop impact onto a flat surfaces with different wettability [Mazloomi et al. 2015]. They further extended the model to simulate large Weber and Reynolds number collisions of two droplets with a novel polynomial equation of state. Accurate three-dimensional simulations involving realistic macro-textured surfaces were performed based on the ELBM. Liu and Lee [Liu & Lee 2009] assumed that the intermolecular forces between solid and fluid can be represented by the inclusion of the surface free energy in the expression of the total free energy. Based on the Cahn theory they proposed three kinds of polynomial boundary conditions: linear, quadratic, and cubic to predict the contact angle and density distribution around the wall and made comparisons. The results shown that these three types of boundary conditions have own particular advantages on specific cases. The cubic boundary scheme was applied in Lee and Liu's work on contact angle simulation and showed good accuracy [Lee & Liu 2010]. Connington and Lee [Connington & Lee 2013] then extended the model [Lee & Liu 2010] to simulate the behavior of droplets on super hydrophobic surfaces with a new implementation of boundary conditions for the complex geometry and an

addition of extra force in 2013. The simulations reproduced the experimental contact angles well both in the Cassie and Wenzel states (on surfaces with different roughness), however, the transition between these states, which is a dynamic process, was not successfully modelled. Therefore, it can be concluded that the moving contact line phenomenon is not easy to reproduce by LB method.

4.2.1 Treatment of wetting wall boundary

When the gas-liquid interface contacts the solid wall, a contact angle is formed. The contact angle at steady state can be obtained by the surface tension between gas-liquid, liquid-solid, and gas-solid (Eq. 48). This equation is the starting point of the wetting boundary treatment in lattice Boltzmann method. The Young equation indicates that the contact angle and is related to the surface tension between the three phases of gas-liquid-solid, and the surface tension can be obtained from the free energy function of the system.

For a two-phase flow system without considering the effect of the wall, the equilibrium state of the fluid can be expressed as follows

$$\Phi_b = \int_V \big(\Phi(T,\rho)\big)\, dV + \frac{\kappa}{2}(\partial_\alpha \rho)^2 \qquad (52.)$$

Where Φ is the free energy density and ρ is the fluid density, the gradient term in the

equation represents the influence on the bulk free energy by flow interface. κ is a constant related to the surface tension and α represents Cartesian coordinate. In the two phase lattice Boltzmann model based on Enskog theory, Φ can be written as follows

$$\Phi = \beta(\rho - \rho_l^{sat})^2\left(\rho - \rho_g^{sat}\right)^2 \tag{53.}$$

In which ρ_l^{sat} and ρ_g^{sat} represents the equilibrium density of liquid phase and gas phase, β is related to the surface tension constant κ, interface thickness D and the equilibrium density ρ_l^{sat} and ρ_g^{sat}. Through variational calculations we can obtain the interface distribution at equilibrium state, which satisfies the following equation

$$\frac{\partial \Phi}{\partial \rho} - \kappa \nabla^2 \rho = \mu = const \tag{54.}$$

By Eq. 53 and 54, the surface tension between gas and liquid is obtained as

$$\sigma_{lg} = \frac{(\rho_l - \rho_g)^3}{6}\sqrt{2\kappa\beta} \tag{55.}$$

When the gas-liquid system encounters a wettable solid wall, Cahn pointed out that the wettability of the solid wall can be expressed by miscibility gap, and the system has a critical point. Cahn suggested that an interface equation to determine the

boundary conditions can be imposed on the system, and the behavior of the critical point behavior can be studied by this interface equation. According to Cahn's theory, the free energy of the system includes solid-fluid coupled freedom in addition to the bulk free energy,

$$\Phi_{total} = \Phi_b + \Phi_s = \int_V \big(\Phi(T,\rho)\big)\, dV + \frac{\kappa}{2}(\partial_\alpha \rho)^2 + \int_S \Phi_s(\rho_s) dS \qquad (56.)$$

In which ρ_s is the density on the solid wall. It can be obtained by minimizing the free energy of solid surface and the bulk phase area at equilibrium state, which is expressed as

$$\frac{\kappa}{2}\left(\frac{d\rho}{dx}\right)^2 = \Phi(T,\rho) \quad x > 0 \qquad (57.)$$

$$\kappa \frac{d\rho}{dx} = \frac{d\Phi_s}{d\rho_s} \qquad x = 0 \qquad (58.)$$

If the solid wall free energy takes the form of a power series, for example,

$$\Phi_s(\rho_s) = -\Phi_1 \rho_s \qquad (59.)$$

The Eq. 58 comes to

$$\kappa \frac{d\rho}{dx} = -\Phi_1 \qquad (60.)$$

Substitute Eq.57 into Eq. 58, we obtain

$$-\Phi_1 = \pm\sqrt{2\kappa\Phi_s(\rho_s)} \tag{61.}$$

By solving this equation we can obtain the equilibrium density at the solid-gas and solid-liquid surface as

$$\rho_{s,g} = \frac{\rho_s^{sat} + \rho_g^{sat} - (\rho_l^{sat} - \rho_g^{sat})\sqrt{1-\omega}}{2} \tag{62.}$$

$$\rho_{s,l} = \frac{\rho_l^{sat} + \rho_g^{sat} + (\rho_l^{sat} - \rho_g^{sat})\sqrt{1-\omega}}{2} \tag{63.}$$

Where ω is the wetting potential,

$$\omega = \frac{4\Phi_1}{\left(\rho_l^{sat} - \rho_g^{sat}\right)^2}\sqrt{2\kappa\beta} \tag{64.}$$

The surface tension between solid and fluid can be obtained by

$$\sigma_{s,f} = -\Phi_1\rho_s + \int_S \sqrt{2\kappa\Phi}\, d\,\rho \tag{65.}$$

The contact angle at equilibrium can be obtained according to the Young equation

$$cos\theta = \frac{(1+w)^{3/2} - (1-w)^{3/2}}{2} \tag{66.}$$

Many researches indicate that a power series of free energy density would cause some errors. The cubic form of surface free energy density is more recommended (Liu & Lee 2009)

$$\Phi_s = -\frac{1}{3}\Phi_3{\rho_s}^3 + \frac{\Phi_3\left(\rho_g^{sat} + \rho_l^{sat}\right){\rho_s}^2}{2} - \Phi_3\rho_g^{sat}\rho_l^{sat}\rho_s \qquad (67.)$$

When the cubic form is used, the surface tension of solid-liquid, solid-gas and liquid-gas are as

$$\sigma_{l,g} = \frac{(\rho_l - \rho_g)^3}{6}\sqrt{2\kappa\beta} \qquad (68.)$$

$$\sigma_{s,g} = \frac{6(\rho_l^{sat})^2\rho_g^{sat} - (\rho_l - \rho_g)^3}{6}w\sqrt{2\kappa\beta} \qquad (69.)$$

$$\sigma_{s,l} = \frac{6(\rho_g^{sat})^2\rho_l^{sat} - (\rho_l - \rho_g)^3}{6}w\sqrt{2\kappa\beta} \qquad (70.)$$

In which

$$w = -\frac{\Phi_3}{\sqrt{2\kappa\beta}} \qquad (71.)$$

According the Young equation, the following boundary condition can be obtained.

$$\boldsymbol{n} \cdot \rho_s = -\frac{6\sigma}{(\rho_l - \rho_g)^3} cos\theta(\rho - \rho_l)(\rho - \rho_g) \quad (72.)$$

4.3 Numerical tests

In this section, the case of equilibrium droplet on wetting surfaces is chosen to validate the proposed wetting boundary treatment method. The cubic form of surface free energy density is taken. The lattice Boltzmann model proposed in Chapter 3 is used to perform the benchmark case.

In this benchmark case, a rectangle computational domain with a grid size of $NX \times NY$ is chosen. A two-dimensional liquid droplet with a radius of R is initially generated at the center of the wetting surface (as shown in Fig 4.5a). The periodic boundaries are implemented at the left and right sides and the developed new wall boundary conditions are applied to the top and bottom boundaries. While the top surface has a fixed contact angle of $\theta^{eq} = 90°$, different contact angles ranging from $30°$ to $150°$ are assumed on the bottom surface.

The density ratio (the heavier over the lighter fluid, ρ^*) is taken as 1000 and $Cn = 20$. The other parameters are set as: $NX = 600, NY = 200, R = 80$. Fig 1 shows the equilibrium states of the droplet on wetting surfaces with contact angles of $\theta^{eq} = 30°, 60°, 90°, 120°$ and $150°$, in which the color represents the density while the red

part and blue part are corresponding to the liquid droplet and the gas, respectively. Eq. 72 gives the theoretical relationship between θ^{eq} and wetting potential *w*. The comparison between the simulated results and analytical solutions is presented in Fig. 3.2. The simulated equilibrium contact angles are measured by the geometric formula of droplet height and the length of contact line based on Fig 4.5 (b) to (f). The figure shows that angles obtained by the present model agree well with the analytical ones. Furthermore, the droplet automatically achieved equilibrium state from initial state after a short period, which indicates that the current model is appropriate to handle the contact angle issue.

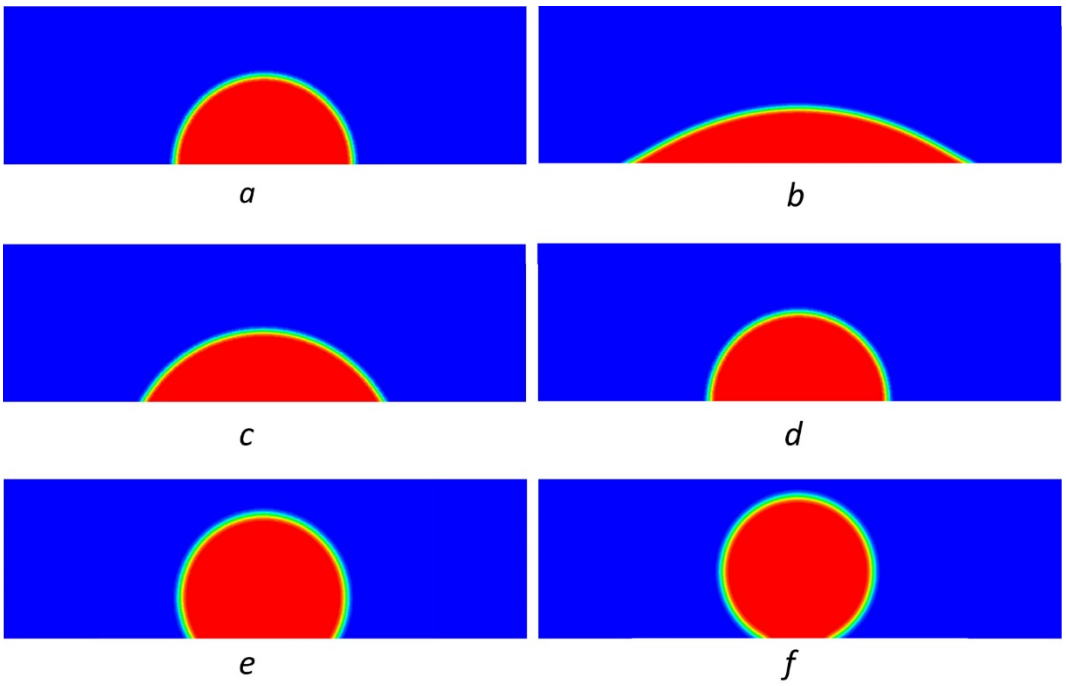

Figure 4.5 Equilibrium state of droplets on surfaces with different contact angles. a: initial state, b: 30º, c: 60º, d: 90º, e: 120º, f: 150º.

4.4 Summary

In falling film research, the wetting area of liquid desiccant is an important parameter in the dehumidifier. In early stage of the simulation model for liquid desiccant dehumidifier, the working plate was usually assumed to be fully wetted by liquid desiccant, which did not comply with the experimental observation. In actual situations, the working surfaces were usually observed to be incompletely wetted by the liquid desiccant. Therefore, it is very important to properly simulate the wetting boundary in falling film.

Surface wettability represents the ability of the liquid wetting on the solid surface. The wettability of the solid surface is mainly determined by surface forces, including the adhesive and cohesive forces. The adhesive forces between the solid force and liquid cause the liquid to spread over the solid surface, while the cohesive forces within the liquid droplet cause the liquid to avoid contact with the solid surface.

In this Chapter, the wetting boundary treatment method is proposed. The cubic form of surface free energy density is taken. The proposed wetting boundary treatment method is used in the lattice Boltzmann model developed in Chapter 3, and numerical

test is performed by this model. The result shows that the proposed wetting boundary treatment method can properly handles the contact angle issue.

CHAPTER 5

DEVELOPMENT OF A MASS CONSERVATIVE LATTICE BOLTZMANN MODEL FOR TWO-PHASE FLOWS WITH MOVING CONTACT LINES AT HIGH DENSITY RATIO

In this chapter, a mass conservative lattice Boltzmann model (LBM) is proposed to simulate the two-phase flows with moving contact lines at high density ratio. The proposed model consists of a phase field lattice Boltzmann equation (LBE) for solving the conservative Allen-Cahn (A-C) equation, and a pressure evolution LBE for solving the incompressible Navier-Stokes equations. In addition, a modified wall boundary treatment scheme is developed to ensure the mass conservation. The wetting dynamics are treated by incorporating the cubic wall energy in the expression of the total free energy. The current model is characterized by mass conservation, proper treatment of wetting boundary and high density ratio. We applied the model on a series of numerical tests including equilibrium droplets on wetting surfaces, co-current flow and a droplet moving by gravity along inclined wetting surfaces. Theoretical analysis and experiments were conducted for model validation. The numerical results show good performances on mass conservation even with a density contrast up to 1000.

Furthermore, the results show that the moving contact line can be successfully recovered, which proves that this model is applicable on the study of moving contact line issue and further related applications.

5.1 Introduction

The behavior of droplets on wetting surfaces is always a popular research topic because it is the multiphase flow fundamental of many engineering applications. The contact angle, which is defined as the angle between the contact line and the solid surface, is an important parameter characterizing the wettability, which significantly influence the behavior of droplets on wetting surfaces. If the solid surface is not horizontal and the gravity exists, the droplet may move on the surface and so as the triple contact line. In this situation, the moving contact line is observed and dynamic contact angles should be defined to feature this phenomenon. The study of the moving contact line is of great significance in engineering applications such like chip cooling, painting, coating and falling film based liquid desiccant technology [Lu & Xiao 2018]. The mechanism of formation of contact line has been studied theoretically by many researchers and it is possible to predict the final equilibrium state of contact lines. However, the transition process, which is important for understanding the mechanism of moving contact line phenomenon, has not been sufficiently understood in previous theoretical studies. Considering the difficulties in conducting experimental study,

numerical methods are more competent for studying the moving contact line.

The lattice Boltzmann method (LBM), which is a numerical method rooted in kinetic theory, is becoming popular in the fields of computational fluid dynamics in last decades. Due to the particle-based mesoscopic nature which connects the micro and macro worlds, the LBM has an advantage in simulation fidelity and computational efficiency especially for multiphase flows. A number of LB models for multiphase flows have been developed in previous researches, such as color-gradient model [Rothman & Keller 1988], Shan-Chen model [Shan & Chen 1993], free energy model [Swift & Osborn 1995] and phase-field model [He et al. 1999]. An extended Shan-Chen method, in which the equation of state (EOS) and surface tension can be tuned independently, was developed by Sbragaglia et al to analyze the physical behavior of a class of mesoscopic models for multiphase flows [Sbragaglia 2007]. Colosqui presented a dynamic optimization strategy to generate customized equations of state for the numerical simulation of non-ideal fluids at high density ratio [Colosqui et al. 2012]. The phase-field LB model, which is originally developed by He et al. [He et al. 1998] in 1998, has been proved applicable to high density ratio issue, which is a key challenge in modelling moving contact angle. Two distribution functions are taken in this model, one is for describing the fluid dynamics and the other is used to track the phase interface, and two macroscopic equations can be recovered from the distribution

functions. The combination of Navier–Stokes (N-S) and Cahn-Hilliard (C-H) equation is applied in many phase field LBMs. Lee and Liu [Lee & Liu 2010] successfully simulate the contact angle at high density ratio with a proposed C-H based LBM. Liang et al [Liang et al 2014] reported their C-H based LBM can properly describe the axisymmetric multiphase flows. However, due to the simplification made in the recovering process, the C-H based phase field LBMs cannot ensure mass conservation. Around 1% of mass change ratio was observed in Connington and Lee's work [Connington & Lee 2013]. Although the error is not large, it may be unacceptable in some special applications. For example, Zheng et al [Zheng et al. 2014] reported that in their modelling, the small droplets disappeared if their radius was below a critical value. A conservative LBM for interface tracking was proposed by Fakhari et al [Fakhari et al. 2016] in 2016. The model was also based on the phase field theory, but it recovered the Allen-Cahn (A-C) equation instead of the Cahn-Hilliard equation, while the former is conservative. Due to its advantages in mass conservation, the A-C based LBM is becoming more popular. The newly developed model by Fakhari et al [Fakhari et al. 2016] has shown great advantage in terms of mass conservation, speed-up and efficiency compared to the Lee and Liu's C-H based model [Lee & Liu 2010] on the contact angle simulation. Liang et al [Liang et al. 2018] investigated the droplet impact on a thin liquid film with a large density ratio of 1000 and successfully reproduced the droplet splashing phenomenon with a A-C based LB model. However,

many A-C based LBMs are proposed for the equilibrium problems, whether the method can be applied on the moving contact line is still unknown.

Another big challenge in moving contact line simulation by LBM is the treatment of wetting boundary. Yan and Zu [Yan & Zu 2007] developed a LB model for simulate the liquid droplet behavior on partial wetting surfaces with density ratio with a simple bounce back boundary scheme applied. While the results of their simulations agreed well with the theoretical prediction in equilibrium situations, the comparison of transient profiles between simulation and theory or experiments was not reported. Mazloomi et al applied the entropic lattice Boltzmann stabilization mechanism to control the dynamics at the liquid-vapor interface and developed a novel entropic lattice Boltzmann model (ELBM) for multiphase flows [Mazloomi et al. 2015]. The model is used to investigate the dynamics of the contact line in a wide range of applications, from capillary filling to liquid drop impact onto a flat surfaces with different wettability [Mazloomi et al. 2015]. They further extended the model to simulate large Weber and Reynolds number collisions of two droplets with a novel polynomial equation of state. Accurate three-dimensional simulations involving realistic macro-textured surfaces were performed based on the ELBM. Liu and Lee [Liu & Lee 2009] assumed that the intermolecular forces between solid and fluid can be represented by the inclusion of the surface free energy in the expression of the total free energy. Based on the Cahn theory they proposed three kinds of polynomial

boundary conditions: linear, quadratic, and cubic to predict the contact angle and density distribution around the wall and made comparisons. The results shown that these three types of boundary conditions have own particular advantages on specific cases. The cubic boundary scheme was applied in Lee and Liu's work on contact angle simulation and showed good accuracy [Lee & Liu 2010]. Connington and Lee [Connington & Lee 2013] then extended the model [Lee & Liu 2010] to simulate the behavior of droplets on super hydrophobic surfaces with a new implementation of boundary conditions for the complex geometry and an addition of extra force in 2013. The simulations reproduced the experimental contact angles well both in the Cassie and Wenzel states (on surfaces with different roughness), however, the transition between these states, which is a dynamic process, was not successfully modelled. Therefore, it is still a challenge to reproduce the moving contact line phenomenon by LB method.

5.2 Description of the developed lattice Boltzmann model

5.2.1 Discrete Boltzmann Equations for Incompressible Two-phase Fluids

The Navier-Stokes equation is usually adopted to describe the fluid dynamics, and it can be recovered by the particle distribution function $\boldsymbol{f}$ in lattice Boltzmann methods. The governing equation of $\boldsymbol{f}$, which is the discrete Boltzmann equations (DBE)

describing the transportation of density and momentum of the incompressible two-phase fluids, is taken as

$$\left(\frac{\partial}{\partial t}+\boldsymbol{e}_{\alpha}\cdot\nabla\right)f_{\alpha}=-\frac{1}{\lambda}\left(f_{\alpha}-f_{\alpha}^{eq}\right)+\frac{1}{{c_s}^2}(\boldsymbol{e}_{\alpha}-\boldsymbol{u})\cdot\boldsymbol{F}\Gamma_{a} \qquad (73.)$$

where f_{α}, e_{α} are the particle distribution function and the velocity of particle in direction α, u is the macro velocity, c_s is the lattice sound speed and λ is the relaxation time, $\Gamma_a = \Gamma_a(\boldsymbol{u}) = f_{\alpha}^{eq}/\rho$, and f_{α}^{eq} is the equilibrium distribution function which is defined by Eq. 74

$$f_{\alpha}^{eq}=\omega_{\alpha}\rho\left[1+\frac{\boldsymbol{e}_{\alpha}\cdot\boldsymbol{u}}{c_s^2}+\frac{(\boldsymbol{e}_{\alpha}\cdot\boldsymbol{u})^2}{2c_s^4}-\frac{(\boldsymbol{u}\cdot\boldsymbol{u})}{2c_s^2}\right] \qquad (74.)$$

where ω_{α} donates the weight factor.

The force terms F in Eq. 73 can have different forms. In this study we take the force scheme proposed by Lee and Liu [Lee & Liu 2010]

$$\boldsymbol{F}=\nabla\rho c_s^2-\nabla p+\mu\nabla\phi+\boldsymbol{F}_b \qquad (75.)$$

in which ϕ is order parameter referring different phases, F_b is the body force and μ represents the chemical potential, which is a function of the order parameter ϕ

$$\mu = 4\beta(\phi - \phi_h)(\phi - \phi_l)\left(\phi - \frac{\phi_h + \phi_l}{2}\right) - \kappa\nabla^2 C \qquad (76.)$$

where ϕ_h and ϕ_l indicate the different phases and are referred as 1 (liquid phase) and 0 (gas phase). κ and β are the parameters related to the surface tension σ and interface width W. This scheme can ensure that the computation of F in collision process is local.

Similar to using the h_α to recover Allen-Cahn equation, a new distribution function, g, is introduced here to describe the evolution of pressure p, which is defined as

$$g_\alpha = f_\alpha c_s^2 + \omega_\alpha(p - \rho c_s^2) \qquad (77.)$$

and the corresponding equilibrium distribution function of g is defined as

$$g_\alpha^{eq} = \omega_\alpha\left[p + \rho c_s^2\left(\frac{\boldsymbol{e}_\alpha \cdot \boldsymbol{u}}{c_s^2} + \frac{(\boldsymbol{e}_\alpha \cdot \boldsymbol{u})^2}{2c_s^4} - \frac{(\boldsymbol{u} \cdot \boldsymbol{u})}{2c_s^2}\right)\right] \qquad (78.)$$

According to Eq. 73 the DBE for the new variable g_α is taken as

$$\left(\frac{\partial}{\partial t} + \boldsymbol{e}_\alpha \cdot \nabla\right) g_\alpha = -\frac{g_\alpha - g_\alpha^{eq}}{\lambda} + (\boldsymbol{e}_\alpha - \boldsymbol{u}) \cdot [\nabla \rho c_s^2(\Gamma_a - \omega_\alpha) + \boldsymbol{F}_b + \mu\nabla\phi)\Gamma_a (79.)$$

Noticing that $\rho = \rho_l + \phi(\rho_h - \rho_l)$, in which ρ_h and ρ_l represent the densities of liquid and gas phases. Accordingly we have

$$\nabla\rho = (\rho_h - \rho_l)\nabla\phi \tag{80.}$$

which can bring a great reduction of computation loads for $\nabla\rho$.

The DBE for g_α can also be split into collision and streaming processes. To simplify the calculation, the modified distribution functions $\bar{g}_\alpha$ as well as their equilibrium functions $\bar{g}_\alpha^{eq}$ are introduced as follows

$$\bar{g}_\alpha = g_\alpha + \frac{1}{2\tau}\left(g_\alpha - g_\alpha^{eq}\right) - \frac{\delta_t}{2}(\boldsymbol{e}_\alpha - \boldsymbol{u}) \cdot [\nabla\rho c_s^2(\Gamma_a - \omega_\alpha) + (\mu\nabla\phi + \boldsymbol{F}_b)\Gamma_a] \tag{81.}$$

$$\bar{g}_\alpha^{eq} = g_\alpha^{eq} - \frac{\delta_t}{2}(\boldsymbol{e}_\alpha - \boldsymbol{u}) \cdot [\nabla\rho c_s^2(\Gamma_a - \omega_\alpha) + (\mu\nabla\phi + \boldsymbol{F}_b)\Gamma_a] \tag{82.}$$

where τ is the dimensionless relaxation time which is defined as $\tau = \lambda/\delta_t$, and δ_t is the time step.

Finally the collision process can be expressed as followed

$$\tilde{g}_a(\boldsymbol{x}, t) = \bar{g}_\alpha(\boldsymbol{x}, t) - \frac{\left(\bar{g}_\alpha - \bar{g}_\alpha^{eq}\right)|_{(\boldsymbol{x},t)}}{\tau} + \delta_t(\boldsymbol{e}_\alpha - \boldsymbol{u}) \cdot [\nabla\rho c_s^2(\Gamma_a - \omega_\alpha) + (\mu\nabla\phi + \boldsymbol{F}_b)\Gamma_a]_{(\boldsymbol{x},t)} \tag{83.}$$

where $\tilde{g}_a(x, t)$ is the updated $\bar{g}_\alpha$ after the collision.

The streaming is then carried out under the perfect shift scheme

$$\bar{g}_\alpha(\boldsymbol{x} + \boldsymbol{e}_\alpha \delta_t, t + \delta_t) = \tilde{g}_a(\boldsymbol{x}, t) \tag{84.}$$

5.2.2 Discrete Boltzmann Equations (DBE) for the Allen-Cahn Equation

The Allen–Cahn equation is a phase field equation which describes the process of phase separation in multi-phase systems. The order parameter $\phi(\boldsymbol{x}, t)$ is used in the phase field model to track the two-phase interface, which satisfies the following conservative Allen-Cahn equation

$$\frac{\partial \phi}{\partial t} + \nabla \cdot \phi \boldsymbol{u} = \nabla \cdot \left[M \left(\nabla \phi - \frac{1 - 4\left(\phi - \frac{(\phi_h + \phi_l)}{2} \right)^2}{W} \right) \boldsymbol{n} \right] \tag{85.}$$

where ϕ_h and ϕ_l indicate the different phases and $(\phi_h + \phi_l)/2$ locates the interface in the impressible two-phase flows (ϕ_h, $\phi_l$are referred as 1 and 0 in this study to represent the two phases). The parameters M, u, W represent the mobility, macroscopic velocity and interface width respectively, and $\boldsymbol{n}$ is the normal vector to the interface, which is defined by

$$\boldsymbol{n} = \frac{\nabla \phi}{|\nabla \phi|} \tag{86.}$$

When the system reaches an equilibrium state, the equilibrium distribution of ϕ along the direction z normal to the interface is assumed as a hyperbolic tangent profile

$$\phi(z) = \frac{(\phi_h + \phi_l)}{2} + \frac{(\phi_h - \phi_l)}{2} \tanh\left(\frac{2z}{W}\right) \quad (87.)$$

A new function h_α, which is the distribution function of ϕ, is introduced for solving Eq. 85, and the LB equation of h_α is

$$\left(\frac{\partial}{\partial t} + \boldsymbol{e}_\alpha \cdot \nabla\right) h_\alpha = -\frac{h_\alpha - h_\alpha^{eq}}{\lambda} \quad (88.)$$

where λ is the relaxation time related to the phase-field parameters.

The equilibrium distribution function of h_α is

$$h_\alpha^{eq} = \phi\Gamma_a + B\omega_\alpha \boldsymbol{e}_\alpha \cdot \boldsymbol{n} \quad (89.)$$

where the term $B\omega_\alpha e_\alpha \cdot n$ accounts for anti-diffusion and in which

$$B = \frac{M}{{c_s}^2}\left[\frac{1 - 4\left(\phi - \frac{(\phi_h + \phi_l)}{2}\right)^2}{W}\right] \quad (90.)$$

Following the original lattice Boltzmann scheme, the distribution function h_α is

going through the collision and streaming processes. In the collision process, h_α satisfies

$$\tilde{h}_a = h_\alpha - \frac{h_\alpha - h_\alpha^{eq}}{\tau_h} \quad (91.)$$

where τ_h is the dimensionless relaxation time and is related to the mobility by

$$\tau_h = 0.5 + \frac{M}{{c_s}^2 \delta t} \quad (92.)$$

After the collision process, the streaming occurs under the perfect shift scheme as followed

$$h_\alpha(x + e_\alpha \delta_t, t + \delta_t) = \tilde{h}_a(x, t) \quad (93.)$$

Then, the hydrodynamic parameters such as the average velocity and dynamic pressure can be calculated by taking the zeroth of the distribution function h_α as shown in Eq. 94

$$\phi = \sum_\alpha h_\alpha \quad (94.)$$

After the streaming step, the hydrodynamic parameters such as the average velocity and the dynamic pressure can be calculated by taking the zeroth and first moments of

the particle distribution.

$$\boldsymbol{u} = \frac{1}{\rho}\left(\frac{1}{c_s^2}\sum_{\alpha}\boldsymbol{e}_\alpha \bar{g}_\alpha + \frac{\delta t}{2}(\mu\nabla\phi + \boldsymbol{F}_b)\right) \tag{95.}$$

$$p = \sum_{\alpha}\bar{g}_\alpha + \frac{\delta t}{2}\boldsymbol{u}\cdot\nabla\rho c_s^2 \tag{96.}$$

5.2.3 Treatment of wetting wall boundary

The wetting wall boundary is treated from two respects: the "ordinary" boundary treatment and the wetting boundary treatment. The former is to obtain the distribution functions at the wall points and the latter is to properly reflect the wetting condition in the wall parameters.

Fig 5.1 shows the lattice node configuration on a flat wall (D2Q9 scheme applied), where layer *N* is the boundary layer and x_b is the boundary point of layer *N*, f is the distribution function and i refers to the direction towards the fluid domain while$\bar{\imath}$ points to the opposite direction (towards wall). The traditional bounce back scheme was widely adopted to the "ordinary" boundary treatment, in which the boundary points on layer *N* are not involved into collision process. However, according to our numerical experiments conducted in this study, the traditional bounce back scheme results to the mass unbalance problem, which may be attributed to the absence of

boundary points in the collision process. Therefore, we proposed a modified bounce back scheme in which the boundary points (layer *N*) are involved the standard collision-streaming process as the points inside fluid field (layer *N*-1). The distribution functions towards the fluid domain of boundary points can be obtained as followed

$$f_i(\boldsymbol{x}_b, t) = f_{\bar{i}}(\boldsymbol{x}_b, t + dt) \tag{97.}$$

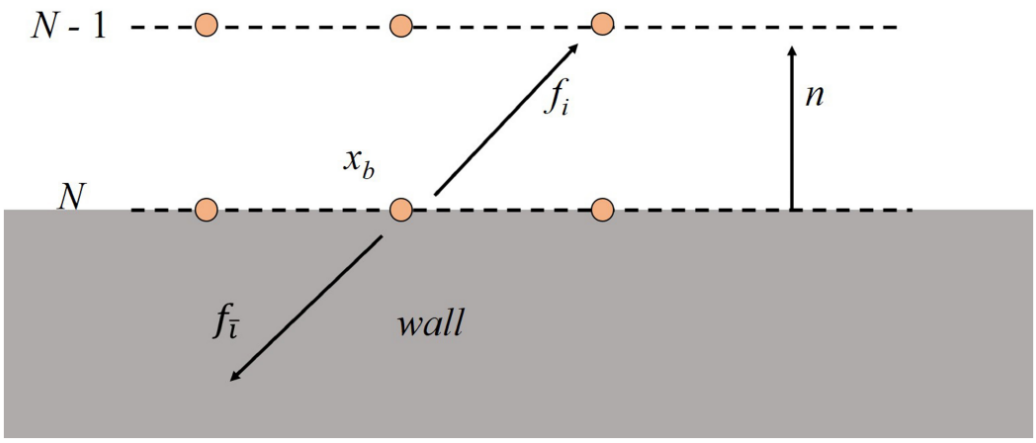

Fig 5.1 Lattice nodes on the flat wall (D2Q9 scheme)

According to the phase-field theory, the free energy of the entire fluid system can be expressed as a function of ϕ

$$\Phi_b + \Phi_s = \int_V \left(E_0(C) + \frac{\kappa}{2}|\nabla\phi|^2\right) dV + \int_S \left(\varphi_0 - \varphi_1\phi_s + \varphi_2{\phi_s}^2 - \varphi_3{\phi_s}^3 + \cdots\right) dS \tag{98.}$$

where E_0 is the bulk energy density and it usually takes the form as $E_0 =$

$\beta C^2(C-1)^2$, κ is a constant related to the surface energy and β is a constant related to bulk energy. The chemical potential is defined as $\mu = \frac{\partial E_0}{\partial C} - \kappa\nabla^2\phi$.

Liu and Lee [Liu & Lee 2009] made an assumption that the fluid behavior along the solid boundary is dominated by the interactions between the solid and liquid-gas interface, so the interactions between the solid and bulk fluids are not taken into consideration. The cubic boundary condition can be constructed based on this assumption and then the parameters in Eq. 98 can be chosen as: $\varphi_0 = \varphi_1$, $\varphi_2 = 1/2\varphi_w$, $\varphi_3 = 1/3\varphi_w$, where φ_w is a constant related to the dimensionless wetting potential *wp* as shown in Eq. 99

$$wp = \varphi_w/\sqrt{2\kappa\beta} \tag{99.}$$

The cubic boundary condition for the order parameter ϕ_s at the wall is finally acquired by neglecting the terms higher than the third order in Φ_s and minimizing the total free energy $\Phi_b + \Phi_s$, which can be expressed as

$$\boldsymbol{n} \cdot \nabla\phi|_s = \left(\phi_s - {\phi_s}^2\right)\varphi_w/\kappa \tag{100.}$$

According to the Young's law, the wetting potential ω can be determined by the equilibrium contact angle θ^{eq}

$$\omega = -\cos\theta^{eq} \tag{101.}$$

Eq. 99, 100 and 101 associate the gradient of order parameter $\nabla\phi$and the contact angle θ^{eq}. The $\nabla\phi$can be calculated with a given θ^{eq}, and then the chemical potential can be obtained by Eq. 100, and finally the macro parameters at the wall can be obtained by Eq. 95, 96.

5.2.4 Calculation of Gradients

Different from the work done by Lee and Liu [20] in which a mixture of central difference and biased difference was taken for the calculation of the gradients, we adopted the central difference to obtain the gradients of the order parameter and the pressure, as defined by Eq. (102)

$$\nabla\phi|_x = \frac{1}{c_s^2\delta_t}\sum_{a\neq 0}\omega_\alpha \boldsymbol{e}_\alpha(\delta_t\boldsymbol{e}_\alpha\cdot\nabla)\phi|_x \tag{102.}$$

$$\delta_t\boldsymbol{e}_\alpha\cdot\nabla^{CD}\phi|_x = \frac{1}{2}[\phi(\boldsymbol{x}+\boldsymbol{e}_\alpha\delta_t)-\phi(\boldsymbol{x}-\boldsymbol{e}_\alpha\delta_t)] \tag{103.}$$

The above DBEs can be discretized by using this finite difference (FD) scheme. For researcher who want to perform a parallel computation algorithm, Fakhari et al [Fakhari et al. 2014] provided a local method using central moments to discretize the

Eq. (86). In this study we choose the finite difference scheme considering it was reported more accurate and stable.

5.3 Numerical tests and discussions

In this section we apply the model on two benchmark cases including equilibrium droplets on wetting surfaces and co-current flow. The results are compared with analytical solutions and experimental results. The behaviors of the water droplets moving by gravity along inclined surfaces such as glass pane and steel plate are then simulated with this model, and the dynamics of moving contact line motion are captured and compared with experimental results.

We adopted the following two dimensionless parameters in analyzing simulation results, the density ratio as defined by Eq. (104) and the Cahn number as defined by Eq. (105)

$$\rho^* = \rho_H/\rho_L \qquad (104.)$$

$$Cn = L_c/W \qquad (105.)$$

where L_c refers the characteristic length and W is the interface width. Cn is often recommended to be greater than 10 to ensure the accuracy of simulations.

5.3.1 Equilibrium droplet on wetting surfaces

In this case, a rectangle computational domain with a grid size of $NX \times NY$ is chosen. A two-dimensional liquid droplet with a radius of R is initially generated at the center of the wetting surface (as shown in Fig 5.2a). The periodic boundaries are implemented at the left and right sides and the developed new wall boundary conditions are applied to the top and bottom boundaries. While the top surface has a fixed contact angle of $\theta^{eq} = 90°$, different contact angles ranging from $30°$ to $150°$ are assumed on the bottom surface.

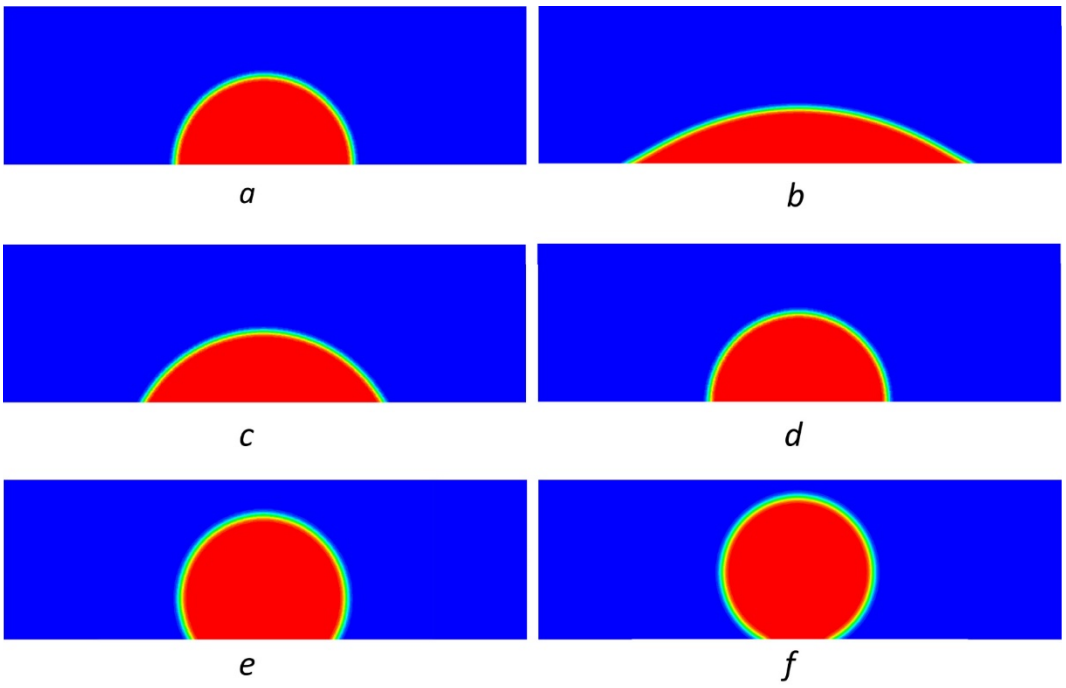

Figure 5.2 Equilibrium state of droplets on surfaces with different contact angles. *a*: initial state, *b*: 30º, *c*: 60º, *d*: 90º, *e*: 120º, *f*: 150º.

The density ratio (the heavier over the lighter fluid, ρ^*) is taken as 1000 and $Cn = 20$. The other parameters are set as: $NX = 600, NY = 200, R = 80$. Fig 1 shows the equilibrium states of the droplet on wetting surfaces with contact angles of $\theta^{eq} = 30°, 60°, 90°, 120°$ and $150°$, in which the color represents the density while the red part and blue part are corresponding to the liquid droplet and the gas, respectively. Eq. (101) gives the theoretical relationship between θ^{eq} and wetting potential *wp*. The comparison between the simulated results and analytical solutions is presented in Fig. 5.3. The simulated equilibrium contact angles are measured by the geometric formula of droplet height and the length of contact line based on Fig 5.2 (b) to (f). The figure shows that the angles obtained by the present model agree well with the analytical ones. Furthermore, the droplet automatically achieved equilibrium state from initial state after a short period, which indicates that the current model is appropriate to handle the contact angle issue.

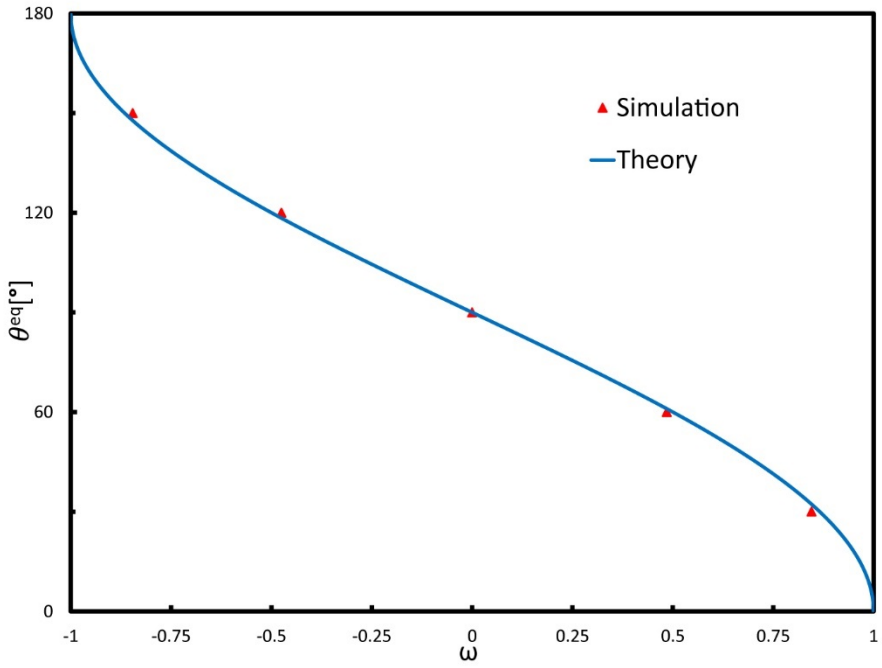

Figure 5.3 The comparison between the equilibrium contact angles between simulation results and analytical data.

Due to the existence of gravity, the actual contact angle may differ from the theoretical ones. The testing-table shown in Fig. 5.4 is used to observe the actual contact angles between water and two surfaces with different materials. Fig. 5.5 compares the experimental and simulation results of different static contact angles while gravity exists, and the difference are $0.2°$ and $0.5°$, respectively. Considering the measuring error, the results by present model agree well with the experiment. It is shown that the actual contact angle can be recovered accurately by our model, which indicates that the incorporation of the gravity works well.

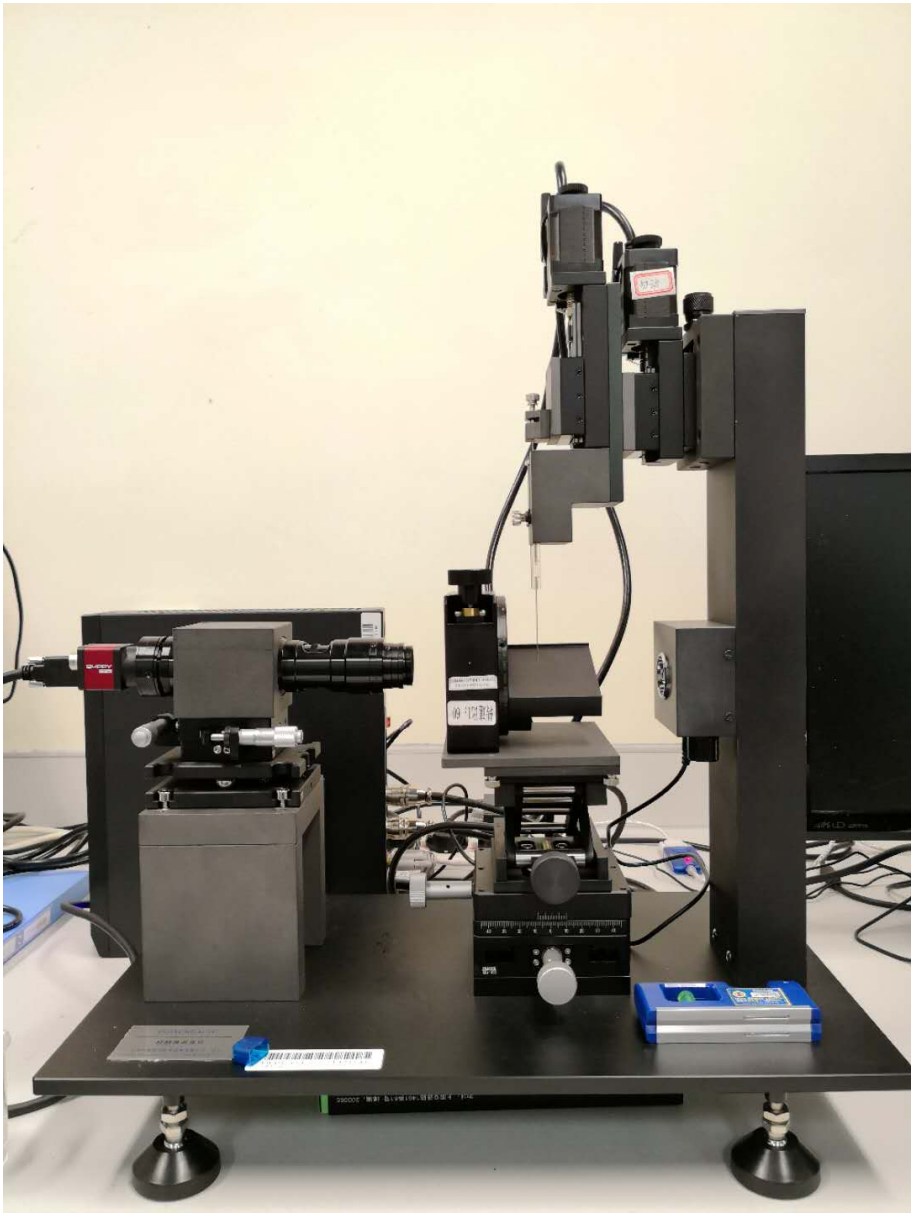

Figure 5.4 Test-table for testing the static and dynamic contact angles.

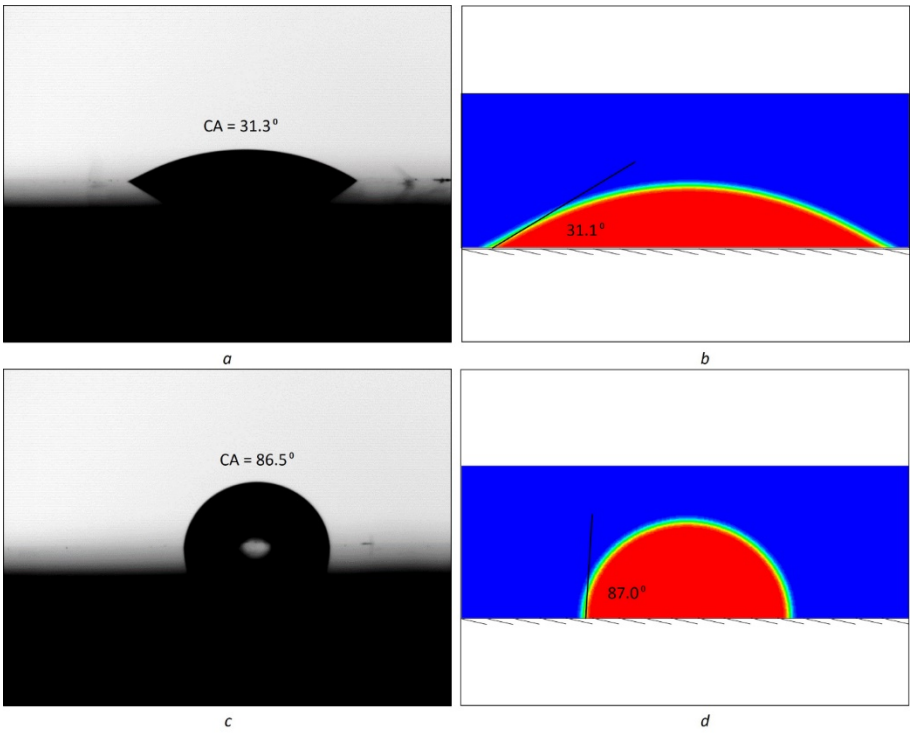

Figure 5.5 Comparison of the experimental and simulation results on actual contact angles. *a*,*c*: experiment, *b*,*d*: simulation.

5.3.2 Mass conservation

One of the most important features of our LB model is that it is mass conservative. The total mass of the system for droplet recovering process shown in Fig. 5.2(b) is checked to verify the mass conservation, and the results obtained from our model are compared with those of the model developed by Lee and Liu [Lee & Liu 2010]. The total mass of the system M is normalized by the initial mass M_0, and its evolution process with dimensionless time is plotted in Fig. 5.6. It can be found that the system mass M gradually decreases with time in the method proposed in Ref. [Lee & Liu

2010]. while the total mass conserves ideally using our model.

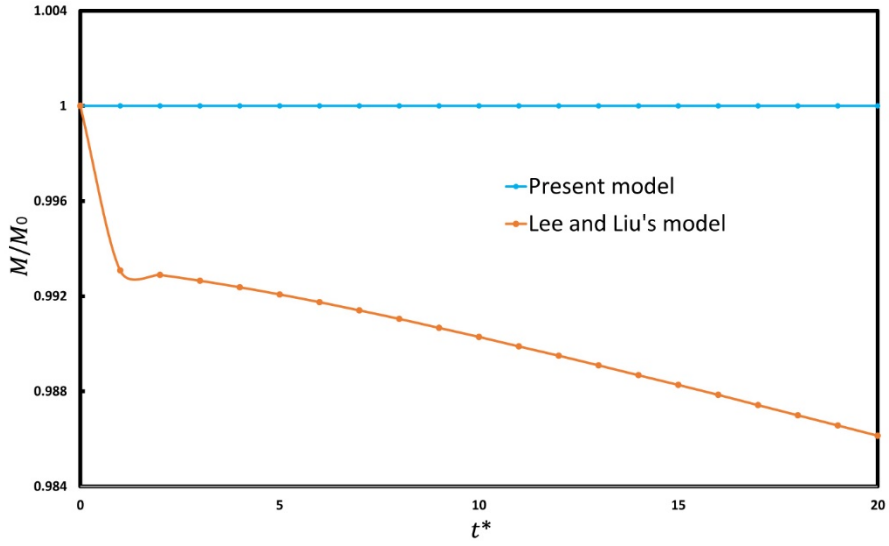

Figure 5.6 Variation of the mass of the system versus time for the droplet recovering process in present model and Lee and Liu's model.

The spurious currents is a considerable issue in the multi-phase LB models. When the magnitude of spurious currents become as large as the characteristic velocities it would severely affected the reliability of the LB simulation results. Fig. 5.7 shows the velocity field around a drop on a surface with contact angle 60 degree (the case of Fig 2 (c)). Vectors are magnified by 3×10^{11} at equilibrium state. It is indicated that the spurious currents have little influence on the results considering the magnitude compared to the characteristic velocity in our model.

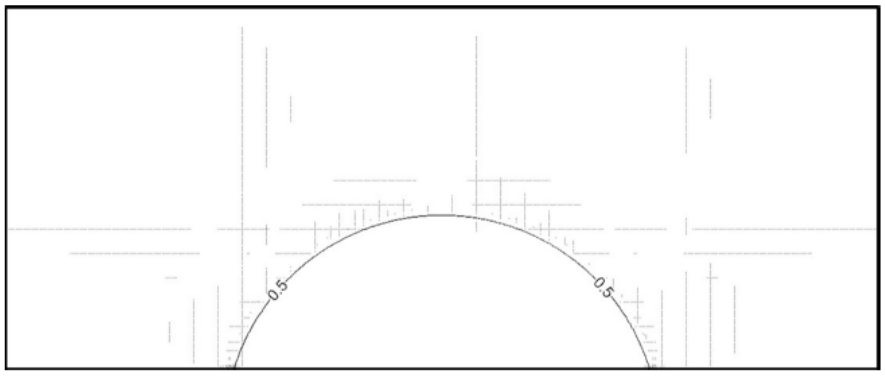

Figure 5.7 Velocity fields around a droplet on a surface with $\theta^{eq} = 60$. Velocity vectors are magnified by 3×10^{11}.The contour level represents ϕ=0.5.

5.3.3 Two-phase co-current flow in the infinite channel

In addition to the static case presented above, the performance of the model in simulating dynamic process is also tested. The two-phase co-current flow driven by an external force $\boldsymbol{F}$ in a channel is simulated. To examine the accuracy and stability of the present model, the symmetric co-current flow in the infinite channel is introduced here and the flow configuration is displayed in Fig. 5.8. The computational domain consists of a rectangle grids system $(NX \times NY)$, while the liquid phase occupies the areas in which $Y = -H1 \sim -H2$ and $Y = H1 \sim H2$, and the remaining area is occupied by the gas phase. Periodic boundaries are implemented at the left and right sides and the developed wall boundary conditions are applied to the top and bottom surfaces. The contact angles θ^{eq} of the top and bottom surfaces are set as $90°$. An external force in x direction, F_x, is exerted on the gas phase or liquid phase,

respectively, which may result in different velocity distributions according to Ref. [Huang et al. 2013].

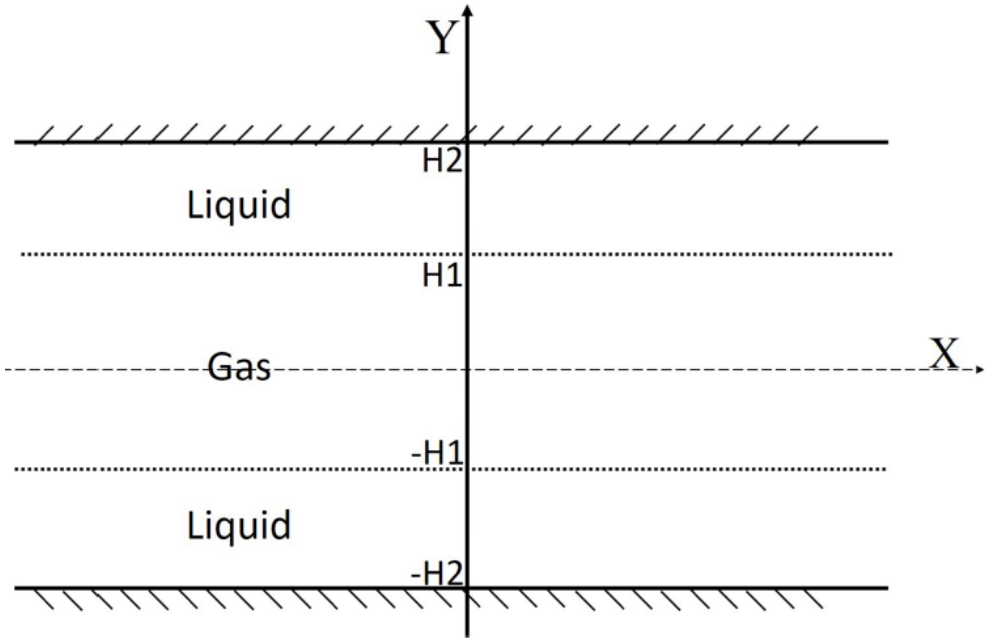

Figure 5.8 The configuration of two-phase co-current flow in the infinite channel.

The density ratio is taken as 1000, i.e. $\rho^* = 1000$ in this case and $Cn = 10$. The other parameters are set as: $NX = 200, NY = 100, H1 = 25, H2 = 50$. Analytical solution for this type of flow can be found in [Huang et al. 2009]. Fig. 5.9 and Fig. 5.10 show the velocity profiles of u_x for cases where F_x is applied on gas and liquid respectively, and the theoretical results are also presented. It can be observed that the velocity profiles obtained from the developed model agree well with analytical solutions.

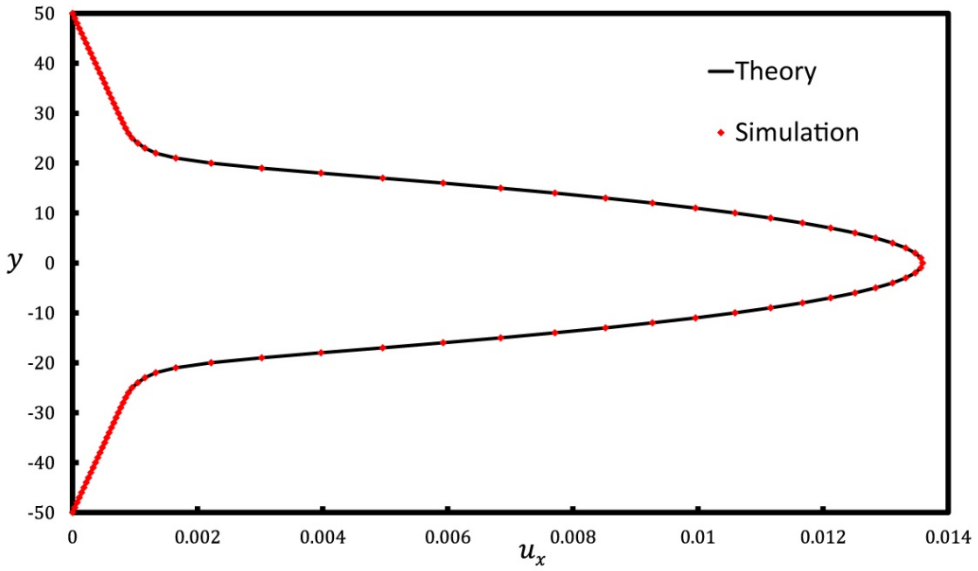

Figure 5.9 Velocity profiles of the co-current flows with F_x applied on the gas.

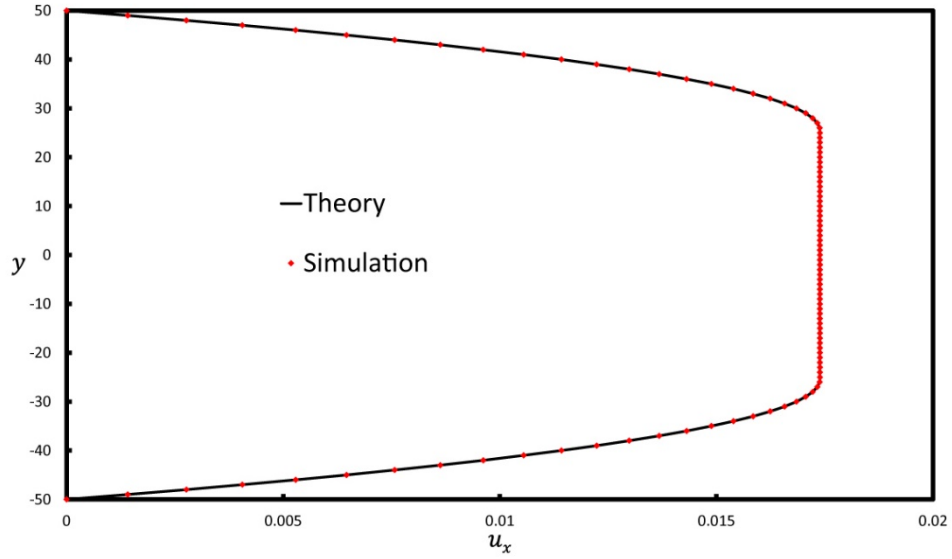

Figure 5.10 Velocity profiles of the co-current flows with F_x applied on the liquid.

5.3.4 Two-phase flow with moving contact line

To investigate the dynamics of two-phase flow with moving contact line, the behaviours of the water droplet moving by gravity along inclined wetting surfaces such as glass pane and steel plate are simulated using the model developed in this study. The computational domain consists of an inclined wall shown in Fig 5.11, where α is the angle of inclination. Similar to the case in 5.3.1, the boundaries in X directions are set as periodic boundaries, and the developed wall boundary conditions are applied to the surfaces in Y directions. The contact angle θ^{eq} is assigned to the inclined wall, which can be adjusted according to the real situations.

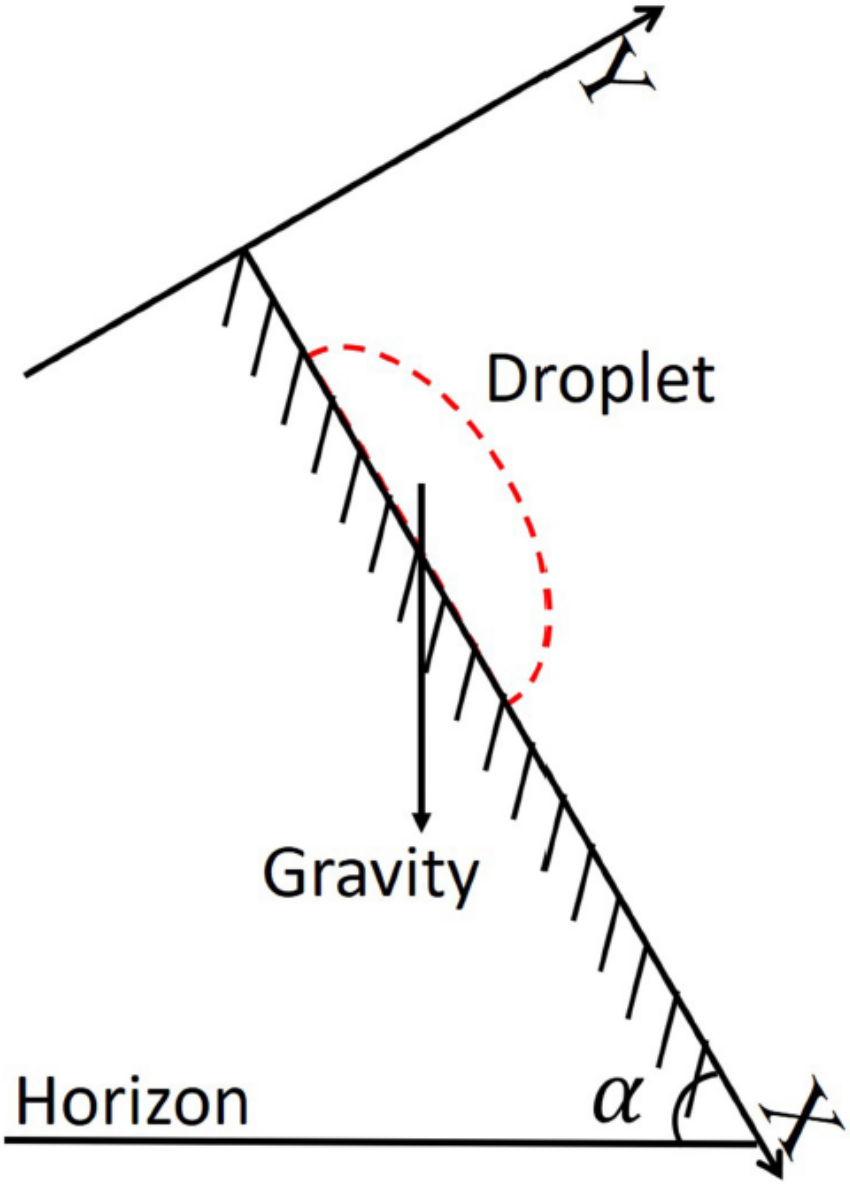

Figure 5.11 Initial state of the moving water droplet.

In this case $\rho^* = 775$ is taken, which represents the density ratio set of water and air, and the Cahn number $Cn = 30$ is taken to ensure the stability and accuracy. The grid system size is 600×2000. The initial condition is shown in Fig 5.11: a droplet starts

to move due to the gravity. The acceleration is set as g. The velocity profiles are set as follows

$$u_{x,liquid} = u_{x,gas} = 0 \quad (106.)$$

$$u_{y,liquid} = u_{y,gas} = 0 \quad (107.)$$

Experiments were also conducted on the test-table shown in Fig 5.4. A glass pane and a steel plate were used as the wall surface, while the working fluid is water in the test.

5.3.5 Advancing and receding contact angles

The contact angle hysteresis phenomenon is observed and discussed by many researchers [Soolaman et al. 2005] which focus on the wetting issue, and rather than static contact angles, they usually defined the contact angle hysteresis as the difference between θ_A and θ_R [Kabov & Zaitsev 2013], where θ_A and θ_R represented the advancing (towards the heading) and receding (towards the backward) contact angles shown in Fig 5.12. The contact angle hysteresis may attribute to various factors such as surface roughness and the moving velocity. A water droplet of volume $20\mu L$ was put on the steel plate with an inclined angle of $60°$ to observe the phenomenon. Fig 5.12a shows the moving droplet and the contact angles captured at certain moment in the experiment. The measured θ_A and θ_R are around $75°$ and $40°$ respectively.

This phenomenon was also recovered by using the current model as shown in Fig 10b. There is a little difference between the simulation and experimental results, which the θ_A and θ_R are about $77°$ and $45°$ in former situation. This may result from the neglect of the surface roughness in our model. The comparison shown in Fig 5.12 indicates that the present model is capable to capture the advancing and receding contact angles in the droplet moving process.

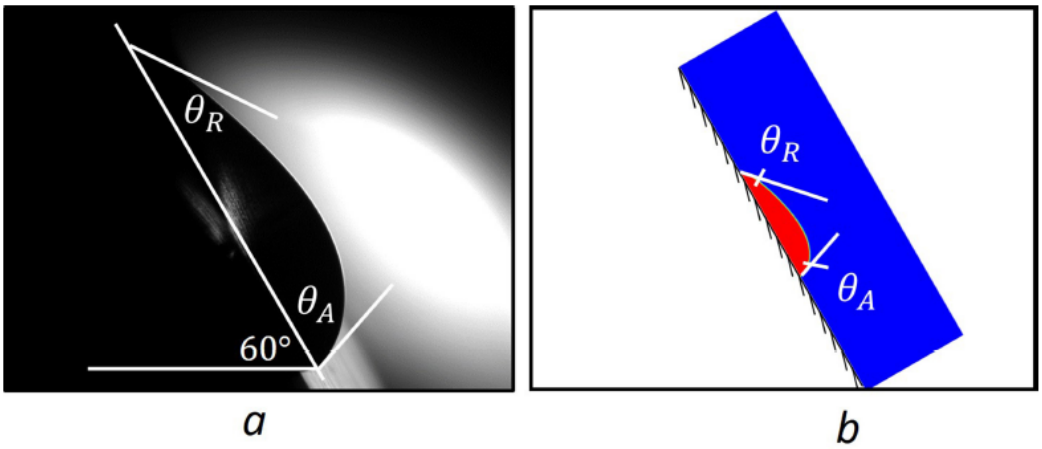

Figure 5.12 The experimental and simulation results of advancing and receding contact angles on inclined steel plate. *a*: experiment; *b*: simulation.

5.3.6 Evolution of moving contact line

The glass pane is a hydrophilic surface with a static contact angle as low as $22.1°$. A water droplet of volume $20\mu L$ was put on the glass pane with an inclined angle of $40°$ in the experiment test. Evolution of the moving droplet along the glass pane is

captured and shown from Fig 5.13a to Fig 5.13d, in which the left pictures are experiment results and right ones are outputs by our proposed model. It can be observed that the droplet moves at a nearly constant velocity after an acceleration at the beginning. The contact angles in Fig 5.13d, both advancing and receding contact angles, are near to $22.1°$ while the former is a little larger and the latter smaller, which indicates the contact angle hysteresis exists. The phenomenon can also be observed in the simulation outputs, which agrees well with the experimental results. By comparing the experiment and simulation results in Fig 5.13 we can conclude that the moving contact line can be recovered accurately by the model developed in this study.

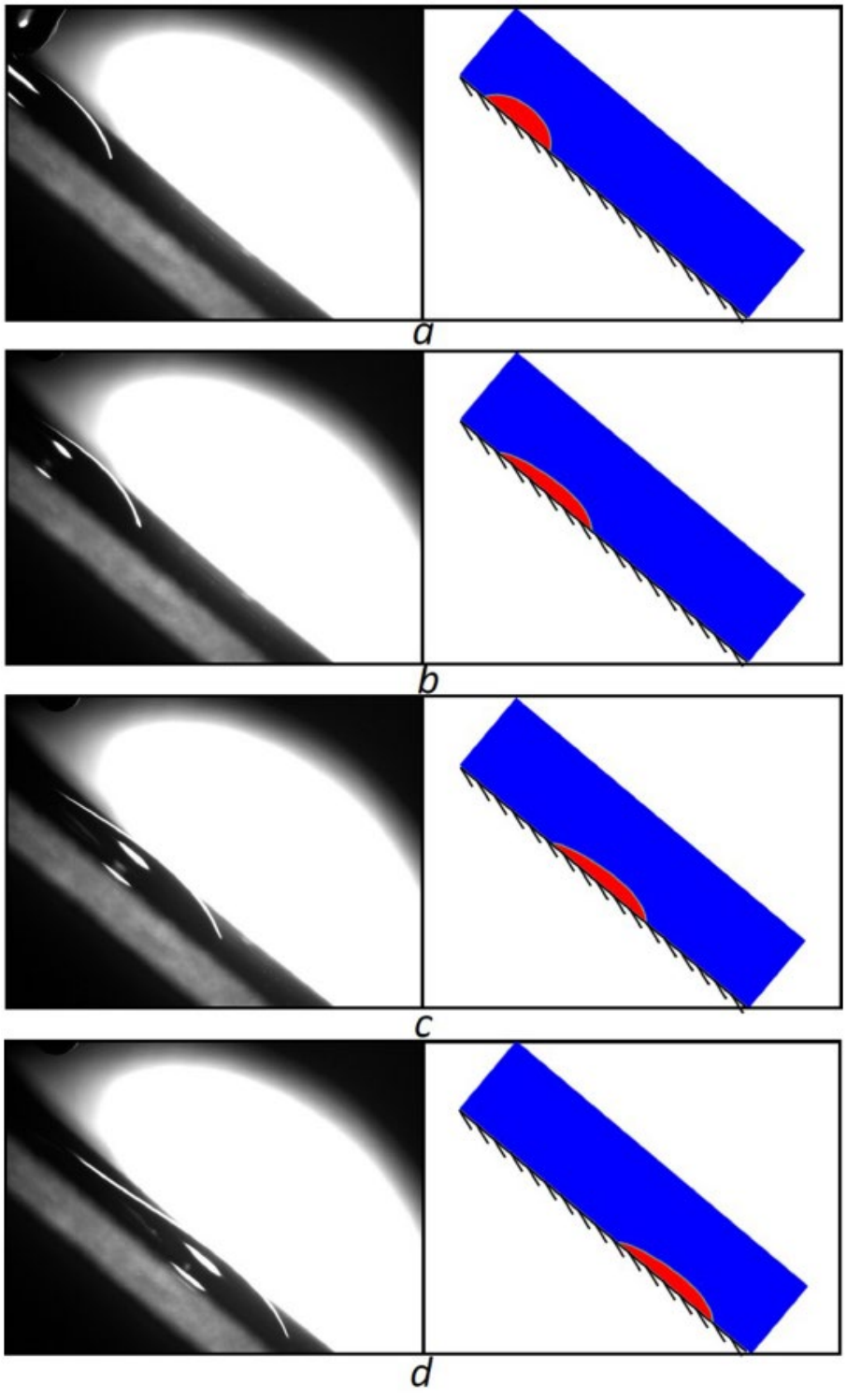

Figure 5.13 Evolution of moving droplet on inclined glass pane (*Left*: experiment results, *Right*: simulation results).

5.3.7 Computational efficiency

The falling droplet simulations are carried out on a computer with CPU i7-3930K and 16 GB RAM. The C++ compiler is the MSVC on windows platform. The computing time for the case in which droplet falls half length of the wall is 403 mins.

5.4 Summary

This chapter presents a conservative lattice Boltzmann model to simulate the two-phase flows with moving contact line at high density ratio. The proposed model consists of a phase field lattice Boltzmann equation for solving the conservative Allen-Cahn equation, and a pressure evolution LBE for solving the incompressible Navier-Stokes equations. A modified wall boundary treatment scheme is developed to ensure the mass conservation. In addition, the wetting dynamics are treated by incorporating the cubic wall energy in the expression of the total free energy. The proposed model is featured with mass conservation property, proper treatment of wetting boundary and high density ratio. Numerical tests including equilibrium droplets on wetting surface, co-current flow and a droplet moving by gravity along inclined wetting surfaces are conducted with our proposed model. The simulation results agree well with analytical solutions and experimental results. The mass conservation is checked and confirmed, the wetting surface is accurately modelled and the density ratio is up to 1000 in the tests. Results show that the proposed model can successfully recover the moving

contact line process, making it applicable to the study of moving contact line problem and lays a solid foundation for the falling film simulation.

CHAPTER 6

DEVELOPMENT OF A THERMAL LATTICE BOLTZMANN MODEL FOR HEAT AND MASS TRANSFER SIMULATION IN FALLING FILM WITH PHASE CHANGE

In this chapter, a thermal lattice Boltzmann model is proposed based on the model developed in chapter 5. This thermal lattice Boltzmann model is proposed to simulate the heat and mass transfer process in fall film. Instead of the traditional continuity hypothesis based numerical methods, the proposed model treats the heat and mass transfer in multi-phase flow from the point of kinetic theory, which has a solid physical background. The proposed model consists of a phase-field lattice Boltzmann equation (LBE) for solving the conservative Allen-Cahn (A-C) equation, a pressure evolution LBE for solving the incompressible Navier-Stokes equations, a temperature evolution LBE for solving the internal energy equation and a concentration evolution LBE for solving the mass diffusivity equation. The proposed model was adopted to simulate the heat and mass transfer process in the falling LiCl solution film at different Reynolds number and the results were compared with the numerical and experimental tests. The comparison results show that the proposed can well predict the temperature

and concentration distribution of the falling film absorption process and has a better computational efficiency than traditional simulation methods.

6.1 Model description

6.1.1 Lattice Boltzmann equations for temperature field

Based on the model proposed in chapter 5, the lattice Boltzmann equations for temperature field are proposed. The passive scalar approach is employed for the evolution of the temperature field in the computational domain. In this model the temperature is passively advected by a fluid velocity and the coupling between energy and momentum equations is done at the macroscopic level. The convection-diffusion equation of the temperature can be solved with a separate distribution function called s_α in the LB framework. The DBE for the new distribution function is written as

$$\frac{\nabla s_\alpha}{\nabla t} + \boldsymbol{e}_\alpha \cdot \nabla s_\alpha = -\frac{s_\alpha - s_\alpha^{eq}}{\lambda_T} \qquad (108.)$$

The equilibrium distribution of s_α reads

$$s_\alpha^{eq} = \omega_\alpha T\left(1 + \frac{\boldsymbol{e}_\alpha \cdot \boldsymbol{u}}{c_s^2}\right) \qquad (109.)$$

It has been shown that the linear equilibrium distribution function, which contains the

terms up to first order in $\boldsymbol{u}$, would be sufficient for solving a typical convection-diffusion equation. The DBE of Eq. (108) is integrated along characteristics to achieve LBE for the temperature. Applying the trapezoidal integration leads to

$$s_\alpha(\boldsymbol{x}+\boldsymbol{e}_\alpha\partial t, t+\partial t) - s_\alpha(\boldsymbol{x},t) = -\frac{s_\alpha - s_\alpha^{eq}}{2\tau_T}[\boldsymbol{x}+\boldsymbol{e}_\alpha\partial t, t+\partial t] - \frac{s_\alpha - s_\alpha^{eq}}{2\tau_T}[\boldsymbol{x},t] \quad (110.)$$

where $\tau_T = \lambda_T/\partial t$ is the nondimensional relaxation time. Since Eq. (110) is implicit in time, the modified distribution function is introduced as follows to make the scheme explicit with second-order accuracy:

$$\bar{s}_\alpha(\boldsymbol{x},t) = s_\alpha(\boldsymbol{x},t) + \frac{s_\alpha - s_\alpha^{eq}}{2\tau_T} \quad (111.)$$

The LBE for the modified distribution function of temperature can be easily derived as

$$\bar{s}_\alpha(\boldsymbol{x}+\boldsymbol{e}_\alpha\partial t, t+\partial t) - \bar{s}_\alpha(\boldsymbol{x},t) = -\frac{1}{\tau_T+0.5}[\boldsymbol{x},t] \quad (112.)$$

The temperature is calculated by taking the zero-order moment of the above distribution function

$$T = \sum_\alpha \bar{s}_\alpha \quad (113.)$$

and the thermal diffusion is related to the relaxation time by

$$a = c_s^2 \tau_T \partial t \qquad (114.)$$

The multiscale Chapman-Enskog expansion of Eq. (112) for recovering the convection-diffusion equation is found extensively in the literature [Guo et al 2002, Mohamad 2011], but some of the authors have ignored to indicate the errors and unwanted terms recovered by multiscale expansion. Chopard et al. [Chopard et al. 2009] discussed the effects of linear and quadratic equilibrium distribution function on the unwanted terms. They showed that with linear equilibrium distribution function, the Chapman-Enskog expansion of Eq. (112) results in

$$\frac{\partial T}{\partial t} + \nabla \cdot (\boldsymbol{u}T) = \alpha \nabla^2 T + \frac{\alpha}{c_s^2} \frac{\partial}{\partial t} \nabla \cdot (\boldsymbol{u}T) \qquad (115.)$$

where the last term in the right-hand side is the error term. It is worth noting that the above equation is second-order accurate in time and space as mentioned by Chopard et al. [Chopard et al. 2009]. However, neglecting the error term of $\frac{\alpha}{c_s^2} \frac{\partial}{\partial t} \nabla \cdot (\boldsymbol{u}T)$ needs more justification.

As assumed previously, bulk phases are considered to be incompressible and the compressibility due to the phase change at the interface is mimicked by a proper source

term. In the next section we declare another important assumption about the temperature. As we will assume, in this study the liquid phase temperature is fixed at saturation temperature and the energy equation is only solved for the gas phase. Thus,

due to incompressibility of the gas phase, the error term of Eq. (115) can be reduced to $\frac{\alpha}{c_s^2}\frac{\partial}{\partial t}\boldsymbol{u}\cdot\nabla T$. Since in incompressible limits the Mach number should be small enough to ensure $\frac{u}{c_s}\ll 1$, the terms of order could be neglected. Hence, the convection-diffusion equation for temperature can be derived as

$$\frac{\partial T}{\partial t}+\nabla\cdot(\boldsymbol{u}T)=\alpha\nabla^2 T \qquad (116.)$$

6.1.2 Computation of the volumetric source due to phase changes

The phase transition from the liquid phase to the gas phase is called vaporization. Evaporation is a type of vaporization which occurs on the liquid surface. From the macroscopic point of view one can assume that the vapor source is present at the phase interface and the gaseous ambience, which is located away from the interface, contains a lower vapor concentration. Thus evaporation can be explained as a continuous diffusion of vapor from the phase interface to the ambience. In this concept the evaporation rate depends on the temperature and the concentration of the different species.

In some practical applications such as droplet heating and evaporating in combustion engines and gas turbines, the transient heating period does not affect the droplet lifetime considerably. Therefore, for studying the evaporating droplets at enginelike conditions, the droplet is sometimes assumed to be at boiling temperature or saturation temperature. Thus the heat which is transferred from the bulk gaseous phase to the liquid interface causes the vaporization at the phase interface. Moreover this postulation eliminates the necessity of solving the energy equation in the liquid phase and the species concentration transport equation in the gas phase.

In this work the liquid phase temperature is assumed at saturation temperature and the driving force for evaporation is the amount of heat which is transferred to the interface. So by applying the energy balance for the interface regions the local vaporizing mass flow rate per unit surface (m'') may be written as

$$m'' = \frac{K\nabla T}{h_{fg}} \cdot \hat{\boldsymbol{n}} \qquad (117.)$$

where h_{fg} is the latent heat of vaporization, K is the thermal conductivity, and ˆn is the unit vector normal to the phase interface. The above vaporization rate is computed per unit surface, so it should be converted to the volumetric form in order to be employed in the convective Cahn-Hilliard equation. The interface area at each computational cell or node is needed for calculation of the volumetric mass source or

sink. As discussed before, the composition C is similar to the volume-fraction function used in the VOF method. Since the proposed phase-field LB framework is physically a diffuse-interface modeling approach, instead of having an exact interface at which the evaporation takes place, we will have a vaporization region in which the liquid phase evaporates continuously. In this context referring to Hardt and Wondra [Hardt & Wondra 2008], one important feature of the gradient of the volume-fraction field is that its integral over a region including a part of the phase interface measures the local interface area. This statement is thus valid for the gradient of the composition field. So by multiplying m''' with the local interface content (i.e., |∇C|) and recalling $\hat{\boldsymbol{n}} = \frac{\nabla C}{\|\nabla C\|}$, the volumetric mass source of evaporation can be obtained as

$$m''' = \frac{K\nabla T}{h_{fg}} \cdot \nabla C \qquad (118.)$$

6.2 Description of experimental test rig

6.2.1 Experimental setup

An experimental setup of single-channel liquid desiccant dehumidifier with substitutable working plates was fabricated to investigate the effect of surface properties on dehumidification performance, as shown in Fig. 6.1. Three commonly-used plate dehumidifiers, i.e., Stainless plate dehumidifier, Titanium plate dehumidifier and Polytetrafluoroethylene (PTFE) plate dehumidifier, were adopted in

this study. The experimental setup mainly consisted of three sub-systems, i.e., the air supply system (green line), the liquid desiccant supply system (red line) and the cooling water system (blue line).

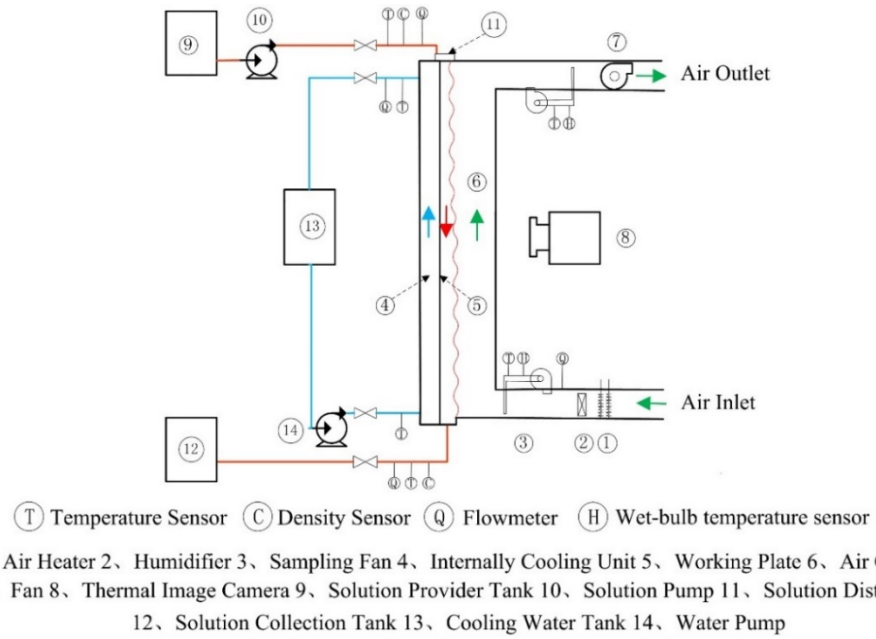

Fig. 6.1 Schematic diagram of the experimental setup

The air was supplied by fans, and then heated and humidified to the required conditions. The processed air interacted with the desiccant solution and the extra moisture exchanged from processed air to desiccant solution. Finally, the dry air flowed out at the top of the dehumidifier.

The liquid desiccant solution was supplied by a plastic magnetic pump and well distributed on working plates by the newly-designed liquid distributor. After absorbing

the extra moisture of processed air, the weak solution was collected and regenerated in regeneration system which was driven by solar energy. The inlet and outlet liquid desiccant temperatures, density and flow rate were measured simultaneously in the experiment.

Besides, the latent heat released in absorption process could increase the solution temperature and deteriorate the dehumidification performance. Therefore, an internally cooling unit was designed to take away the released latent heat. In addition, ⑤ in Fig. 3.1 represents the working plate which is substitutable during the experiment. Different plate dehumidifiers, i.e., Stainless plate dehumidifier, Titanium plate dehumidifier and PTFE plate dehumidifier, were used to analyse the influence of plate properties on dehumidification performance.

As contact area between processed air and desiccant solution was critical to dehumidification capacity, a thermal image camera was utilized to record the shapes of the solution film and then to calculate the wetting area on different working plates. Besides, the film thickness was measured by a capacitance micrometer.

To achieve the even distribution of the liquid desiccant falling film, a new solution distributor was designed, as shown in Fig. 6.2. Three entrance holes were set up at the top of the distributor to ensure the even inlet of the desiccant solution. It was observed

that some eddies occurred as the desiccant solution flowed from the inlet pipe to the chamber of the distributor. These eddies could lead to unstable solution levels, which seriously affected the distribution of the desiccant solution. To reduce the effect of the solution eddies on the solution distribution, a baffle was fixed inside the distributor which separated the chamber into two parts. The desiccant solution firstly flowed into Chamber I and stored. When the solution level was above the baffle, the solution began to flow over the baffle smoothly. The effect of the solution eddies was effectively eliminated by the baffle. In addition, an outlet slot was opened in Chamber II and the even distribution of the falling film could be achieved once the solution level was above the outlet slot.

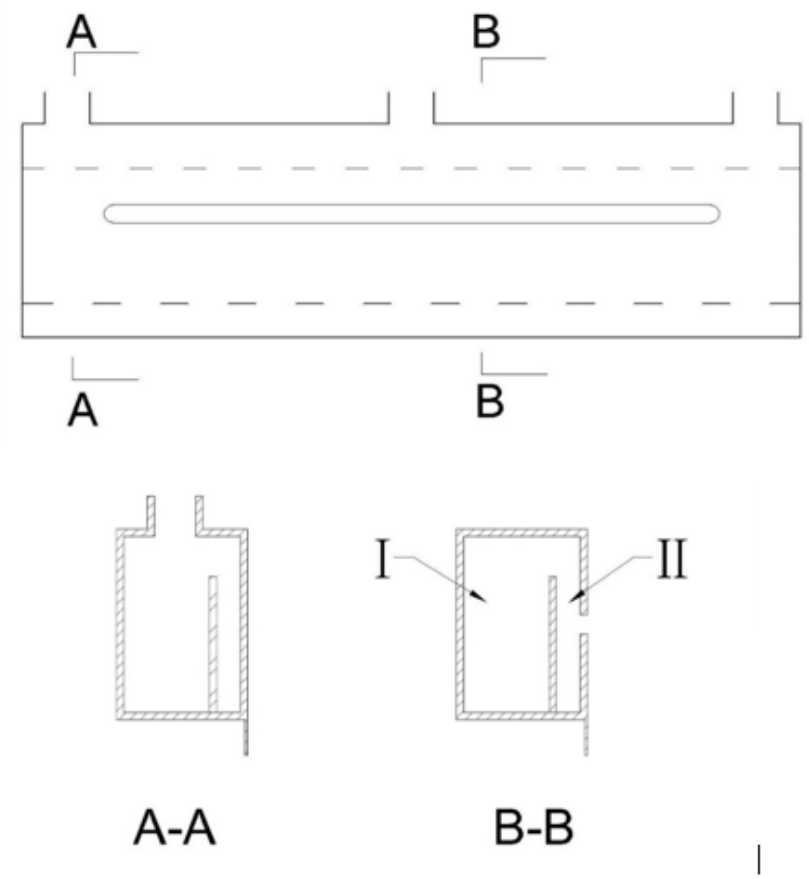

Fig. 6.2 Schematic diagram of the solution distributor

6.2.2 Measuring and controlling devices

In the experiment, the inlet parameters of processed air, liquid desiccant solution and cooling water were controlled and adjusted. The air flow rate was controlled by the voltage regulator of the fan. The air temperature was regulated by the air heater with PID controller and the air humidity by the electromagnetic humidifier which was controlled by adjusting the input voltage. In addition, the solution flow rate was regulated by the valve installed at the outlet of the pump and the temperature was

controlled by the heat exchanger fixed inside the solution tank. These main devices in the experiment are presented in Fig. 6.3.

(a) Air humidifier

(b) Air heater

(c) Water chiller

(d) Air fan

(e) Magnetic pump

(f) Control board

Fig. 6.3 Main devices in the experimental setup

The inlet and outlet parameters of processed air, liquid desiccant solution and cooling water were measured for each test. The temperature was measured by platinum resistance temperature detectors (Pt RTDs). The air flow rate was measured by air velocity sensors with the accuracy of 0.3%. The desiccant solution and cooling water flow rates were measured by turbine flow rate sensors. Besides, the concentration of the liquid desiccant solution was calculated based on temperature and density which was measured by a specific gravity hydrometer. As the wetting area was one of the key parameters in dehumidification process, a thermal image camera was used to record the wetting area in the experiment. Each test lasted for more than ten minutes under steady conditions and the data were acquired by a data logger. The main measuring devices are shown in Fig. 6.4 and the specifications are listed in Table 6.1.

(a) Air velocity sensor

(b) Turbine flow rate sensor

(c) Specific gravity hydrometer

(d) Thermal image camera

(e) Data logger

Fig. 6.4 Measuring devices in the experimental setup

Table 6.1 Specifications of different measuring devices

Parameter	Device	Brand	Model	Accuracy	Operational range
Air dry-/wet-bulb temperature	Pt RTD	Heraeus	LN222-A	0.1 K	223-573 K
Air flow rate	Air velocity sensor	Shielur	ASF-100	0.3%	9-10000 Pa
Solution temperature	Pt RTD	Heraeus	LN222-A	0.1 K	223-573 K
Solution flow rate	Turbine flow rate sensor	Gems Sensors	173936-C	3%	0.5-5 L/min
Solution density	Specific gravity hydrometer	Daho	DH-300x	1 kg/m^3	1-99, 999 kg/m^3
Cooling water temperature	Pt RTD	Heraeus	LN222-A	0.1 K	223-573 K
Cooling water flow rate	Turbine flow rate sensor	Sea	YF-S201	2%	1-30 L/min

6.2.3 Measurement of falling film thickness

As the liquid desiccant spreads as falling film on the working plates and absorbs the extra moisture of the processed air, the flow characteristics of the falling film are very important to dehumidification performance. Thus, the falling film thickness and its

fluctuation are measured. To investigate the flow characteristics of falling film along the flow direction, two test points are selected to measure the local falling film thickness, as shown in Fig. 6.5. The instantaneous falling film thickness is measured by a Capacitance micrometer (JDC-2008). The fluctuation of the falling film can result in various capacitance between the capacitance probe and the falling film as well as the output voltage of the Capacitance micrometer. As the output voltage is proportional to the falling film thickness, the time-varied falling film thickness is measured accurately.

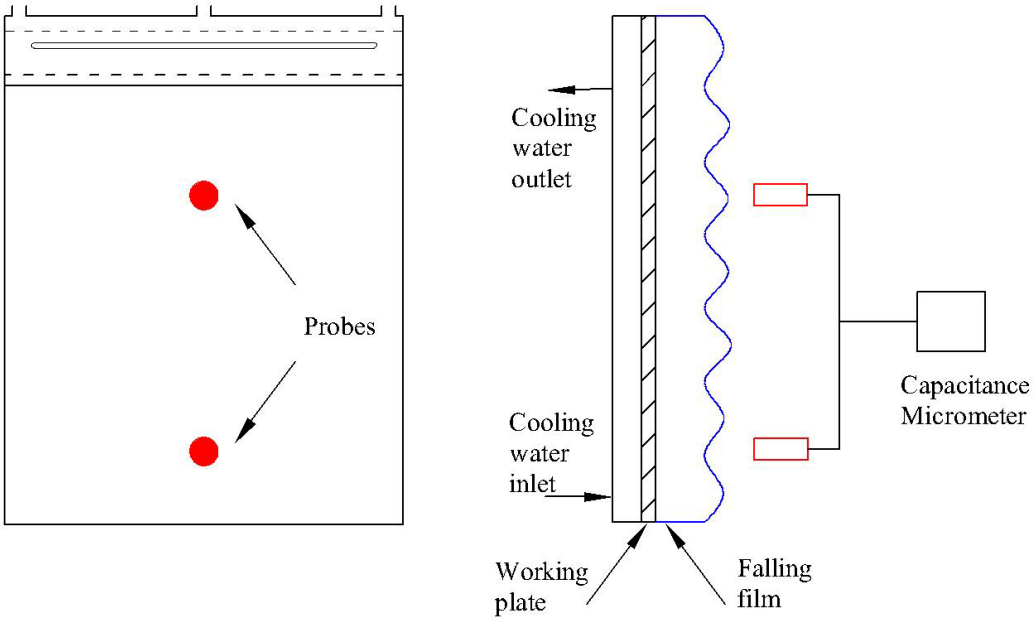

Fig. 6.5 Schematic diagram of falling film measuring system

As the Capacitance micrometer is sensible to the surroundings, calibration is necessary

before the experiment. Static calibration is adopted in this experiment. The calibration of Capacitance micrometer is conducted using both deionized water and LiCl aqueous solution (39 wt.%). The detailed procedure is presented as follows.

(1) Fill the metal container with deionized water or LiCl aqueous solution (39 wt.%) and make sure that the bottom of the metal container is fully covered by liquid.

(2) Put the container on the calibration platform.

(3) Adjust the lifting platform to linear region of the Capacitance micrometer and make sure that the output voltage of is around 4000 mV.

(4) Adjust the output voltage of the Capacitance micrometer to zero and lift the metal container with certain distance (around 100 μm). Then record the measured film thickness by the Capacitance micrometer and the accurate lifting distance as well.

(5) Repeat Sept (4) to obtain the calibration curve.

The calibration curves of the Capacitance micrometer using deionized water or LiCl aqueous solution (39 wt.%) are shown in Fig. 3.6. The calibration results indicate that the measured thickness agrees well with the real thickness for both deionized water or

LiCl aqueous solution (39 wt.%).

6.3 Falling film simulation with proposed thermal lattice Boltzmann model

6.3.1 Physical model

Fig 6.6 shows the physical falling film model. The main factors which influence the simulations are listed: Liquid-gas interaction, solid-liquid interaction, gravity and boundary conditions. Fig 6.7 describes the numerical model and the key points in simulation.

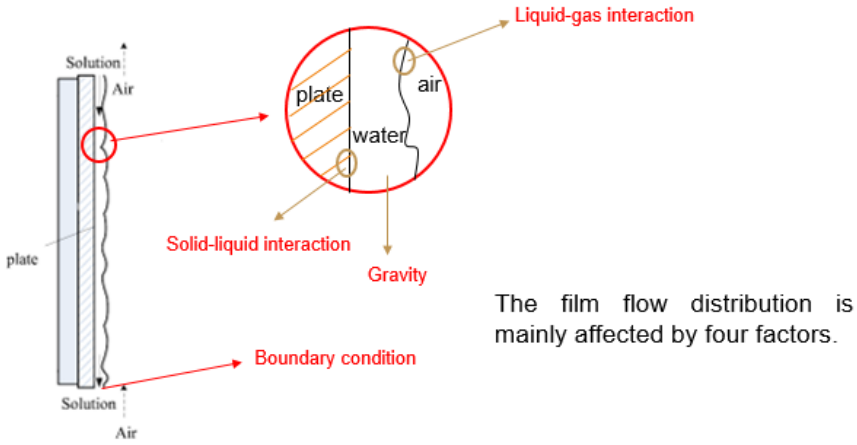

Figure 6.6 schematic of falling film

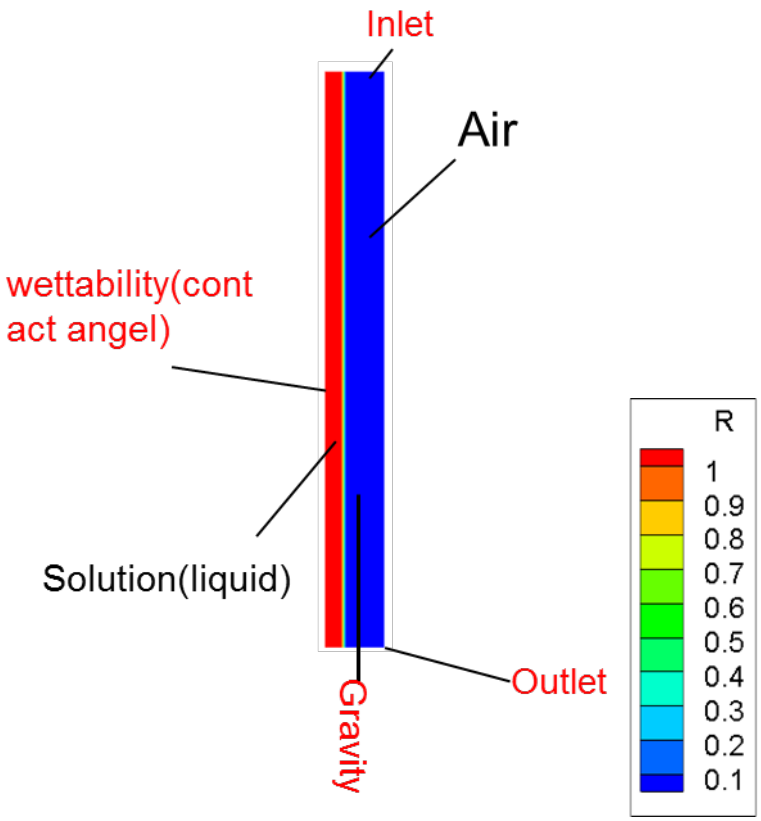

Figure 6.7 Schematic of falling film Simulation area (density distribution)

6.3.2 Validity of the model

A grid sensitivity test was conducted on three different grids of 30×300, 60×600, 100×1000 $(NX \times NY)$ at Reynolds number 20. Fig. 6.8 shows the velocity profiles of u_y at $NY = 150, t/t_0 = 1.0, Re = 20$. The velocity profile obtained on the finest grid of 60×600 agrees well with that obtained on the grid of 100×1000 except for a small fraction near the interface, which indicates that the grid of 60×600 is fine enough to capture the liquid-gas interface in this case.

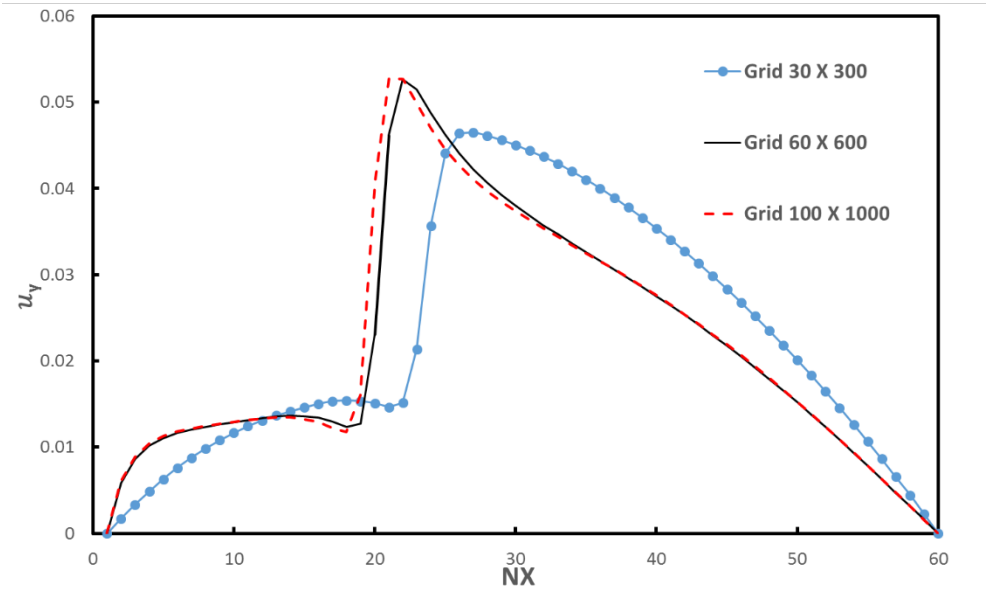

Figure 6.8 Grid sensitivity test for the falling film simulation at $NY = 150, Re = 20, t/t_0 = 0.5$

6.3.3 Results and discussion

6.3.3.1 Parameter lists

With the above established model, the dehumidification processes of the moist air were simulated in a range of different flow conditions. Table 4.1 presents the summary of different calculating conditions.

Table 6.1 Summary of calculating conditions

Desiccant solution				
Parameter	$T_{in}(K)$	$C_{in}(\%)$	$u_{in}(m/s)$	Reynolds number
Basic point	293	30	0.07	20
Range	288-308	30-45	0.05-0.2	10-180

6.3.3.2 Dynamic simulation of development of falling film

The computational domain is a rectangle area shown in Fig 6.6. As above mentioned, the upper boundary was set as velocity inlet, the lower boundary was a fully developed outlet, and both the left and right boundaries were no-slip walls. The contact angles of the left and right boundary were both set as $90°$. In this case, $\rho^* = 1000$, which represents the density ratio of desiccant solution and air. The initial condition was set as follows: at the very beginning, the whole simulation domain was occupied by the gas phase and then the liquid phase flows from the upper boundary with a velocity U. The velocity profile at the inlet was set as follows:

$$u_{y,liquid} = U \quad x < h_{film}$$

$$u_{y,gas} = 0 \quad x > h_{film}$$

$$u_{x,liquid} = u_{x,gas} = 0$$

The Reynolds number was defined as

$$Re = \frac{Uh_{film}}{\nu}$$

where U and h_{film} are the film velocity and film thickness at the inlet, and ν is the viscosity of the liquid. For the convenience of discussion, the dimensionless time t/t_0 is taken, where $t_0 = \rho\nu h_{film}/\sigma$ is the viscous time of the liquid phase.

Fig. 6.9 shows the dynamic falling film formation process with Reynolds number 20. The red part represents the liquid phase while the blue part represents the gas phase. It can be observed that the film pattern is slightly unstable and there are many small waves on the liquid interface. At the beginning, the flow is quite slow and it is then accelerated by gravity. The distance between the film heads is getting larger in the time period $t/t_0 = 1.5 - 2.0$ than $t/t_0 = 0 - 0.5$, which indicates that the average velocity of the film is increasing. The film becomes smooth and small waves disappear when it reaches the outlet at around $t/t_0 = 2.0$ and it remains unchanged after 2.5,

which means the film becomes totally laminar after a short unstable period.

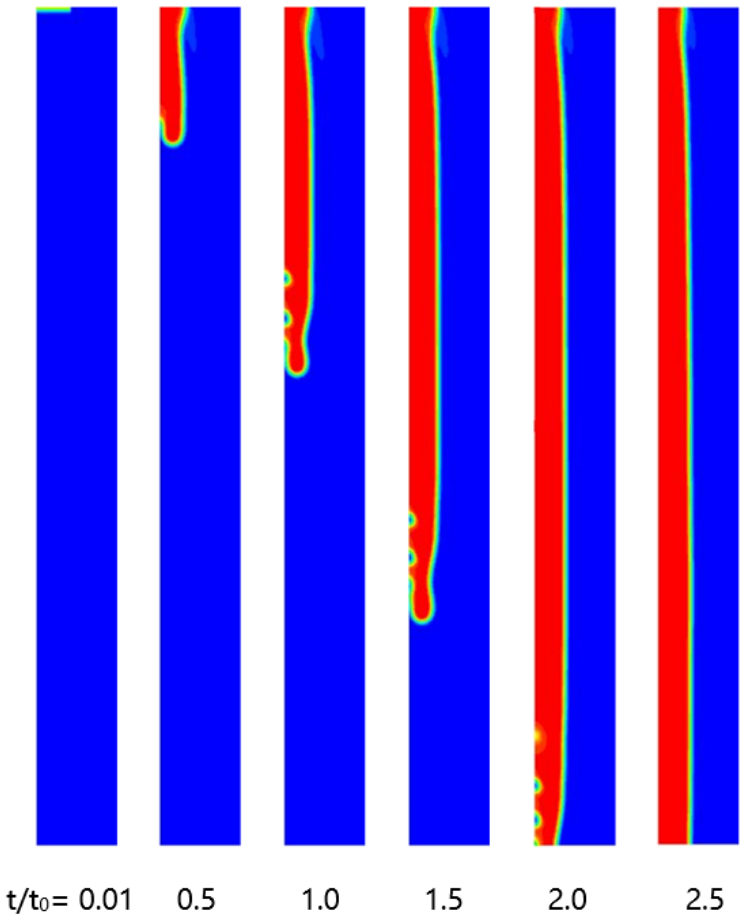

Figure 6.9 Time sequence of falling film with Reynolds number 20

At $t/t_0 = 1.0, 1.5, 2.0$ in Fig. 9, it can be observed that separation takes place between liquid and the wall. This phenomenon is also reported in the CFD simulation done by Luo *et .al* [Luo et al. 2013] and they attributed it to the low wettability. The velocity profiles of u_y at $NY = 220$ and $NY = 260$ when $t/t_0 = 1.0, Re = 20$ are shown in Fig. 6.10. It can be found that separation occurs at $NY = 260$ since there

are three different velocity sections while at $NY = 220$ there are only two. In both pictures we can find that the outer liquid layer always has larger velocity than the inner layer and the liquid behind ($NY = 220$) flows faster than the liquid ahead ($NY = 260$), which may result in the separation.

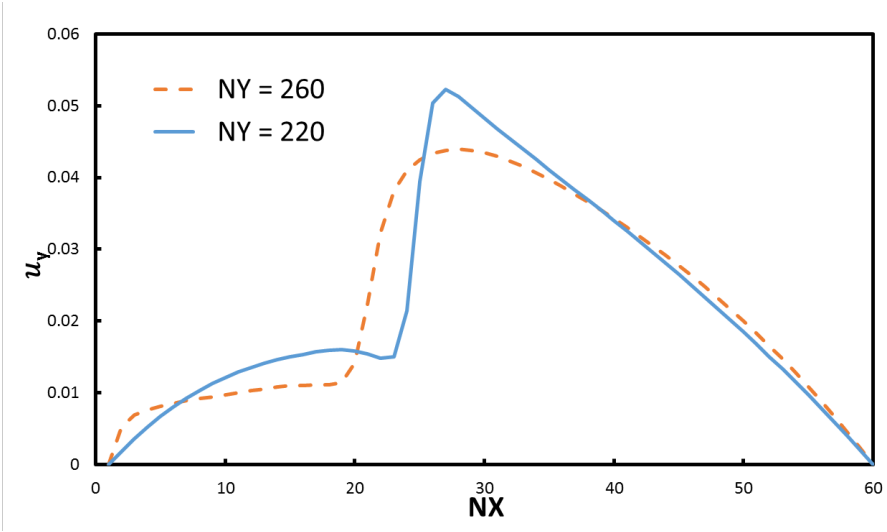

Figure 6.10 Velocity profiles of u_y at $NY = 220$ and $NY = 260, t/t_0 = 1.0, Re = 20$

The film interface at the time $t/t_0 = 1.5$ for falling film with different Reynolds numbers ranging from 1 to 20 are shown in Fig. 6.11. It can be observed that the film patterns are quite similar, which indicates that the flow type within the Reynolds range are similar. It shows that the average velocity under different Reynolds numbers are quite close, this may be because the film is dominated by surface tension under low Reynolds number so the inlet velocity has little influence on the film flow. All of the

four falling films after stabilization are totally laminar, which agree with the experimental results by Miyara [Miyara 1999].

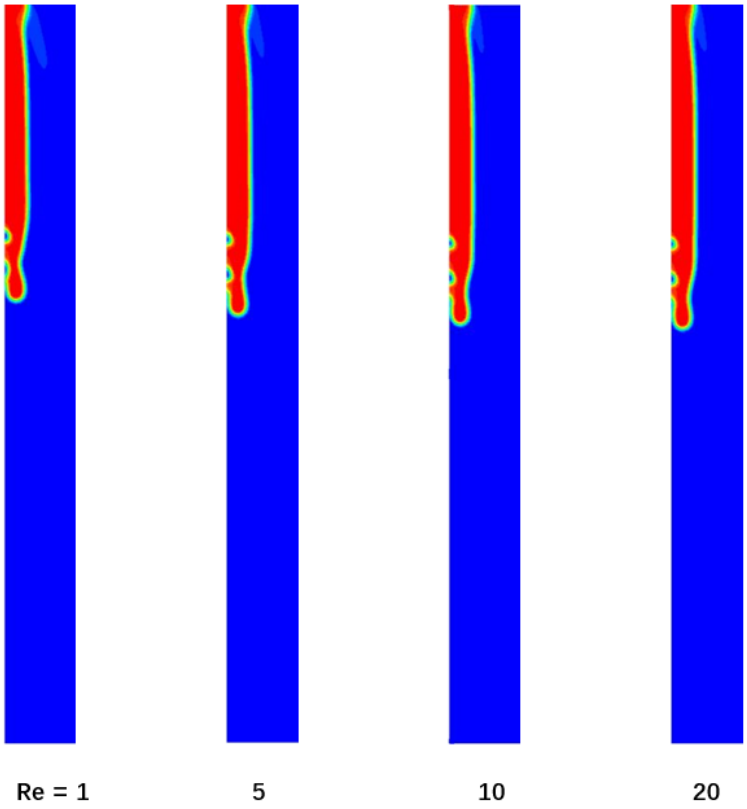

Figure 6.11 Film interface at $t/t_0 = 1.5$ under different Reynolds numbers

6.3.3.3 Temperature distribution

Fig 6.12(a) shows the PLIF (thermal) image of thin liquid-film taken by Zadrazil et al [Zadrazil et al 2014]. It can be observed that the temperature decreases gradually from film surface to the plate. The high temperature mainly occurs between the film surface and fluid foil interface, while we can obviously see the same phenomenon from Fig

6.12(b), which is the simulation results by the proposed model. It indicates that the proposed model can reproduce the temperature distribution of falling film accurately.

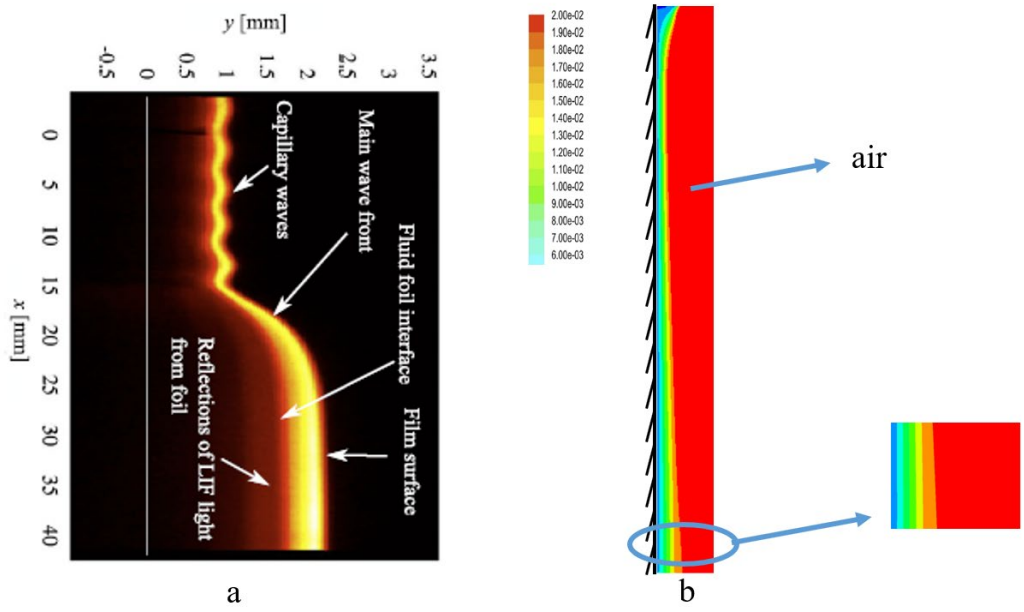

Figure 6.12 Temperature distribution of liquid-film by experimental (a) and proposed model (b)

6.3.3.4 Concentration distribution

Fig 6.13 shows the water vapor fraction of falling LiCl film, which is so-called the concentration distribution. The film Reynolds number is 10 in this case, in which the film will finally be laminar smooth flow according to the film theory. Fig6 (a) is the simulation by traditional CFD tool [Luo], in which the film and the air are in counter

flow while Fig6 (b) is the results by the proposed model in which the air has no initial velocity. Fig6 (b) shows the concentration distribution at t = 3.7s, while the film head is arriving the lower edge, which means near steady state. In Fig 6.13 (a) the film head has already arrived the lower edge at t = 3.7s, which means the average film velocity in simulation (a) is larger than (b) even through it is counter flow. The variation trends of concentration are similar in both figures. It is obvious to tell the influence of the peaking film head in Fig 6.13 (b), in which the slope of concentration is quite different around the peaking from other area, however, in Fig 6.13(a) it seems that the peaking head causes no difference, which is not reasonable. This may attribute to the incorrect use of the continuity hypothesis in small scale. It reveals the proposed lattice Boltzmann model performs better than traditional CFD tool especially in small scale.

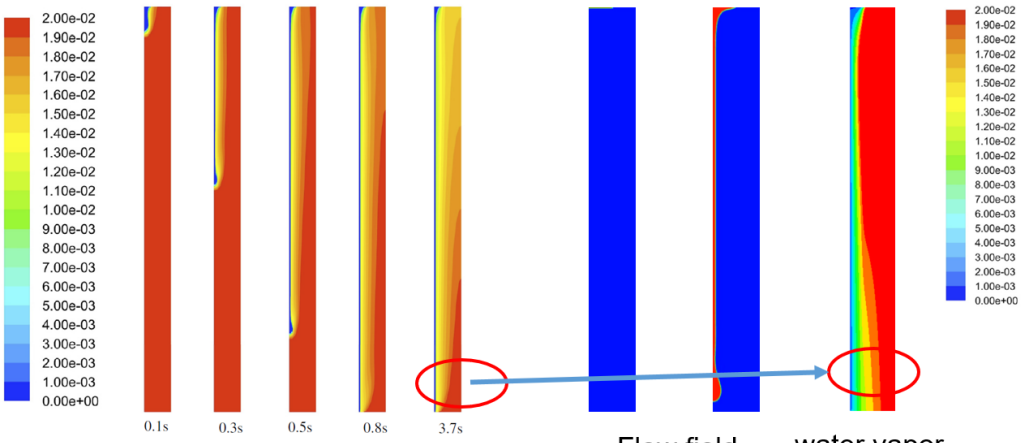

Fig. 8. Stages of film formation and mass transfer in the dehumidifier.

Figure 6.13 Flow and water vapor fraction of falling film with Re = 10 by [Luo] (a) and proposed model (b).

6.3.4 Influence of inlet desiccant concentration

In the section, the local film thickness profiles of the simulations with various inlet 128 desiccant concentrations are illustrated in Fig. 6.14. It was observed that with a relatively lower desiccant concentration, the liquid films were almost smooth. When the inlet desiccant concentration increased, the liquid film thickness increased and the surface waves became more and more evident correspondingly. It was concluded that the obvious surface waves were generated by the more drastic absorption processes, when significant momentums were exchanged at the vapor-liquid interface.

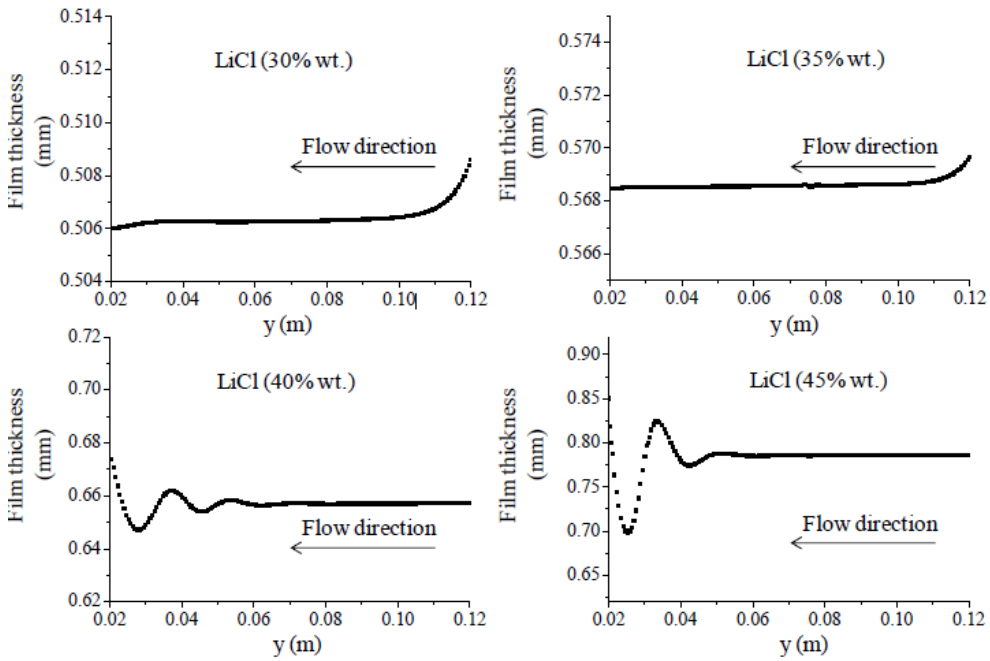

Fig 6.14 Liquid film thickness profiles for various inlet desiccant concentrations

6.3.4.1 Influence of inlet solution flow rate

Under different inlet solution flow rate, the mass fraction of water vapor and temperature of outlet air had the similar variation trend. As shown in Fig. 6.15, it was observed that the initial increase of inlet solution flow rate would improve the dehumidification performance significantly while the effect would reduce with further increase of inlet solution flow rate. By looking into the contours of temperature and mass fraction of water vapor under different inlet solution flow rate in Fig. 6.13, a common point was found, that is, the thermal diffusion was faster than the mass diffusion. It meant Le > 1 for all the cases. In early research, through comparing the simulation results with the experimental data of Fumo and Goswami (Fumo and Goswami 2002), Babakhani (Babakhani 2009) had pointed out that instead of 1.0 was more preferable for the prediction of the performance of the dehumidifier. Thus, it could be verified that the present model possessed high accuracy.

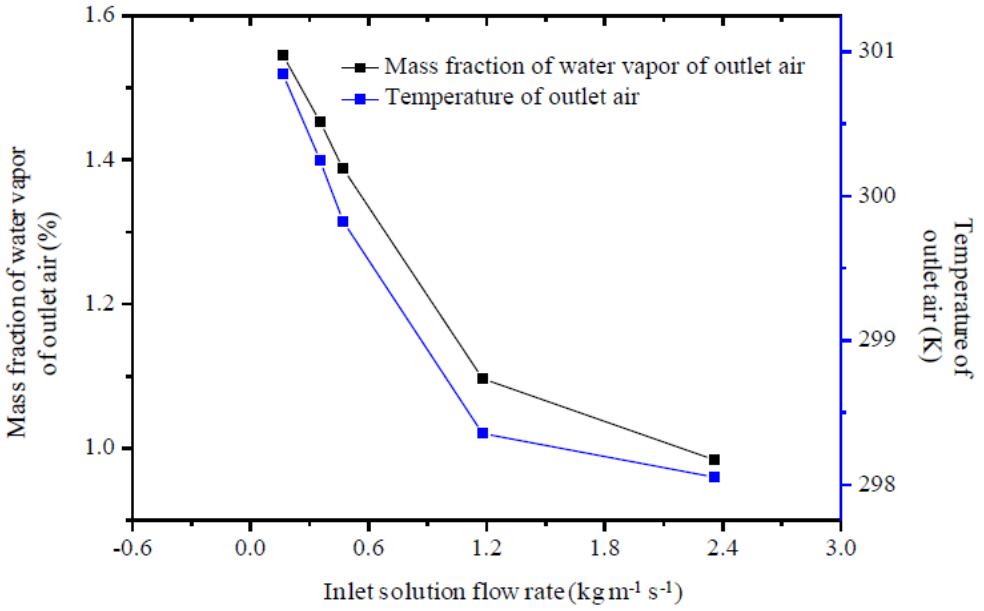

Fig 6.15 Mass fraction of water vapor and temperature of outlet air under different inlet solution flow rate

6.4 Summary

In this chapter, a thermal lattice Boltzmann model is proposed based on the model developed in chapter 5. This thermal lattice Boltzmann model is proposed to simulate the heat and mass transfer process in fall film. Instead of the traditional continuity hypothesis based numerical methods, the proposed model treats the heat and mass transfer in multi-phase flow from the point of kinetic theory, which has a solid physical background. The proposed model consists of a phase-field lattice Boltzmann equation (LBE) for solving the conservative Allen-Cahn (A-C) equation, a pressure evolution LBE for solving the incompressible Navier-Stokes equations, a temperature evolution

LBE for solving the internal energy equation and a concentration evolution LBE for solving the mass diffusivity equation. The proposed model was adopted to simulate the heat and mass transfer process in the falling LiCl solution film at different Reynolds number and the results were compared with the numerical and experimental tests. The comparison results show that the proposed can well predict the temperature and concentration distribution of the falling film absorption process and has a better computational efficiency than traditional simulation methods.

CHAPTER 7

CONSLUSIONS AND ORIGINAL CONTRIBUTIONS

7.1 Summary of contributions

This thesis aims to propose a lattice Boltzmann model to study the falling film based liquid desiccant air conditioning. This work may have origin contribution in following aspects:

(1) developed a lattice Boltzmann model which can properly capture the density distribution of two phase flow with high density ratio, which is applicable on the realistic two phase flow problem.

(2) developed a dynamic, mass conservative lattice Boltzmann model which can simulate the two phase flows with moving contact lines at high density ratio. This proposed model can dynamically reproduce the development of two phase flow with moving contact line

(3) developed a thermal lattice Boltzmann mode which can simulate the heat and mass transfer in the falling film dehumidifier. This model can well predict the performance of the falling film dehumidifier, which promotes the design and application of falling

film based air conditioning system.

7.2 Conclusions

This thesis aims to propose a lattice Boltzmann model to study the falling film based liquid desiccant air conditioning. First, a mass conservative lattice Boltzmann model is proposed to simulate the two-phase flows with moving contact lines at high density ratio. The proposed model consists of a phase field lattice Boltzmann equation (LBE) for solving the conservative Allen-Cahn equation, and a pressure evolution LBE for solving the incompressible Navier-Stokes equations. This model is characterized by mass conservation, proper treatment of wetting boundary and high-density ratio. Theoretical analysis and experiments are conducted for model validation. Based on this, a thermal lattice Boltzmann model for simulating the heat and mass transfer process in falling film dehumidifier is further established. A temperature evolution LBE for solving the internal energy equation and a concentration evolution LBE for solving the mass diffusivity equation are proposed to deal with the heat and mass transfer problem. The proposed model is adopted to simulate the heat and mass transfer process in the falling LiCl solution film at different Reynolds number and the results are compared with the numerical and experimental tests by other researchers. The comparison results show that the proposed model can well predict the temperature and concentration distribution of the falling film absorption process and has a better

computational efficiency than traditional simulation methods. The model has made contributions in the aspects of two-phase flow interaction, high density ratio flow and phase-change problems and provides suggestions in the future design and optimization of the falling film based liquid desiccant air conditioning.

Reference

A. A. Mohamad, Lattice Boltzmann Method, Fundamentals and Engineering Applications with Computer Codes (Springer, London, 2011).

A. Ali, K. Vafai, A.R.A. Khaled. Analysis of heat and mass transfer between air and falling film in a cross flow configuration. International Journal of Heat and Mass Transfer 47 (2004): 743-755.

A. Faghri, Y.W. Zhang. John Howell. Advanced Heat and Mass Transfer. Global Digital Press. 2010.

A. Lowenstein, K.E. Slyzak. A zero carry over liquid desiccant air conditioner for solar applications. ASME International Solar Energy Conference (ISEC 2006), 2006, Denver, Colarodo.

A. Ulman, An introduction to ultrathin organic films: from Langmuir-Blodgett to Self-Assembly, Academic Press, Inc, Boston, 1991.

A.A. Ertas, E.E. Anderson, I. Kiris. Properties of a new liquid desiccant solution-lithium chloride and calcium chloride mixture. Solar Energy 49(3) (1992):205-12.

A.A. Farayedhi, A.P. Gandhidasan, et al. Regeneration of liquid desiccants using membrane technology. Energy Conversion and Management 40(13) (1999): 1405-1411.

A.B.D. Cassie, S. Baxter. Wettability of porous surfaces. Transactions of the Faraday Society 40(1944): 546-551.

A.B.D. Cassie, S. Baxter. Wettability of porous surfaces. Transactions of the Faraday

Society 40(1944): 546-551.

A.S.A. Mohamed , M.S. Ahmed, A.A.M. Hassan, M. Salah Hassan, Performance evaluation of gauze packing for liquid desiccant dehumidification system, Case Studies in Thermal Engineering 8 (2016) 260-276.

A.T. Conlisk. Semi-analytical design of a falling film absorber. Journal of heat transfer 116 (1994):1055-1058.

A.Y. Khan, H.D. Ball. Development of a generalized model for performance evaluation of packed-type liquid sorbent dehumidifiers and regenerators. ASHRAE Transactions 98 (1992): 525-33.

Ahn, J., Kim, J., and Kang, B.H., Performance of a Hybrid Desiccant Cooling System in a Residential Environment, Heat Transfer Engineering, vol. 37, no. 7-8, pp. 633-639, 2016.

B. Chopard, J. L. Falcone, and J. Latt, Eur. Phys. J.: Spec. Top. 171, 245 (2009).

B.G. Ganchev, V.M. Koglov, V.V. Lozovetskiy. A study of heat transfer to a falling film at a vertical surface. Heat transfer-Soviet Research (4) (1972): 102-110.

B.G. Ganchev, V.M. Koglov, V.V. Lozovetskiy. A study of heat transfer to a falling film at a vertical surface. Heat transfer-Soviet Research (4) (1972): 102-110.

Brauner, M., J. S. Briggs, and H. Klar. "Triply-differential cross sections for ionisation of hydrogen atoms by electrons and positrons." Journal of Physics B: Atomic, Molecular and Optical Physics 22.14 (1989): 2265.

C. Decker, K. Zahouily. Photodegradation and photooxidation of thermoset and UV-cured acrylate polymers. Polymer Degradation and Stability 64(2) (1999): 293-304.

C. Li, Z. Wang, P.I. Wang, Y. Peles, N. Koratkar and G.P. Peterson. Nanostructured copper interfaces for enhanced boiling. Small, 4(8) (2008): 1084-1088.

C. M. Chan, T. M. Ko, H. Hiraoka. Polymer surface modification by plasmas and photons. Surface Science Reports 24(1-2) (1996): 3-54.

C.H.E. Nielsen, S. Kiil, H.W. Thomsen, K. Dam-Johansen. Mass transfer in wetted-wall columns: Correlations at high Reynolds numbers. Chemical Engineering Science 53 (3) (1998): 495-503.

C.J. van Oss, M.K. Chaudhury, R.J. Good. Interfacial Lifshitz-van der Waals and polar interactions in macroscopic systems, Chemical Review 88 (1988): 927-940.

C.J. van Oss, M.K. Chaudhury, R.J. Good. Interfacial Lifshitz-van der Waals and polar interactions in macroscopic systems, Chemical Review 88 (1988): 927-940.

C.Q. Ren, M. Tu, H.H. Wang. An analytical model for heat and mass transfer processes in internally cooled or heated liquid desiccant-air contact units. International Journal of Heat and Mass Transfer 50(17) (2007): 3545-3555.

Chatain D. Experimental study of wetting hysteresis on surfaces with controlled geometrical and/or chemical defects. Acta metallurgica et materialia, 1995, 43(4): 1505-1515.

Chowdhury I, Prasher R, Lofgreen K, et al. On-chip cooling by superlattice-based thin-film thermoelectrics. Nature nanotechnology, 2009, 4(4): 235.

Connington K, Lee T. Lattice Boltzmann simulations of forced wetting transitions of drops on superhydrophobic surfaces. Journal of Computational Physics, 2013, 250: 601-615.

Cox R G. The dynamics of the spreading of liquids on a solid surface. Part 1. Viscous flow. Journal of Fluid Mechanics, 1986, 168: 169-194.

Cox R G. The dynamics of the spreading of liquids on a solid surface. Part 2. Surfactants. Journal of Fluid mechanics, 1986, 168: 195-220.

Cristea A, Sofonea V. Reduction of spurious velocity in finite difference lattice Boltzmann models for liquid–vapor systems. Int. J. Mod. Phys. C, 2003, 14:1251–1266.

D. Pietruschka, U. Eicker, M. Huber, Schumacher J. Experimental performance analysis and modelling of liquid desiccant cooling systems for air conditioning in residential buildings. International Journal of Refrigeration 29(1) (2006): 110-124.

D.I. Stevens, J.E. Braun, S.A. Klein. An effectiveness model of liquid-desiccant system heat/mass exchangers. Solar Energy142(6) (1989): 449-55.

D.K. Owens, R.C. Wendt. Estimation of the surface free energy of polymers. Journal of Applied Polymer Science 13 (1969): 1741-1747

D.L. Elbert, J.A. Hubbell. Surface treatments of polymers for biocompatibility. Annual Review of Materials Research 26(1996): 365-394.

D.Q. Kern, Process Heat Transfer, McGraw-Hill, Japan, 1950.

E. B. Nauman. Chemical Reactor Design, Optimization, and Scaleup. McGraw-Hill Professional, 2002.

E. Elsarrag. Dehumidification of air by chemical liquid desiccant in a packed column and its heat and mass transfer effectiveness. HVAC&R Research 12 (1) (2006): 3-16.

E. Hihara, T. Saito. Effect of surfactant on falling film absorption. International

Journal of Refrigeration 16(5) (1993): 339-346.

EMSD. Performance-based Building Energy Code, 2003 edition. Electrical and Mechanical Services Department, Hong Kong, 2003.

F. Zhang, D.L. Tang, J. Geng, Z.X. Wang, Z.B. Zhang. Study on the temperature distribution of heated falling liquid films. Physica D: Nonlinear Phenomena, 237(7) (2008): 867-872.

F. Zhang, Z.B. Zhang, J. Geng. Study on shrinkage characteristics of heated falling liquid films. AIChE Journal 51(11) (2005): 2899-2907.

F. Zhang, Z.B. Zhang, J. Geng. Study on shrinkage characteristics of heated falling liquid films. AIChE Journal 51(11) (2005): 2899-2907.

Fakhari A, Geier M, Lee T. A mass-conserving lattice Boltzmann method with dynamic grid refinement for immiscible two-phase flows. Journal of Computational Physics, 2016, 315: 434-457.

Falcucci G, Ubertini S, Biscarini C, et al. Lattice Boltzmann methods for multiphase flow simulations across scales[J]. Communications in Computational Physics, 2011, 9(2): 269-296.

G. Karimi, M Kawaji. Flow characteristics and circulatory motion in wavy falling films with and without counter-current gas flow. International Journal of Multiphase Flow 25(6-7) (1999): 1305-1319.

G.J. Gambutis. Heat transfer in film heat exchangers. Proceeding of 14th International Conference of Refrigeration. Moscow 195 (2)1-7.

G.J. Gambutis. Heat transfer in film heat exchangers. Proceeding of 14th International

Conference of Refrigeration. Moscow 195 (2)1-7.

G.M. Ge, F. Xiao, X.F. Niu. Control strategies for a liquid desiccant air-conditioning system. Energy and buildings, 43(6) (2011): 1499-1507.

G.O.G. Lof. Cooling with solar energy. Congress on Solar Energy, Tucson, USA, 1955, 171-189.

G.W. Brundrett. Hand Book of Dehumidification technology, Drying Technology. 1989 7:1 (1989) 143-147, DOI: 10.1080/07373938908916580.

Geier M, Fakhari A, Lee T. Conservative phase-field lattice Boltzmann model for interface tracking equation. Physical Review E, 2015, 91(6): 063309.

H. Fujita, T. Ueda. Falling liquid films in absorption machines. International Journal of Refrigeration 16(1993): 281-292.

H. Takahama, S. Kato. Longitudinal flow characteristics of vertically falling liquid film without concurrent gas flow. International Journal of Multiphase Flow 6(20) (1980) 203-215.

H. Takahama, S. Kato. Longitudinal flow characteristics of vertically falling liquid film without concurrent gas flow. International Journal of Multiphase Flow 6(20) (1980) 203-215.

H.C. Cho, Y.T. Kang, C.D. Kim. Effect of surface roughness of micro-scale hatched tubes on the absorption performance. Proceeding of the International Sorption Heat Pump Conference, Shanghai, China, 2002, 300-304.

H.W. Coleman, W.G. Steele, Experimentation, Validation and Uncertainty Analysis for Engineers, John Wiley & Sons, Inc., 2009.

He X, Chen S, Zhang R. A lattice Boltzmann scheme for incompressible multiphase flow and its application in simulation of Rayleigh¡VTaylor instability. Journal of Computational Physics, 1999, 152(2): 642-663.

Hong Kong Energy End Use Data, Electrical and Mechanical Services, Department of Hong Kong Special Administrative Region, 2017.

Hong Kong Government. Code of practice for overall thermal transfer value in buildings. Hong Kong, 1995.

Hong Kong Government. Code of practice for overall thermal transfer value in buildings. Hong Kong, 1995.

Huang H, Huang J J, Lu X Y, et al. On simulations of high-density ratio flows using color-gradient multiphase lattice Boltzmann models. International Journal of Modern Physics C, 2013, 24(04): 1350021.

Huang H, Lu X. Relative permeabilities and coupling effects in steady-state gas-liquid flow in porous media: A lattice Boltzmann study. Physics of Fluids, 2009, 21(9): 092104.

I. Blom, L. Itard, A. Meijer. Environmental impact of building-related and user-related energy consumption in dwellings, Building and Environment 46(8) (2011): 1657-1669.

J. Benaman. A systematic approach to uncertainty analysis for a distributed watershed model. PhD dissertation, Cornell University, Ithaca, N.Y. 2002.

J. F. Roques, V. Dupont, J. R. Thome. Falling film transitions on plain and enhanced tubes. Journal of Heat Transfer 124(2002):491-499.

J. Geng. Influence of Marangoni Effect on Distillation in Packing Tower. PhD

Dissertation. : Nanjing University, Nanjing, China, 2002.

J.K. Kim, C. W. Park, Y. T. Kang. The effect of micro-scale surface treatment on heat and mass transfer performance for a falling film H2O/LiBr absorber. International Journal of Refrigeration 26 (2003): 575-585.

J.K. Kim, J.Y. Jung, Y.T. Kang. Mass transfer enhancement of a binary nano-fluid for absorption application.The13th International Heat Conference, Australia, 2006.

J.K. Kim, J.Y. Jung, Y.T. Kang. The effect of nano-particles on the bubble absorption performance in a binary nanofluid. International Journal of Refrigeration, 29(1) (2006): 22-29.

J.K. Kim, Y.T. Kang, C.W. Park. The effect of micro-scale surface treatment on heat and mass transfer performance for a falling film H2O/LiBr absorber. Proceeding of the International Sorption Heat Pump Conference, Shanghai, China, 2002, 277-282.

J.R. Howell, E.C.H. Bantel, Design of liquid desiccant dehumidification and cooling systems. Solar Energy Utilization 129 (1987): 374-386.

J.R. Reker, C.A. Plank, E.R. Gerhard. Liquid surface area in wetted-wall column, AICHE Journal 12(5) (1966): 1008-1010.

J.W. Studak, J.L.Peterson. A preliminary evaluation of alternative liquid desiccants for a hybrid desiccant air conditioner. Proceedings of the Fifth Symposium on Improving Building Systems in Hot and Humid Climates, Houston, TX, 1988.

K. Nakao, E. Ozaki, G. Yamanaka. Study on vertical type heat exchanger for absorption heat transformer. National Heat Transfer Symposium of Japan, 1986: 367-369.

K. Onda, H. Takeuchi, Y. Kumoto. Mass transfer coefficients between gas and liquid phases in packed columns. Journal of Chemical Engineering of Japan 1(1) (1968): 56-62.

K. S. Siow, L. Britcher, S. Kumar, H. J. Griesser. Plasma methods for the generation of chemically reactive surfaces for biomolecule immobilization and cell colonization-a review. Plasma Processes and Polymers 3(6-7) (2007): 392-418.

K.I. Lee, H.J. Kim, J.H. Jung. An experimental study on the falling film heat transfer for binary nano-fluids. The 18th International Symposium on Transports Phenomena, Korea, 2007: 1107-1110.

K.R. Morison, Q.A.G. Worth, N.P. O'dea. Minimum Wetting and Distribution Rates in Falling Film Evapourators. Food and Bioproducts Processing 84 (4) (2006): 302-310.

Kabov O A, Zaitsev D V. The effect of wetting hysteresis on drop spreading under gravity. Doklady Physics. Springer US, 2013, 58(7): 292-295.

Keyhani, Majid, and W. A. Miller. The correlation of coupled heat and mass transfer experimental data for vertical falling film absorption. No. ORNL/CP-103983. Oak Ridge National Laboratory (ORNL), Oak Ridge, TN, 1999.

L. McNelly. Thermodynamic properties of aqueous solutions of lithium bromide. ASHRAE Transactions 85 (1979):412-34.

L. Mei, Y.J. Dai. A technical review on use of liquid-desiccant dehumidification for air-conditioning application. Renewable and Sustainable Energy Reviews 12 (2008): 662-689.

L. Perez-Lombard, J. Ortiz, J.F. Coronel, I.R. Maestre. A review of HVAC systems

requirements in building energy regulations, Energy and Buildings 43(2-3) (2011): 255-268.

L.A. Girifalco, R.J. Good. A theory for the estimation of surface and interfacial energies. I. Derivation and application to interfacial tension. The Journal of Physical Chemistry 61 (1957): 904-909.

L.A. Girifalco, R.J. Good. A theory for the estimation of surface and interfacial energies. I. Derivation and application to interfacial tension. The Journal of Physical Chemistry 61 (1957): 904-909.

L.C.S. Mesquita. S.J. Harrison, D. Thomey. Modeling of heat and mass transfer in parallel plate liquid-desiccant dehumidifiers. Solar Energy 80 (2006): 1475-1482.

Lee T, Liu L. Lattice Boltzmann simulations of micron-scale drop impact on dry surfaces. Journal of Computational Physics, 2010, 229(20): 8045-8063.

Li D, Qiao Z, Tang T. Characterizing the stabilization size for semi-implicit Fourier-spectral method to phase field equations[J]. SIAM Journal on Numerical Analysis, 2016, 54(3): 1653-1681.

Liang H, Chai Z H, Shi B C, et al. Phase-field-based lattice Boltzmann model for axisymmetric multiphase flows. Physical Review E, 2014, 90(6): 063311.

Liang H, Xu J, Chen J, et al. Phase-field-based lattice Boltzmann modeling of large-density-ratio two-phase flows. arXiv preprint arXiv:1710.09541, 2017.

Liu L, Lee T. Wall free energy based polynomial boundary conditions for non-ideal gas lattice Boltzmann equation. International Journal of Modern Physics C, 2009, 20(11): 1749-1768.

Lowenstein, A., Review of Liquid Desiccant Technology for Hvac Applications, Hvac&R Research, vol. 14, no. 6, pp. 819-839, 2008.

Lu T, Xiao F. Lattice Boltzmann Simulation of Falling Film Flow under Low Reynolds Number. Heat Transfer Engineering, 2017: 1-12.

M. M. Rafique, P. Gandhidasan, H.M.S. Bahaidarah. Liquid desiccant materials and dehumidifiers-A review. Renewable and Sustainable Energy Reviews 56 (2016): 179-195.

M. Nie, P. Patel, S. Kai, D.D. Meng. Superhydrophilic anti-fog polyester film by oxygen Plasma Treatment. 4th IEEE International Conference on Nano/Micro Engineered and Molecular Systems, Shenzhen, 2009, 1017-1020.

M. Ozdemir, C. U. Yurteri, H. Sadikoglu. Physical polymer surface modification methods and applications in food packaging polymers. Critical Reviews in Food Science and Nutrition 39(5) (1999): 457-477.

M. R. Islam, N. E. Wijeysundera, J. C. Ho. Performance study of a falling-film absorber with a film-inverting configuration. International Journal of Refrigeration 26(8) (2003): 909-917.

M. Yin, J.B. Chen, P. Chen, X.H. Ma, S.P. Li. Study on the heat-mass transfer in falling film outside the vertical tube for water vapor absorption into aqueous lithium bromide. Journal of Chemical Engineering of Chinese Universities 16(6) (2002): 604-607. (In Chinese)

M. Żenkiewicz. Methods for the calculation of surface free energy of solids. Journal of Achievements in Materials and Manufacturing Engineering 24(1) (2007): 137-145.

M.R. Conde. Properties of aqueous solutions of lithium and calcium chlorides:

formulations for use in air conditioning equipment design. International Journal of Thermal Sciences 43 (2004):367-82.

M.R. Islam, J.C. Ho, N.E. Wijeysundera. A study of heat and mass transfer in falling films of film-inverting absorbers. 13th International Heat Transfer Conferenee, 2006, Sydney, Australia.

M.R. Islam, N.E. Wijeysundera, J.C. Ho. Performance study of a falling-film absorber with a film-inverting configuration. International Journal of Refrigeration, 26(8) (2003): 909-917.

M.R. Swift, W.R. Osborn, J.M. Yeomans, Lattice Boltzmann simulation of nonideal fluids. Phys. Rev. Lett. 75 (1995) 830¡V833.

M.S. Buker, S.B. Riffat. Recent developments in solar assisted liquid desiccant evaporative cooling technology-a review. Energy and Buildings 96 (2015): 95-108.

M.S. Park, J.R. Howell, G.C. Vliet, J. Peterson. Numerical and experimental results for coupled heat and mass transfer between a desiccant film and air in cross flow, International Journal of Heat and Mass Transfer 37 (1994): 395-402.

Mazloomi, Ali, Shyam S. Chikatamarla, and Iliya V. Karlin. "Entropic lattice Boltzmann method for multiphase flows: Fluid-solid interfaces." Physical Review E 92.2 (2015): 023308.

Miyara, A. "Numerical analysis on flow dynamics and heat transfer of falling liquid films with interfacial waves." Heat and Mass Transfer 35.4 (1999): 298-306.

Morioka, Itsuki, Masanori Kiyota, and Ryuuji Nakao. "Absorption of water vapor into a film of aqueous solution of LiBr falling along a vertical pipe." JSME International Journal Series B Fluids and Thermal Engineering 36.2 (1993): 351-356.

N. Nishimura, T. Nomura, H. Lyota. Investigation of absorption enhancement by a surfactant. Proeeeding of the Intemational Sorption Heat Pump Conferenee, Shanghai, China, 2002, 373-377.

N. Nusselt, Die Oberflachenkondensation des Wasserdampfes. Zeit. Ver. D. Ing. 60(1916) 541-569.

N. Nusselt, Die Oberflachenkondensation des Wasserdampfes. Zeit. Ver. D. Ing. 60(1916) 541-569.

O.A. Kabov, B. Scheid, I.A. Sharina, J.C. Legros. Heat transfer and rivulet structures formation in a falling thin liquid film locally heated. International Journal of Thermal Science 427 (2002): 664-672.

ows on partial wetting surface with large density ratio. Journal of Computational Physics, 2007, 227(1): 763-775.

P. Chen. Investigation on the heat-mass transfer on vertical tube of falling film of water vapor absorption aqueous lithium bromide. Dalian University of Technology, Dalian, China, 2002. (In Chinese)

P. Mazzei, F. Minichiello, D. Palma. HVAC dehumidification systems for thermal comfort: a critical review. Applied Thermal Engineering 25 (2005): 677-707.

P. Patel, C. K. Choi and D.D. Meng. Superhydrophilic surfaces for antifogging and antifouling microfluidic devices. Journal of Laboratory Automation, 15(2) (2010): 114-119.

P. Tuominen, R. Holopainen, L. Eskola, J. Jokisalo, M. Airaksinen. Calculation method and tool for assessing energy consumption in the building stock, Building and Environment 75 (2014): 153-160.

P.N. Yoshimura, T. Nosoko, T. Nagata. Enhancement of mass transfer into a falling laminar liquid film by two-dimensional surface waves-some experimental observations and modeling. Chemical Engineering Science, 51(8) (1996): 1231-1240.

Pooley C, Furtado K. Eliminating spurious velocities in the free-energy lattice Boltzmann method. Phys. Rev. E, 2008, 77:046702. Sbragaglia M, Benzi R, Biferale L et al. Generalized lattice Boltzmann method with multirange pseudopotential. Phys. Rev. E, 2007, 75:026702.

Principles of Colloid and Surface Chemistry, Third Edition, Marcel Dekker, Inc. 1997.

Principles of Colloid and Surface Chemistry, Third Edition, Marcel Dekker, Inc. 1997.

Qian Y H. Simulating thermohydrodynamics with lattice BGK models. Journal of Scientific Computing, 1993, 8(3): 231-242.

Qiao Z, Sun S. Two-phase fluid simulation using a diffuse interface model with Peng--Robinson equation of state[J]. SIAM Journal on Scientific Computing, 2014, 36(4): B708-B728.

Qiao Z, Zhang Z, Tang T. An adaptive time-stepping strategy for the molecular beam epitaxy models[J]. SIAM Journal on Scientific Computing, 2011, 33(3): 1395-1414.

R. Chen, M.C. Lu, V. Srinivasan, Z. Wang, H. H. Cho and A. Majumdar. Nanowires for enhanced boiling heat transfer, Nano Letters, 9(2) (2009): 548-553.

R. Yang, D. Jou. Heat and mass transfer of absorption process for the falling film flow inside a porous medium. International Journal of Heat and Mass Transfer 38(6) (1995):1121-1126.

R.E. Treybal, Mass Transfer Operations, 3rd ed., McGraw-Hill, New York, 1981.

R.H. Qi, L. Lu, H.X. Yang, F. Qin. Influence of plate surface temperature on the wetted area and system performance for falling film liquid desiccant regeneration system. International Journal of Heat and Mass Transfer 64 (2013): 1003-1013.

R.H. Qi, L. Lu, H.X. Yang, F. Qin. Influence of plate surface temperature on the wetted area and system performance for falling film liquid desiccant regeneration system. International Journal of Heat and Mass Transfer 64 (2013): 1003-1013.

R.H. Qi, L. Lu, H.X. Yang, F. Qin. Investigation on wetted area and film thickness for falling film liquid desiccant regeneration system. Applied Energy, 112 (2013): 93-101.

R.H. Qi, L. Lu, H.X. Yang. Development of simplified prediction model for internally cooled/heated liquid desiccant dehumidification system. Energy and Buildings 59 (2013): 133-142.

R.H. Qi, Y. Hu, Y.H. Wang, L. Lu. A new approach to enhance the heat and mass transfer of liquid desiccant dehumidification with a titanium dioxide super-hydrophilic self-cleaning coating. Journal of Cleaner Production 112 (2016): 3555-3561.

R.H. Qi. Study on Heat and mass transfer of internally heated liquid desiccant regeneration for solar-assisted air-conditioning system. Phd dissertation. The Hong Kong Polytechnic University, Hong Kong China, 2013.

R.N. Wenzel. Resistance of solid surface to wetting by water. Journal of Industrial & Engineering Chemistry 28(1936): 988-994.

A. A. Mohamad, Lattice Boltzmann Method, Fundamentals and Engineering Applications with Computer Codes (Springer, London, 2011).

A. Ali, K. Vafai, A.R.A. Khaled. Analysis of heat and mass transfer between air and falling film in a cross flow configuration. International Journal of Heat and Mass

Transfer 47 (2004): 743-755.

A. Faghri, Y.W. Zhang. John Howell. Advanced Heat and Mass Transfer. Global Digital Press. 2010.

A. Lowenstein, K.E. Slyzak. A zero carry over liquid desiccant air conditioner for solar applications. ASME International Solar Energy Conference (ISEC 2006), 2006, Denver, Colarodo.

A. Ulman, An introduction to ultrathin organic films: from Langmuir-Blodgett to Self-Assembly, Academic Press, Inc, Boston, 1991.

A.A. Ertas, E.E. Anderson, I. Kiris. Properties of a new liquid desiccant solution-lithium chloride and calcium chloride mixture. Solar Energy 49(3) (1992):205-12.

A.A. Farayedhi, A.P. Gandhidasan, et al. Regeneration of liquid desiccants using membrane technology. Energy Conversion and Management 40(13) (1999): 1405-1411.

A.B.D. Cassie, S. Baxter. Wettability of porous surfaces. Transactions of the Faraday Society 40(1944): 546-551.

A.S.A. Mohamed , M.S. Ahmed, A.A.M. Hassan, M. Salah Hassan, Performance evaluation of gauze packing for liquid desiccant dehumidification system, Case Studies in Thermal Engineering 8 (2016) 260-276.

A.T. Conlisk. Semi-analytical design of a falling film absorber. Journal of heat transfer 116 (1994):1055-1058.

A.Y. Khan, H.D. Ball. Development of a generalized model for performance evaluation of packed-type liquid sorbent dehumidifiers and regenerators. ASHRAE

Transactions 98 (1992): 525-33.

Ahn, J., Kim, J., and Kang, B.H., Performance of a Hybrid Desiccant Cooling System in a Residential Environment, Heat Transfer Engineering, vol. 37, no. 7-8, pp. 633-639, 2016.

B. Chopard, J. L. Falcone, and J. Latt, Eur. Phys. J.: Spec. Top. 171, 245 (2009).

B.G. Ganchev, V.M. Koglov, V.V. Lozovetskiy. A study of heat transfer to a falling film at a vertical surface. Heat transfer-Soviet Research (4) (1972): 102-110.

Balotaki, Hassan Kavoosi, et al. "Modelling of free convection heat transfer in a triangular cavity equipped using double distribution functions (DDF) lattice Boltzmann method (LBM)." Thermal Science and Engineering Progress (2020): 100495.

Benzi R, Succi S, Vergassola M. The lattice Boltzmann equation: theory and applications[J]. Physics Reports, 1992, 222(3): 145-197.

Bösch F, Dorschner B, Karlin I. Entropic multi-relaxation free-energy lattice Boltzmann model for two-phase flows[J]. EPL (Europhysics Letters), 2018, 122(1): 14002.

Brauner, M., J. S. Briggs, and H. Klar. "Triply-differential cross sections for ionisation of hydrogen atoms by electrons and positrons." Journal of Physics B: Atomic, Molecular and Optical Physics 22.14 (1989): 2265.

C. Decker, K. Zahouily. Photodegradation and photooxidation of thermoset and UV-cured acrylate polymers. Polymer Degradation and Stability 64(2) (1999): 293-304.

C. Li, Z. Wang, P.I. Wang, Y. Peles, N. Koratkar and G.P. Peterson. Nanostructured

copper interfaces for enhanced boiling. Small, 4(8) (2008): 1084-1088.

C. M. Chan, T. M. Ko, H. Hiraoka. Polymer surface modification by plasmas and photons. Surface Science Reports 24(1-2) (1996): 3-54.

C.H.E. Nielsen, S. Kiil, H.W. Thomsen, K. Dam-Johansen. Mass transfer in wetted-wall columns: Correlations at high Reynolds numbers. Chemical Engineering Science 53 (3) (1998): 495-503.

C.J. van Oss, M.K. Chaudhury, R.J. Good. Interfacial Lifshitz-van der Waals and polar interactions in macroscopic systems, Chemical Review 88 (1988): 927-940.

C.Q. Ren, M. Tu, H.H. Wang. An analytical model for heat and mass transfer processes in internally cooled or heated liquid desiccant-air contact units. International Journal of Heat and Mass Transfer 50(17) (2007): 3545-3555.

Chatain D. Experimental study of wetting hysteresis on surfaces with controlled geometrical and/or chemical defects. Acta metallurgica et materialia, 1995, 43(4): 1505-1515.

Chiappini D, Bella G, Succi S, et al. Improved lattice Boltzmann without parasitic currents for Rayleigh-Taylor instability[J]. Communications in Computational Physics, 2010, 7(3): 423.

Chowdhury I, Prasher R, Lofgreen K, et al. On-chip cooling by superlattice-based thin-film thermoelectrics. Nature nanotechnology, 2009, 4(4): 235.

Colosqui C E, Falcucci G, Ubertini S, et al. Mesoscopic simulation of non-ideal fluids with self-tuning of the equation of state[J]. Soft Matter, 2012, 8(14): 3798-3809.

Connington K, Lee T. Lattice Boltzmann simulations of forced wetting transitions of

drops on superhydrophobic surfaces. Journal of Computational Physics, 2013, 250: 601-615.

Cox R G. The dynamics of the spreading of liquids on a solid surface. Part 1. Viscous flow. Journal of Fluid Mechanics, 1986, 168: 169-194.

Cox R G. The dynamics of the spreading of liquids on a solid surface. Part 2. Surfactants. Journal of Fluid mechanics, 1986, 168: 195-220.

Cristea A, Sofonea V. Reduction of spurious velocity in finite difference lattice Boltzmann models for liquid–vapor systems. Int. J. Mod. Phys. C, 2003, 14:1251–1266.

D. Pietruschka, U. Eicker, M. Huber, Schumacher J. Experimental performance analysis and modelling of liquid desiccant cooling systems for air conditioning in residential buildings. International Journal of Refrigeration 29(1) (2006): 110-124.

D.I. Stevens, J.E. Braun, S.A. Klein. An effectiveness model of liquid-desiccant system heat/mass exchangers. Solar Energy142(6) (1989): 449-55.

D.K. Owens, R.C. Wendt. Estimation of the surface free energy of polymers. Journal of Applied Polymer Science 13 (1969): 1741-1747

D.L. Elbert, J.A. Hubbell. Surface treatments of polymers for biocompatibility. Annual Review of Materials Research 26(1996): 365-394.

D.Q. Kern, Process Heat Transfer, McGraw-Hill, Japan, 1950.

E. Elsarrag. Dehumidification of air by chemical liquid desiccant in a packed column and its heat and mass transfer effectiveness. HVAC&R Research 12 (1) (2006): 3-16.

E. Hihara, T. Saito. Effect of surfactant on falling film absorption. International

Journal of Refrigeration 16(5) (1993): 339-346.

EMSD. Performance-based Building Energy Code, 2003 edition. Electrical and Mechanical Services Department, Hong Kong, 2003.

F. Zhang, D.L. Tang, J. Geng, Z.X. Wang, Z.B. Zhang. Study on the temperature distribution of heated falling liquid films. Physica D: Nonlinear Phenomena, 237(7) (2008): 867-872.

F. Zhang, Z.B. Zhang, J. Geng. Study on shrinkage characteristics of heated falling liquid films. AIChE Journal 51(11) (2005): 2899-2907.

Fakhari A, Geier M, Lee T. A mass-conserving lattice Boltzmann method with dynamic grid refinement for immiscible two-phase flows. Journal of Computational Physics, 2016, 315: 434-457.

Falcucci G, Ubertini S, Biscarini C, et al. Lattice Boltzmann methods for multiphase flow simulations across scales[J]. Communications in Computational Physics, 2011, 9(2): 269-296.

G. Karimi, M Kawaji. Flow characteristics and circulatory motion in wavy falling films with and without counter-current gas flow. International Journal of Multiphase Flow 25(6-7) (1999): 1305-1319.

G.J. Gambutis. Heat transfer in film heat exchangers. Proceeding of 14th International Conference of Refrigeration. Moscow 195 (2)1-7.

G.M. Ge, F. Xiao, X.F. Niu. Control strategies for a liquid desiccant air-conditioning system. Energy and buildings, 43(6) (2011): 1499-1507.

G.O.G. Lof. Cooling with solar energy. Congress on Solar Energy, Tucson, USA, 1955,

171-189.

G.W. Brundrett. Hand Book of Dehumidification technology, Drying Technology. 1989 7:1 (1989) 143-147, DOI: 10.1080/07373938908916580.

Gaedtke, Maximilian, et al. "Total enthalpy-based lattice Boltzmann simulations of melting in paraffin/metal foam composite phase change materials." International Journal of Heat and Mass Transfer 155 (2020): 119870.

Geier M, Fakhari A, Lee T. Conservative phase-field lattice Boltzmann model for interface tracking equation. Physical Review E, 2015, 91(6): 063309.

Guo, Lin, G. H. Tang, and Satish Kumar. "Droplet Morphology and Mobility on Lubricant-Impregnated Surfaces: A Molecular Dynamics Study." Langmuir 35.49 (2019): 16377-16387.

H. Fujita, T. Ueda. Falling liquid films in absorption machines. International Journal of Refrigeration 16(1993): 281-292.

H. Takahama, S. Kato. Longitudinal flow characteristics of vertically falling liquid film without concurrent gas flow. International Journal of Multiphase Flow 6(20) (1980) 203-215.

H.C. Cho, Y.T. Kang, C.D. Kim. Effect of surface roughness of micro-scale hatched tubes on the absorption performance. Proceeding of the International Sorption Heat Pump Conference, Shanghai, China, 2002, 300-304.

H.W. Coleman, W.G. Steele, Experimentation, Validation and Uncertainty Analysis for Engineers, John Wiley & Sons, Inc., 2009.

He X, Chen S, Zhang R. A lattice Boltzmann scheme for incompressible multiphase

flow and its application in simulation of Rayleigh¡VTaylor instability. Journal of Computational Physics, 1999, 152(2): 642-663.

He, Ya-Ling, et al. "Lattice Boltzmann methods for single-phase and solid-liquid phase-change heat transfer in porous media: A review." International Journal of Heat and Mass Transfer 129 (2019): 160-197.

Hong Kong Energy End Use Data, Electrical and Mechanical Services, Department of Hong Kong Special Administrative Region, 2017.

Hong Kong Government. Code of practice for overall thermal transfer value in buildings. Hong Kong, 1995.

Hosseini, Seyed Ali, Nasser Darabiha, and Dominique Thévenin. "Lattice Boltzmann advection-diffusion model for conjugate heat transfer in heterogeneous media." International Journal of Heat and Mass Transfer 132 (2019): 906-919.

Huang H, Huang J J, Lu X Y, et al. On simulations of high-density ratio flows using color-gradient multiphase lattice Boltzmann models. International Journal of Modern Physics C, 2013, 24(04): 1350021.

Huang H, Lu X. Relative permeabilities and coupling effects in steady-state gas-liquid flow in porous media: A lattice Boltzmann study. Physics of Fluids, 2009, 21(9): 092104.

I. Blom, L. Itard, A. Meijer. Environmental impact of building-related and user-related energy consumption in dwellings, Building and Environment 46(8) (2011): 1657-1669.

J. Benaman. A systematic approach to uncertainty analysis for a distributed watershed model. PhD dissertation, Cornell University, Ithaca, N.Y. 2002.

J. F. Roques, V. Dupont, J. R. Thome. Falling film transitions on plain and enhanced tubes. Journal of Heat Transfer 124(2002):491-499.

J. Geng. Influence of Marangoni Effect on Distillation in Packing Tower. PhD Dissertation. : Nanjing University, Nanjing, China, 2002.

J.K. Kim, C. W. Park, Y. T. Kang. The effect of micro-scale surface treatment on heat and mass transfer performance for a falling film H2O/LiBr absorber. International Journal of Refrigeration 26 (2003): 575-585.

J.K. Kim, J.Y. Jung, Y.T. Kang. Mass transfer enhancement of a binary nano-fluid for absorption application.The13th International Heat Conference, Australia, 2006.

J.K. Kim, J.Y. Jung, Y.T. Kang. The effect of nano-particles on the bubble absorption performance in a binary nanofluid. International Journal of Refrigeration, 29(1) (2006): 22-29.

J.K. Kim, Y.T. Kang, C.W. Park. The effect of micro-scale surface treatment on heat and mass transfer performance for a falling film H2O/LiBr absorber. Proceeding of the International Sorption Heat Pump Conference, Shanghai, China, 2002, 277-282.

J.R. Howell, E.C.H. Bantel, Design of liquid desiccant dehumidification and cooling systems. Solar Energy Utilization 129 (1987): 374-386.

J.R. Reker, C.A. Plank, E.R. Gerhard. Liquid surface area in wetted-wall column, AICHE Journal 12(5) (1966): 1008-1010.

J.W. Studak, J.L.Peterson. A preliminary evaluation of alternative liquid desiccants for a hybrid desiccant air conditioner. Proceedings of the Fifth Symposium on Improving Building Systems in Hot and Humid Climates, Houston, TX, 1988.

K. Nakao, E. Ozaki, G. Yamanaka. Study on vertical type heat exchanger for absorption heat transformer. National Heat Transfer Symposium of Japan, 1986: 367-369.

K. Onda, H. Takeuchi, Y. Kumoto. Mass transfer coefficients between gas and liquid phases in packed columns. Journal of Chemical Engineering of Japan 1(1) (1968): 56-62.

K. S. Siow, L. Britcher, S. Kumar, H. J. Griesser. Plasma methods for the generation of chemically reactive surfaces for biomolecule immobilization and cell colonization-a review. Plasma Processes and Polymers 3(6-7) (2007): 392-418.

K.I. Lee, H.J. Kim, J.H. Jung. An experimental study on the falling film heat transfer for binary nano-fluids. The 18th International Symposium on Transports Phenomena, Korea, 2007: 1107-1110.

K.R. Morison, Q.A.G. Worth, N.P. O'dea. Minimum Wetting and Distribution Rates in Falling Film Evapourators. Food and Bioproducts Processing 84 (4) (2006): 302-310.

Kabov O A, Zaitsev D V. The effect of wetting hysteresis on drop spreading under gravity. Doklady Physics. Springer US, 2013, 58(7): 292-295.

Keyhani, Majid, and W. A. Miller. The correlation of coupled heat and mass transfer experimental data for vertical falling film absorption. No. ORNL/CP-103983. Oak Ridge National Laboratory (ORNL), Oak Ridge, TN, 1999.

Krüger, Timm, et al. "The lattice Boltzmann method." Springer International Publishing 10 (2017): 978-3.

L. McNelly. Thermodynamic properties of aqueous solutions of lithium bromide.

ASHRAE Transactions 85 (1979):412-34.

L. Mei, Y.J. Dai. A technical review on use of liquid-desiccant dehumidification for air-conditioning application. Renewable and Sustainable Energy Reviews 12 (2008): 662-689.

L. Perez-Lombard, J. Ortiz, J.F. Coronel, I.R. Maestre. A review of HVAC systems requirements in building energy regulations, Energy and Buildings 43(2-3) (2011): 255-268.

L.A. Girifalco, R.J. Good. A theory for the estimation of surface and interfacial energies. I. Derivation and application to interfacial tension. The Journal of Physical Chemistry 61 (1957): 904-909.

L.C.S. Mesquita. S.J. Harrison, D. Thomey. Modeling of heat and mass transfer in parallel plate liquid-desiccant dehumidifiers. Solar Energy 80 (2006): 1475-1482.

Latt, Jonas, et al. "Palabos: Parallel Lattice Boltzmann solver." Computers & Mathematics with Applications (2020).

Lee T, Liu L. Lattice Boltzmann simulations of micron-scale drop impact on dry surfaces. Journal of Computational Physics, 2010, 229(20): 8045-8063.

Li D, Qiao Z, Tang T. Characterizing the stabilization size for semi-implicit Fourier-spectral method to phase field equations[J]. SIAM Journal on Numerical Analysis, 2016, 54(3): 1653-1681.

Li, Zhixiong, et al. "Nanofluid heat transfer in a porous duct in the presence of Lorentz forces using the lattice Boltzmann method." The European Physical Journal Plus 134.1 (2019): 1-10.

Liang H, Chai Z H, Shi B C, et al. Phase-field-based lattice Boltzmann model for axisymmetric multiphase flows. Physical Review E, 2014, 90(6): 063311.

Liang H, Xu J, Chen J, et al. Phase-field-based lattice Boltzmann modeling of large-density-ratio two-phase flows. arXiv preprint arXiv:1710.09541, 2017.

Liu L, Lee T. Wall free energy based polynomial boundary conditions for non-ideal gas lattice Boltzmann equation. International Journal of Modern Physics C, 2009, 20(11): 1749-1768.

Lowenstein, A., Review of Liquid Desiccant Technology for Hvac Applications, Hvac&R Research, vol. 14, no. 6, pp. 819-839, 2008.

Lu T, Xiao F. Lattice Boltzmann Simulation of Falling Film Flow under Low Reynolds Number. Heat Transfer Engineering, 2017: 1-12.

Lu, J. H., H. Y. Lei, and C. S. Dai. "Lattice Boltzmann equation for mass transfer in multi solvent systems." International Journal of Heat and Mass Transfer 132 (2019): 519-528.

M. M. Rafique, P. Gandhidasan, H.M.S. Bahaidarah. Liquid desiccant materials and dehumidifiers-A review. Renewable and Sustainable Energy Reviews 56 (2016): 179-195.

M. Nie, P. Patel, S. Kai, D.D. Meng. Superhydrophilic anti-fog polyester film by oxygen Plasma Treatment. 4th IEEE International Conference on Nano/Micro Engineered and Molecular Systems, Shenzhen, 2009, 1017-1020.

M. Ozdemir, C. U. Yurteri, H. Sadikoglu. Physical polymer surface modification methods and applications in food packaging polymers. Critical Reviews in Food Science and Nutrition 39(5) (1999): 457-477.

M. R. Islam, N. E. Wijeysundera, J. C. Ho. Performance study of a falling-film absorber with a film-inverting configuration. International Journal of Refrigeration 26(8) (2003): 909-917.

M. Yin, J.B. Chen, P. Chen, X.H. Ma, S.P. Li. Study on the heat-mass transfer in falling film outside the vertical tube for water vapor absorption into aqueous lithium bromide. Journal of Chemical Engineering of Chinese Universities 16(6) (2002): 604-607. (In Chinese)

M. Żenkiewicz. Methods for the calculation of surface free energy of solids. Journal of Achievements in Materials and Manufacturing Engineering 24(1) (2007): 137-145.

M.R. Conde. Properties of aqueous solutions of lithium and calcium chlorides: formulations for use in air conditioning equipment design. International Journal of Thermal Sciences 43 (2004):367-82.

M.R. Islam, J.C. Ho, N.E. Wijeysundera. A study of heat and mass transfer in falling films of film-inverting absorbers. 13th International Heat Transfer Conferenee, 2006, Sydney, Australia.

M.R. Swift, W.R. Osborn, J.M. Yeomans, Lattice Boltzmann simulation of nonideal fluids. Phys. Rev. Lett. 75 (1995) 830 V833.

M.S. Buker, S.B. Riffat. Recent developments in solar assisted liquid desiccant evaporative cooling technology-a review. Energy and Buildings 96 (2015): 95-108.

M.S. Park, J.R. Howell, G.C. Vliet, J. Peterson. Numerical and experimental results for coupled heat and mass transfer between a desiccant film and air in cross flow, International Journal of Heat and Mass Transfer 37 (1994): 395-402.

Ma, Yuan, et al. "Numerical investigation of MHD effects on nanofluid heat transfer

in a baffled U-shaped enclosure using lattice Boltzmann method." Journal of Thermal Analysis and Calorimetry 135.6 (2019): 3197-3213.

Mazloomi A, Chikatamarla S S, Karlin I V. Entropic lattice Boltzmann method for multiphase flows: Fluid-solid interfaces[J]. Physical Review E, 2015, 92(2): 023308.

Mazloomi M A, Chikatamarla S S, Karlin I V. Entropic Lattice Boltzmann Method for Multiphase Flows[J]. Physical Review Letters, 2015, 114(17).

Mazloomi Moqaddam A, Chikatamarla S S, Karlin I V. Simulation of binary droplet collisions with the entropic lattice Boltzmann method[J]. Physics of Fluids, 2016, 28(2): 022106.

Mazloomi, Ali, Shyam S. Chikatamarla, and Iliya V. Karlin. "Entropic lattice Boltzmann method for multiphase flows: Fluid-solid interfaces." Physical Review E 92.2 (2015): 023308.

Miyara, A. "Numerical analysis on flow dynamics and heat transfer of falling liquid films with interfacial waves." Heat and Mass Transfer 35.4 (1999): 298-306.

Mohebbi, Rasul, et al. "Forced convection of nanofluids in an extended surfaces channel using lattice Boltzmann method." International Journal of Heat and Mass Transfer 117 (2018): 1291-1303.

Montessori A, Falcucci G, La Rocca M, et al. Three-dimensional lattice pseudo-potentials for multiphase flow simulations at high density ratios[J]. Journal of Statistical Physics, 2015, 161(6): 1404-1419.

Moqaddam A M, Chikatamarla S S, Karlin I V. Drops bouncing off macro-textured superhydrophobic surfaces[J]. Journal of Fluid Mechanics, 2017, 824: 866-885.

Morioka, Itsuki, Masanori Kiyota, and Ryuuji Nakao. "Absorption of water vapor into a film of aqueous solution of LiBr falling along a vertical pipe." JSME International Journal Series B Fluids and Thermal Engineering 36.2 (1993): 351-356.

N. Nishimura, T. Nomura, H. Lyota. Investigation of absorption enhancement by a surfactant. Proeeeding of the Intemational Sorption Heat Pump Conferenee, Shanghai, China, 2002, 373-377.

N. Nusselt, Die Oberflachenkondensation des Wasserdampfes. Zeit. Ver. D. Ing. 60(1916) 541-569.

O.A. Kabov, B. Scheid, I.A. Sharina, J.C. Legros. Heat transfer and rivulet structures formation in a falling thin liquid film locally heated. International Journal of Thermal Science 427 (2002): 664-672.

P. Chen. Investigation on the heat-mass transfer on vertical tube of falling film of water vapor absorption aqueous lithium bromide. Dalian University of Technology, Dalian, China, 2002. (In Chinese)

P. Mazzei, F. Minichiello, D. Palma. HVAC dehumidification systems for thermal comfort: a critical review. Applied Thermal Engineering 25 (2005): 677-707.

P. Patel, C. K. Choi and D.D. Meng. Superhydrophilic surfaces for antifogging and antifouling microfluidic devices. Journal of Laboratory Automation, 15(2) (2010): 114-119.

P. Tuominen, R. Holopainen, L. Eskola, J. Jokisalo, M. Airaksinen. Calculation method and tool for assessing energy consumption in the building stock, Building and Environment 75 (2014): 153-160.

P.N. Yoshimura, T. Nosoko, T. Nagata. Enhancement of mass transfer into a falling

laminar liquid film by two-dimensional surface waves-some experimental observations and modeling. Chemical Engineering Science, 51(8) (1996): 1231-1240.

Pooley C, Furtado K. Eliminating spurious velocities in the free-energy lattice Boltzmann method. Phys. Rev. E, 2008, 77:046702. Sbragaglia M, Benzi R, Biferale L et al. Generalized lattice Boltzmann method with multirange pseudopotential. Phys. Rev. E, 2007, 75:026702.

Principles of Colloid and Surface Chemistry, Third Edition, Marcel Dekker, Inc. 1997.

Qian Y H. Simulating thermohydrodynamics with lattice BGK models. Journal of Scientific Computing, 1993, 8(3): 231-242.

Qiao Z, Sun S. Two-phase fluid simulation using a diffuse interface model with Peng--Robinson equation of state[J]. SIAM Journal on Scientific Computing, 2014, 36(4): B708-B728.

Qiao Z, Zhang Z, Tang T. An adaptive time-stepping strategy for the molecular beam epitaxy models[J]. SIAM Journal on Scientific Computing, 2011, 33(3): 1395-1414.

R. Chen, M.C. Lu, V. Srinivasan, Z. Wang, H. H. Cho and A. Majumdar. Nanowires for enhanced boiling heat transfer, Nano Letters, 9(2) (2009): 548-553.

R. Yang, D. Jou. Heat and mass transfer of absorption process for the falling film flow inside a porous medium. International Journal of Heat and Mass Transfer 38(6) (1995):1121-1126.

R.E. Treybal, Mass Transfer Operations, 3rd ed., McGraw-Hill, New York, 1981.

R.H. Qi, L. Lu, H.X. Yang, F. Qin. Influence of plate surface temperature on the wetted area and system performance for falling film liquid desiccant regeneration system.

International Journal of Heat and Mass Transfer 64 (2013): 1003-1013.

R.H. Qi, L. Lu, H.X. Yang, F. Qin. Investigation on wetted area and film thickness for falling film liquid desiccant regeneration system. Applied Energy, 112 (2013): 93-101.

R.H. Qi, L. Lu, H.X. Yang. Development of simplified prediction model for internally cooled/heated liquid desiccant dehumidification system. Energy and Buildings 59 (2013): 133-142.

R.H. Qi, Y. Hu, Y.H. Wang, L. Lu. A new approach to enhance the heat and mass transfer of liquid desiccant dehumidification with a titanium dioxide super-hydrophilic self-cleaning coating. Journal of Cleaner Production 112 (2016): 3555-3561.

R.H. Qi. Study on Heat and mass transfer of internally heated liquid desiccant regeneration for solar-assisted air-conditioning system. Phd dissertation. The Hong Kong Polytechnic University, Hong Kong China, 2013.

R.N. Wenzel. Resistance of solid surface to wetting by water. Journal of Industrial & Engineering Chemistry 28(1936): 988-994.

Roques, J.F. and Thome, J., Falling Films on Arrays of Horizontal Tubes with R-134a, Part Ii: Flow Visualization, Onset of Dryout, and Heat Transfer Predictions, Heat Transfer Engineering, vol. 28, no. 5, pp. 415-434, 2007.

Rothman D H, Keller J M. Immiscible cellular-automaton fluids. Journal of Statistical Physics, 1988, 52(3): 1119-1127.

S. Farris, S. Pozzoli, P. Biagioni, L. Duo, S. Mancinelli, L. Piergiovanni. The fundamentals of flame treatment for the surface activation of polyolefin polymers-a review. Polymer 51(16) (2010): 3591-3605.

S. Hardt and F. Wondra, J. Comput. Phys. 227, 5871 (2008).

S. Jain, P.K. Bansal. Performance analysis of liquid desiccant dehumidification systems. International Journal of Refrigeration, 30(5) (2007): 861-872.

S.R. Broome. Liquid Distribution And Falling Film Wetting In Dairy Evapourators. Master Dissertation. University of Canterbury, Christchurch, New Zealand, 2005.

Sbragaglia M, Benzi R, Biferale L et al. Generalized lattice Boltzmann method with multirange pseudopotential. Phys. Rev. E, 2007, 75:026702.

Seta T, Okui K. Effects of Truncation Error of Derivative Approximation for Two-Phase Lattice Boltzmann Method. J. Fluid Sci. Technol., 2007, 2:139.

Shan X, Chen H. Lattice Boltzmann model for simulating flows with multiple phases and components. Physical Review E, 1993, 47(3): 1815.

Shan X. Analysis and reduction of the spurious current in a class of multiphase lattice Boltzmann models. Phys. Rev. E, 2006, 73:047701.

Shi, Y., et al. "An improved phase-field-based lattice Boltzmann model for droplet dynamics with soluble surfactant." Computers & Fluids 179 (2019): 508-520.

Shi, Y., G. H. Tang, and L. Y. Shen. "Study of coalescence-induced droplet jumping during phase-change process in the presence of noncondensable gas." International Journal of Heat and Mass Transfer 152 (2020): 119506.

Soolaman D M, Yu H Z. Water microdroplets on molecularly tailored surfaces: correlation between wetting hysteresis and evaporation mode switching. The Journal of Physical Chemistry B, 2005, 109(38): 17967-17973.

T. Inamuro, M. Yoshino, H. Inoue, R. Mizuno, and F. Ogino, J. Comput. Phys. 179,

201 (2002).

T. Young. An easy on the cohesion of fluids, Philosophical Transactions of the Royal Society of London 95 (1805):65-87.

T.D. Karapantsios, S.V. Paras, A.J. Karabelas. Statistical characteristics of free falling film at high Reynolds number. International Journal of Multiphase Flow 15 (1) (1989): 1-21.

T.W. Chung, C.M. Luo. Vapor Pressures of the Aqueous Desiccants. Journal of Chemical & Engineering Data 44 (5) (1999): 1024-1027.

Uddholm, H., and F. Setterwall. "Model for dimensioning a falling film absorber in an absorption heat pump." International journal of refrigeration 11.1 (1988): 41-45.

V.H. Ramm, Absorption of gases, in: Israel Program for Scienti®c Translations, Jerusalem, 1968.

Vliet, G. C., and F. B. Cosenza. "Absorption phenomena in water-lithium bromide films." Proceedings of the International Absorption Heat Pump Conference. 1991.

W. Kessling, E. Laevemann, C. Kapfhammer. Energy storage for desiccant cooling systems component development. Solar Energy 64(4-6) (1998): 209-21.

W.F. Stoecker, Design of Thermal Systems, 3rd ed., McGraw-Hill, New York, 1989.

W.L. Cheng, R. Zhao, C. Liu, S.L. Jiang, Z.S. Chen. Experimental study of influence of additives on ammonia bubble absorption. Journal of Refrigeration 27(3) (2006): 35-40. (In Chinese)

W.L. Cheng, Z.S. Chen. Experimental study of steam absorption into aqueous lithium bromide with vapor of additive. Fluid Machinery 30(12) (2002): 40-43. (In Chinese)

Wang, Chun-Sheng, et al. "Lattice Boltzmann study of flow pulsation on heat transfer augmentation in a louvered microchannel heat sink." International Journal of Heat and Mass Transfer 148 (2020): 119139.

X. H. Liu, Y. Jiang, X.M. Chang, X.Q. Yi. Experimental investigation of the heat and mass transfer between air and liquid desiccant in a cross-flow regenerator. Renewable Energy 32 (10) (2007) 1623-1636.

X.H. Liu, Y. Jiang, K.Y. Qu. Heat and mass transfer model of cross flow liquid desiccant air dehumidifier/regenerator. Energy Conversion and Management 48 (2) (2007): 546-554.

X.H. Ma, F.M. Su, J.B. Chen. Heat and mass transfer enhancement of the bubble absorption for a binary nanofluid. Journal of Mechanical Science and Technology 21(2007): 1338-1343.

X.M. Ye, H. X, S.D. Ma. Review on experimental research on wetting of surfactant solutions. Journal of North China Electric Power University, 38(3) (2011): 72-77.

X.Y. Cui, J.Z. Shi, C. Tan. Investigation of plate falling film absorber with film-inverting configuration. Journal of Heat Transfer 131(2009): 072001-9.

Xu, Ao, Le Shi, and Heng-Dong Xi. "Lattice Boltzmann simulations of three-dimensional thermal convective flows at high Rayleigh number." International Journal of Heat and Mass Transfer 140 (2019): 359-370.

Y. Im, Y. Joshi, C. Dietz and S. Lee. Enhanced boiling of a dielectric liquid on copper nanowire surfaces. International Journal of Micro-Nano Scale Transport 1(1) (2010): 79-96.

Y. Jiang, Z. Li, X.L. Chen, X.H. Liu. Liquid desiccant air conditioning system and its

applications. Journal of HV&AC 34 (2004): 88-98.

Y. Kaita. Thermodynamic properties of lithium bromide-water solutions at high temperatures. International Journal of Refrigeration 24 (2001):371-90.

Y. T. Kang, T. Kashiwagi. Heat transfer enhancement by Marangoni convection process. Proceeding of the International Sorption Heat Pump Conference, Shanghai, China, 2002, 283-288.

Y. Takata, S. Hidaka, M. Masuda and T. Ito. Pool boiling on a superhydrophilic surface. International Journal of Energy Research 27 (2003): 111-119

Y. Yang, X.G. Li, W.Y. Li, C.C. Fang, X.L., Qi. Experimental study on the characteristics of solar powered liquid dehumidification system. Acta Energiae Solaris Sinica 21 (2) (2000): 155-159.

Y.G. Yin, X.S. Zhang, G. Wang, L. Luo. Experimental study on a new internally cooled/heated dehumidifier/regenerator of liquid desiccant systems. International Journal of Refrigeration 31(5) (2008): 857-866.

Y.G. Yin, X.S. Zhang, Z.Q. Chen, Experimental study on dehumidifier and regenerator of liquid desiccant cooling air conditioning system, Building and Environment, 42 (2007): 2505-2511.

Y.M. Luo Study on the coupled flow, heat and mass transfer processes in a liquid desiccant dehumidifier. PhD Thesis. The Hong Kong Polytechnic University, Hong Kong, China, 2015.

Y.T. Kang, T. Kashiwagi. Heat transfer enhancement by Marangoni convectionin NH3-H2O absorption process. International Journal of Refrigeration 25 (2002): 780-788.

Yan Y Y, Zu Y Q. A lattice Boltzmann method for incompressible two-phase flows on partial wetting surface with large density ratio. Journal of Computational Physics, 2007, 227(1): 763-775.

Yang X, Shi B, Chai Z, et al. A coupled lattice Boltzmann method to solve Nernst Planck model for simulating electro-osmotic flows[J]. Journal of Scientific Computing, 2014, 61(1): 222-238.

Yang X, Shi B, Chai Z. Coupled lattice Boltzmann method for generalized Keller Segel chemotaxis model[J]. Computers and Mathematics with Applications, 2014, 68(12): 1653-1670.

Yin, Y., Qian, J., and Zhang, X., Recent Advancements in Liquid Desiccant Dehumidification Technology, Renewable and Sustainable Energy Reviews, vol. 31, pp. 38-52, 2014.

Z. Jiang, W. Tyan. Experimental studies on surface wave characteristics of free-falling liquid films. Proceeding of 4th International Symposium on Heat Transfer. Beijing High Education Process, 1966, 200-205.

Z. Li. Liquid desiccant air conditioning and independent humidity control air conditioning systems. Journal of HV&A 33 (2003): 26-31.

Zadrazil, Ivan, and Christos N. Markides. "An experimental characterization of liquid films in downwards co-current gas–liquid annular flow by particle image and tracking velocimetry." International Journal of Multiphase Flow 67 (2014): 42-53.

Zheng L, Lee T, Guo Z, et al. Shrinkage of bubbles and drops in the lattice Boltzmann equation method for nonideal gases. Physical Review E, 2014, 89(3): 033302.